TNO innovation for life

Theory and numerical models for acoustic insertion loss of bubble curtains

Bubbles JIP WP2B

TNO Publiek › TNO 2023 R10893
May 2023

Defence, Safety & Security
www.tno.nl
+31 88 866 10 00
info@tno.nl

TNO 2023 R10893 – May 2023

Bubbles JIP WP2B

Theory and numerical models for acoustic insertion loss of bubble curtains

Author(s)	M.J.J. Nijhof, T. van Abcoude, C.A.F. de Jong
Classification report	TNO Publiek
TitleTitle	TNO Publiek
Report text	TNO Publiek
Appendices	TNO Publiek
Number of pages	107 (excl. front and back cover)
Number of appendices	4
Sponsor	GROW
Project name	Bubbles JIP
Project number	060.47267

Summary

The study described in this report was carried out in the scope of the GROW Bubbles JIP. The objective of the Bubbles JIP is to achieve more efficient and effective use of bubble curtains for noise mitigation in offshore piling projects by improved engineering of the bubble curtain.

The objective of WP2 was to further develop hydrodynamic and acoustic models of bubble curtains, and validate these models against lab and offshore measurements. Models for bubble generation (i.e. how the air will be released from the hose that produces the bubble curtain, based on equipment and settings) are developed by TU Delft in WP5. In WP2A, MARIN develops hydrodynamic models to describe the geometry of the bubble curtain and the distribution of bubbles in the curtain, under influence of environmental conditions such as water depth and (tidal) currents. In WP2B, TNO further investigated the details of acoustic modelling of bubble curtains, and included bubble curtain models in the Aquarius marine piling noise modelling framework. In WP2C, TU Delft tested another acoustic modelling approach, implemented in the SILENCE piling noise model and compared results with field measurements.

This WP2B report presents the results of a literature review and evaluation of various available modelling approaches. This revealed that the interaction of an underwater sound field with the dynamic water-bubble mixture in a realistic bubble curtain is not fully captured by state-of-the-art models. At lower frequencies, where the performance of the bubble curtain is mainly due to the compressibility of the bubble curtain, the models seem to capture the main parameter dependencies reasonably well, but at higher frequencies, where models predict additional damping due to bubble resonances, the predictions differ widely. Note that frequencies at which most acoustic energy is released into the water by impact pile driving are typically found in the low frequency regime of the models (below the onset of bubble resonance), while the frequencies at which the noise reduction by the bubble curtain is maximal is usually found at higher frequencies (i.e. at or close to bubble resonance frequencies).

The applicability of the available models was tested against data from acoustic measurements in the Concept Basin at MARIN, performed by TNO and MARIN in WP4. Three different bubble curtain generation configurations (hoses) were compared, at three different air flow rates. Air void fractions and bubble size distributions were measured by MARIN, assisted by Twente University, at various locations across height and width of the bubble curtain. Because hydrodynamic modelling of the bubble curtain was not timely available, the input parameters for the acoustic models (void fraction and bubble size distribution as a function of position in the bubble screen) could not be generated using these models. Instead, the measurement data available at a limited set of positions was extrapolated across the curtain and then used as input for acoustic models. Subsequently, these models predict the acoustic insertion loss of the bubble curtain configurations and are compared with the measured insertion loss. This comparison confirmed that the models describe the effect of the compressibility of the bubble curtain reasonably well, but overestimate the damping associated with bubble resonances (which becomes dominant from ca. 1 kHz and above for the considered cases). The effect of the applied variations in bubble curtain configuration and air flow rate on the acoustic insertion loss appeared to be smaller than

the uncertainties in measurements and modelling. Direct quantitative comparison of results from models and measurements is complicated by uncertainties in the measurements and extrapolation of the bubble curtain parameters, as well as by uncertainties in the modeling of the acoustic field in the concept basin. Extrapolation of the conclusions from this comparison to offshore piling conditions is not warranted without further study. Recommendation for further development and validation of the models to arrive at predictive models for the case of offshore piling conditions are identified.

In general, it can be concluded that insertion loss of bubble curtains increases with increasing void fraction, which can be achieved by increasing the air flow rate and limiting the dispersion of the bubbles. This effect can be predicted by models that describe the distribution of compressibility in the curtain. Effects of bubbles size distribution on the insertion loss remain unclear.

Contents

Summary 3
Contents 5
1 Introduction 6
1.1 Background 6
1.2 Acoustic bubble screen models 6
1.3 Work Package 2 objectives 7
1.4 Outline 8
2 Sound mitigation by bubble curtains 9
2.1 Sources of sound reduction 9
2.2 Equivalent fluid properties 9
2.3 Sound reduction through dissipation 9
2.4 Sound reduction through reflection 10
2.5 Effects of difference in impedance and material damping in a bubble screen 11
2.6 Effects of environment 11
3 Bubble curtain insertion loss modelling 13
3.1 Insertion loss 13
3.2 Equivalent fluids 13
3.3 Modelling approaches 21
4 One-dimensional models for waveguides with a layer of water-bubble mixture 23
4.1 Insertion loss for 1D plane waves 23
4.2 Homogenous layer of water using Wood's equation 24
4.3 Homogeneous layer of water with resonant bubbles of equal bubble radius 26
4.4 Homogeneous layer of water with resonant bubbles and a bubble size distribution 31
4.5 Range dependent void fraction 35
4.6 Depth dependence 42
4.7 Summary 43
5 Two-dimensional models for a waveguide with a layer of water-bubble mixture 45
5.1 Overview modeling approach 45
5.2 Coordinate system 47
5.3 Implementation of the bubble screen in COMSOL 53
5.4 Notes on mesh size 53
6 Results Concept Basin 55
6.1 Bubble curtain measurements at MARIN 55
6.2 Effective speed of sound 57
6.3 Insertion loss 59
6.4 Difference in insertion loss between model and measurement results 63
6.5 Difference in insertion loss between flow speeds 64
6.6 Difference in insertion loss between bubble curtain types 67
6.7 Discussion 68
7 Summary and conclusions 76
7.1 Literature 76
7.2 1D models 76
7.3 2D models 77
7.4 Conclusions regarding bubble curtain performance 78
7.5 Recommendations for further research 79
References 81

Appendices
Appendix A: Literature overview 83
Appendix B: Adiabatic vs Isothermal speed of sound 100
Appendix C: Bubble damping 101
Appendix D: Derivation of the power transmission coefficient 103

1 Introduction

1.1 Background

The studies described in this report where carried out in the scope of the GROW Bubbles JIP. The objective of the Bubbles JIP is to achieve more efficient and effective use of bubble curtains/bubble screens for noise mitigation in offshore installation projects by improved engineering of the bubble curtain. At present, many offshore construction projects depend on pile driving to secure structures such as wind turbines to the seafloor. Depending on the dimensions of the piles that are driven and the technique that is employed the noise that is produced may surpasses the levels that are deemed acceptable (from an environment impact perspective) and mitigating measures are needed. A common method that is universally applicable for noise mitigation in shallow water environments is the use of bubble curtains.
An important step towards better engineered bubble curtains is an understanding of the various physical mechanisms at play and their effects on the acoustic properties. Using this knowledge allows to better control the noise levels and (by extension) the risks of not complying with specific noise requirements in a cost-effective manner. For a broader background of the Bubbles JIP see https://grow-offshorewind.nl/project/bubbles-jip

1.2 Acoustic bubble screen models

An assessment of the impact of noise on the environment is often required prior to the start of engineering activities. Acoustic models are critical tools in this assessment step since they provide the means to predict the expected sound levels for proposed scenarios. Ideally these models are capable of capturing the effects of:

- Properties of the source (i.e. the hammer and pile properties);
- Propagation through the environment which is influenced by the ocean wave guide properties (i.e. the properties of water, bottom and sea surface);
- Mitigating measures which are in this case determined by the bubble curtain properties (i.e. the bubble size distribution and void fraction in the curtain as a function of range and depth).

Most acoustic models for impact pile driving consist of multiple coupled or nested models. The way these models can be coupled or nested depends on the specific sub-models that are used. Note that while the overall acoustic model is linear some of the physical processes involved may not be linear (hammer impact, sediment deformation, bubble resonance). The different sub-models that can be distinguished usually include:

- Source/Excitation model. This model predicts how much energy is being put into the acoustic propagation model at different frequencies and the form of the excitation. For some model setups the source model includes the pile or even a section of the surrounding water, while for other model setups the source model only includes the hammer. In general, this model involves capturing the non-linearity of hammer/anvil impact (and of sediment deformation if included). For the type of model setup described in this report the source/excitation model only includes the hammer. For the laboratory test that are described in this report the source model is simply an omnidirectional point source.

- Acoustic propagation model. This model takes the excitation of the source model and propagates the results to the receiver points. This model is in general a linear acoustic model. In some model setups the pile is included in the propagation model and the non-linear behavior of the bottom surrounding the pile is represented by equivalent linear material properties. For the type of model setup described in this report the propagation model is included in the pile. However, for the laboratory test that are described there is no pile (the point source creates a sound field directly).
- Model of mitigating measures. If mitigating measures are present a separate model is usually used to represent its behavior in the setup. For some model setups the equivalent model forms a bridge between a short range propagation model (from source to mitigating system) and a long range propagation model (from mitigating system to receivers). For other model setups, the mitigation model is nested in or part of the propagation model. For the type of model setup described in this report the mitigation model is part of the propagation model. The mitigation model provides equivalent fluid properties that represent the bubble curtain, which are applied in the propagation model at the location of the bubble curtain.

Modelling of the source and sound propagation through the environment have been investigated in previous research projects. For lower frequencies (below ca. 500 Hz) a satisfactory general purpose model for impact pile driving (using a solid mass to store impulse) is available [1]. For higher frequencies more detailed models or data from measurements are needed to represent the source. For other hammer types (such as vibratory pile driving or Blue Piling) source models are lacking or currently in development and input data from measurements is needed. A range of propagation models is available, each offering different strengths and limitations. The main focus of the current JIP project is on development and validation of the capabilities to model mitigation using bubble curtains and to gather knowledge on the phenomena determining the performance of bubble curtains.

1.3 Work Package 2 objectives

The objective of WP2 is to (further) develop hydrodynamic and acoustic models, and validate the models against lab and offshore measurements. In addition, the influence of bubble curtain parameters on the acoustic performance of the bubble curtain are studied to aid bubble curtain design optimization. The interaction of a sound field with a bubble curtain results in complex physical behavior, and – perhaps unsurprisingly - the state of the art models that are available don't capture the behavior fully. Therefore, two different existing acoustic modelling approaches (TNO's Aquarius model and TU Delft's SILENCE) are compared and validated against experimental data independently, to be able to evaluate the applicability and effectiveness of the different modelling approaches. Models for bubble generation (i.e. how a specific bubble curtain will form based on bubble curtain equipment and settings) are developed by TU Delft in WP5 and in WP2A MARIN develops hydrodynamic models to describe the geometry of the bubble curtain and the density and distribution of bubble sizes in the curtain, under influence of environmental conditions such as water depth and (tidal) currents and possibly also water quality (salinity and surfactants).

The objectives of WP2 and the acoustic models that are used and developed in this work package can be linked to the following sub-objectives of the Bubbles JIP:

- To understand the sound propagation of piling noise through water and soil;
- To understand the physical mechanism of noise attenuation by air bubbles;
- To determine the parameters influencing the noise attenuation by air bubbles;
- To develop a practical numerical model which can be used to calculate the noise reduction of piling noise for realistic air bubble curtain configurations.

1.4 Outline

A short summary of relevant aspect related to sound mitigation using bubble screens is given in Chapter 2. An introduction to the calculation of the acoustic insertion loss for bubble curtains is given in Chapter 3, together with an overview of the models for equivalent fluid properties of bubble-water mixtures that are used in this study. In Chapter 4 the results of one-dimensional models for waveguides with a layer of water-bubble mixture are presented. Chapter 5 contains a description of the two-dimensional models for a waveguide with a layer of water-bubble mixture considered in this study. The results of the measurement carried out in the MARIN concept basin are presented in Chapter 6, together with the results of modelling this setup. Chapter 7 contains a summary of the presented work and the conclusions and recommendations that can be given based on the outcomes of the study.

2 Sound mitigation by bubble curtains

A short summary of relevant aspects related to sound mitigation using bubble screens is given below. Certain aspects that are described concisely below will be elaborated on more extensively in other sections of the text.

2.1 Sources of sound reduction

The reduction in sound level that is accomplished by placing a bubble screen between source and receiver is due to both absorption of sound while travelling through the bubble screen and reflection of sound on the layer of bubbly water, which has different acoustic propagation properties than pure water.
The amount of reduction of the transmitted wave and the strength of the reflected wave caused by both phenomena is dependent on many aspects including:

- composition of the bubble screen: the amount and size of the bubbles (which are potentially depth and width dependent);
- the bubble screen dimensions: extent of the bubble screen in the width direction (which is potentially depth dependent);
- properties of the environment:
- water depth and properties;
- sub-sediment layering and composition;
- distance between source and screen and source depth;
- distance between receiver and screen and receiver depth.

2.2 Equivalent fluid properties

For cases where the bubble sizes are much smaller than the acoustic wavelength, acoustic waves in the bubbly water can be described by an equivalent fluid with 'averaged' fluid properties. In the most simple approximation (which is useful in the low frequency limit, i.e. well below bubble resonance) the density and compliance, i.e. the reciprocal of the bulk stiffness, are the material properties that are averaged [2] [3]. At low volume fractions the equivalent density is hardly different from that of water, but the equivalent bulk modulus changes drastically (due to the reciprocal relation of bulk modulus with compliance, which is the quantity that is averaged). As a consequence, very low sound speeds can be observed in bubbly water (sound speeds as low as ca. 50 m/s for air volume fractions of ca. 1% are observed instead of 1500 m/s or 344 m/s which are typical for pure water and air, respectively).

2.3 Sound reduction through dissipation

The equivalent fluid will also exhibit material damping (i.e. attenuation of the amplitude of acoustic waves as these propagates through the equivalent fluid), especially at higher frequencies. This damping is related to the forced expansion and contraction of the air bubbles due to the fluctuations in pressure associated with passing acoustic waves. For

bubbles in vibration, damping is most pronounced at/near their resonance frequencies, especially at the first breathing mode (i.e. a bubble motion involving simultaneous radial contraction/expansion of the entire bubble surface) [3] [4].
Depending on the size of the bubble the main cause of damping at resonance is either viscous losses, thermal losses or radiation [4]. Viscous losses are due to compression/expansion of the water directly surrounding the bubble. Thermal losses are due to heat transport from the trapped gas into the water, a process that is harmonic, but partially out of phase with compression leading to a net transport of heat to the water. Radiation 'losses' are due to incoherent re-radiation of acoustic energy by systems consisting of many bubbles. The acoustic energy due to this incoherent part of the sound field is not dissipated (i.e. it is not converted to heat), but will not contribute (on average) to the response of the bubble curtain [5]. For air bubbles in water, the main contribution to the damping is viscosity for small bubbles (< ca. 0.003 mm), thermal losses for medium bubbles (> ca. 0.003 mm, and < ca. 4 mm) and radiation for large bubbles (> ca. 4 mm) [4]. In bubble curtains generated under operational conditions a distribution of bubble sizes is encountered. Measurements performed by Marin (in a laboratory setting with fresh water) show that bubbles with sizes that contribute significantly to the volume fractions are typically between ca. 0.1 mm and 50 mm in diameter (smaller and larger bubbles are present but in very small concentrations). As was mentioned above, the observed dissipation is maximal at the frequency associated with a resonance of the first breathing mode. This resonance frequency is dependent on the size of the bubble, and for a bubble size distribution various bubbles will be at or close to resonance over a wide range of frequencies. In addition, the volume fraction for bubbles in a certain range will also influence the amount of material damping that is observed. This leads to a complex dependency of the amount of material damping with frequency (and bubble distribution). Below the resonance frequency of the largest bubbles (having the lowest resonance frequencies) the amount of material damping of the equivalent fluid representing a bubbly liquid will decrease with decreasing frequency.

2.4 Sound reduction through reflection

Reduction in sound due to reflection of incident sound on the bubble curtain interface can be associated with the 'contrast' in fluid properties between pure water and bubbly water. To be more specific, the amount of reflection is closely related to the difference in acoustic impedance. The characteristic specific acoustic impedance is defined as the product of density and sound speed. If the acoustic impedances at two sides of a fluid-fluid interface are identical no sound will be reflected at the interfaces, and all sound will be transmitted from one side of the interface to the other side. As the difference in acoustic impedance between the two fluids grows the amount of reflection will also increase while the amount of transmission decreases.
If a planar layer of a fluid is embedded in a host fluid, two parallel fluid-fluid interfaces exist with similar reflection/transmission properties. For such cases, the reflection/transmission of the layer (as a whole) depends not only on the reflection/transmission of the interfaces, but also on the thickness of the layer (i.e. the distance between the reflective interfaces). If the layer is much thinner than a wavelength (based on the sound speed in the layer), the wave appears to mostly 'tunnel' through the layer (i.e. the effect of the layer is limited). The amount of reflection decreases with decreasing thickness while the amount of transmission increases. On the other hand, if the layer is ca. half a wavelength or thicker (based on the sound speed in the layer) resonances and anti-resonance occur (depending how well an integer number of half-wavelengths fits in the layer thickness) making the layer either almost transparent (independent of the difference in impedance) or maximally reflective

(with the maximum dependent on the difference in impedance). Examples of this behavior are demonstrated in Section 3.
If sound is incident at an angle, diffraction takes place at the interface (i.e. the angle of transmission is not identical to the angle of incidence). The angle of incidence has an effect on the amount of reflection/transmission that occurs at an interface (for instance, above the critical angle sound will be fully reflected while at normal incidence a high transmission may be observed). For a wave interacting with a planar layer at an angle the distance that determines if the response of the layer involves a resonance of the layers is the distance that the diffracted wave travels in the layer (i.e. the 'width' in the direction of the diffracted wave). For layers of non-constant thickness, the behavior is more complex, especially if the wavelengths are in the order of the thickness of the layer or smaller.

2.5 Effects of difference in impedance and material damping in a bubble screen

It was already mentioned above that the sound speed of a bubble liquid can be much lower than that of pure water, while the density in both media is very similar.
Due to this much lower equivalent sound speed (and virtually unchanged density) the acoustic impedance of bubbly water is much lower than that of pure water. This can lead to large reflections depending on the width of the bubble curtain and the angle of incidence on the interface as was described above. In general, at very low frequencies the sound reduction due to a bubble curtain is small. If the bubble screen is substantially smaller in width than a wavelength (based on the sound speed in the curtain) reflections on the screen will be small. In addition, at low frequencies the number of wavelengths that sound travels in the curtain is small (even at the very low sound speeds observed in bubble liquids), and as a consequence damping due to interaction with bubbles is small. Furthermore, material damping of an equivalent fluid will be small for frequencies much below bubble resonance frequencies.
On the other hand, as frequencies increase and approach the lowest bubble resonance frequency the amount of damping increases significantly. If a distribution of bubble sizes is present multiple bubbles will be at or near resonance at higher frequencies and the effects of material damping becomes significant. For these frequencies the screen is often also multiple wavelengths thick (based on the sound speed in the curtain) implying that dissipation through material damping grows width frequency and reflections on the screen can also be significant adding to the sound mitigating effect of the screen.
For frequencies above the bubble resonance of the smallest bubbles, the material damping diminishes with frequency and the sound speed will approach the speed in bubble-free water as the frequencies become very large [3], This suggests the effect of the screen will reduce with frequency for frequencies well above the resonance frequency of the smallest bubbles.

2.6 Effects of environment

Sound can travel under the bubble screen depending on sub-bottom layering. If a layer of soil/sediment of significant thickness that is relatively well matched with the properties of water (for instance mud) sits on top of a relatively good reflecting layer (for instance sand) sound paths that travel through the sediment below the screen may carry significant amounts of acoustic energy to the shadow side of the screen. This can reduce the effectiveness of the bubble screen significantly, since contributions from sound paths traveling under the screen will not be reduced. The contribution of such paths to the total sound field on the shadow side of the screen is dependent on many factors including: the

reduction the screen achieves for the direct path (i.e. paths that do travel through the screen), the directivity of the source, environmental properties (such as the material properties and thickness of the bottom layers and sound speed in the water column), the depth of the source and its distance to the bubble screen and the distance of receiver positions to the source and screen. The contribution of all sound paths is in general frequency dependent, necessitating a per frequency analysis to establish which path is dominant and how effective the bubble screen is in reducing the total field.

3 Bubble curtain insertion loss modelling

3.1 Insertion loss

The effectiveness of a bubble curtain for reducing underwater sound can be quantified in terms of its acoustic insertion loss. This is defined in the German measurement standard DIN SPEC 45653 (Offshore wind farms - In-situ determination of the insertion loss of control measures underwater), which has been submitted to the International Organization for Standardization (ISO) for development as an international standard.

The insertion loss (IL) of a bubble curtain is defined here as the decrease of the single strike sound exposure level (abbreviation SEL, symbol L_E) from the piling sound at a specified position due to the insertion of the bubble curtain. In this report it is determined and reported as a frequency-depended quantity of the difference of the SELs without and with bubble curtain.

$$\mathrm{IL} = L_{E,\mathrm{screen}} - L_{E,\mathrm{ref}} \tag{3.1}$$

Unless stated otherwise it is plotted for decidecade[1] frequency bands. With SEL defined as

$$L_E = 10 \log_{10} \frac{E}{E_0} \ \mathrm{dB} \tag{3.2}$$

with $E_0 = 1\ \mu\mathrm{Pa}^2\mathrm{s}$, the reference sound exposure and the sound exposure E defined as

$$E = \int_{t_0}^{t_1} p(t)^2 dt \tag{3.3}$$

with p the sound pressure.

3.2 Equivalent fluids

As the number of bubbles in a bubble cloud grows, taking the contribution of individual bubbles to the response of the bubble curtain into account explicitly becomes an intractable problem quite quickly. Apart from rare exceptions models of bubble clouds do usually not consider individual bubbles. Instead the most common solution is to derive equivalent acoustic properties (density, sound speed and damping) of the bubbly liquid which can then be used in regular acoustic models. In the scope of this study only equivalent fluid models are considered.

[1] Decidecade bands are also referred to as 'one-third octave (base-10)' bands, see the ISO 18405 Terminology standard for underwater sound.

Roughly four types of equivalent fluid models can be identified:

1. **Models without bubble response:** In these models, bubble resonances are neglected and the only effect of adding gas to a liquid that is considered is the average loss in mass and stiffness. The most commonly adopted equations that follow from this approach are known as Wood's equation [6].
2. **Models including single bubble interaction:** A way to incorporate the resonant response of individual bubbles without having to explicitly track the contribution of individual bubbles is to adopt a statistical approach. The most commonly used approach is to consider the average behavior of bubble ensembles that correspond with a description of the bubble curtain in terms of statistical properties. A mathematical framework to evaluate the average properties of such bubble ensembles was proposed by Foldy [5]. This work only includes abstract scatters and does not include a specific model for the response of an individual bubble, however. The most widely used model, that is based on Foldy's approach, which includes a detailed model for the response of individual bubbles is the model of Commander and Prosperetti [7]. This model is also applicable to cases with a bubble size distribution. However, the model does not include bubble to bubble interaction (only the interaction of individual bubbles with the incident field is considered). Bubble to bubble interaction may become relevant for higher bubble concentrations due to smaller distance between neighboring bubbles.
3. **Models including bubble-bubble interaction using a scattering series:** Foldy already recognized the importance of bubble to bubble interaction and suggests it can be incorporated in the theory by including terms accounting for the response of bubbles to the fields scattered by other bubbles. A simple method to implicitly include bubble to bubble interactions based on a recursive scheme in which the incident field is repeatedly update to include the response from other bubbles was suggested by Kargl [8]. Alternative approaches are provided by Ye [9] and Henyey [10], who derive analytical expressions for the equivalent speed of sound that include terms accounting for (higher order) bubble-bubble interaction. Henyey claims his model captures the full scattering series using a closed form expression, which in theory makes it superior to the models presented by Foldy and Ye. These models are also applicable to cases with a bubble size distribution. However, validation against measurement data is lacking for the models presented by Ye and Henyey. Only the paper by Kargl includes a few data points from measurement allowing to assess the quality of the predictions.
4. **Models including bubble-bubble interaction using a self-consistent approach:** An alternative way to incorporate bubble to bubble interactions was proposed by Feuillade [11]. He argues that if bubble to bubble interaction is strong (because of close proximity of bubbles and bubble resonance) the scattering series solution as proposed by Foldy is no longer valid (the scattering series diverges). The approach adopted by Feuillade is self-consistent. In the theory, the total field incident on any bubble is defined as the sum of the external field plus the scattered fields from all the other bubbles, where these other bubbles are considered to have already experienced all of the interactions which affect them. A downside to the method is that one of the parameters (determining the range within which neighboring bubbles are considered coupled) does not follow from the theory and has to be determined by fitting measurements. The method has been extended to cases with a bubble size distribution, but the approximation provided is expected to be useful only under the assumption that the distribution of bubble radii is narrow compared to the mean radius. The results from validation against measurement data presented by Feuillade are promising, although differences between model prediction and measurement data remain.

These models and other work are discussed in more detail in the literature overview in Appendix A. A number of the models mentioned above were implemented and used in the

scope of this study to predict the acoustic performance of the bubble curtains that was measured in tests at MARIN (WP4). The next sub-sections contain a concise description of the main four models that were used.

Note that these models do not include the work of Ye [9] and Henyey [10]. Although the model of Henyey is in theory superior to the other models based on a scattering series that are presented (including the work of Ye), the results have not been validated against measurement. Moreover, the solutions that are obtained are somewhat problematic. Solving the model analytically leads to three solutions. Two of these solutions produces unphysical results for certain frequency ranges (i.e. they predict a growth in signal with propagation instead of attenuation due to damping). The remaining solution does not converge to known solution for the low-frequency limit (it converges to zero). See Appendix A for a more detailed description of the results obtained with the model of Henyey.

3.2.1 Wood's equation

In the simplest approximation, the bubble curtain is represented as a homogeneous gas-water mixture. An expression for the equivalent/effective density ρ_{eff} and speed of sound c_{eff} of such a mixture was first given by Mallock [6]. He supposed a constant density ρ and sound speed c in the gas and water, and defines β as the volume occupied by the gas in a unit volume of the mixture, also known as the void fraction. The effective density of the mixture is given by the arithmetic mean of the densities of gas and water, accounting for the fraction of volume they occupy.

$$\rho_{\text{eff}} = \rho_w(1-\beta) + \rho_g\beta \tag{3.4}$$

where the subscripts w and g refer to the water and gas fractions of the mixture, respectively. The bulk modulus is related to the sound speed and density by

$$c^2 = K/\rho \tag{3.5}$$

The effective bulk modulus of the mixture is given by the harmonic mean of the densities of gas and water, accounting for the fraction of volume they occupy.

$$K_{\text{eff}} = \frac{1-\beta}{K_w} + \frac{\beta}{K_g} \tag{3.6}$$

Or using equation (3.5) this can be expressed in terms of density and speed of sound in the water and gas

$$K_{\text{eff}} = \frac{1-\beta}{\rho_w c_w^2} + \frac{\beta}{\rho_g c_g^2} \tag{3.7}$$

The effective speed of sound of the gas-water mixture can (after some re-writing) be expressed using equation (3.4), (3.5) and (3.7) as

$$c_{\text{eff}} = \left\{ \frac{(1-\beta)^2}{c_w^2} + \frac{\beta^2}{c_g^2} + \frac{\beta(1-\beta)(c_g^2\rho_g^2 + c_w^2\rho_w^2)}{c_g^2\rho_g c_w^2\rho_w} \right\}^{-1/2} \tag{3.8}$$

Equations (3.4) through (3.6) or equation (3.8) and variations thereof are often referred to as Wood's equation since he seems to have popularized this representation of the speed of sound for liquid-gas mixtures [2].

Equation (3.8) is only expected to be useful for low frequency waves (i.e. frequencies well below the resonance frequencies of the bubbles), because it does not take into account the resonance effects of the bubbles [12]. Moreover, the obtained speed of sound is frequency independent and is real-valued, implying that there is no damping associated with propagating though the bubbly liquid. From measurements it is known that the speed of sound in bubble liquids is frequency-dependent and propagating waves attenuate due to damping [7].

Note that some authors [13] explicitly mention that they use the isothermal speed of sound of the gas in these equations, while others (like Wood [2]) don't explicitly make a choice or use the more commonly used adiabatic speed of sound. Using a more complex theory including thermal effects it can be shown that which choice is more appropriate is frequency and bubble size dependent[2]. Unless mentioned otherwise the isothermal speed of sound is taken for calculations using Wood's equation described in this report. Furthermore, it may be worth mentioning that in some cases also approximations to equation (3.8) are referred to as Wood's equation (see Appendix B for an example).

Error! Reference source not found. shows that the equivalent speed of sound in the m ixture is lower than the speed of sound in air (337 m/s) at void fractions β between 10-3 and 0.99. This can be understood by deriving from equation (3.8) that to first approximation $c_{\text{eff}} \approx c_g\sqrt{\rho_g/\rho_w\beta(1-\beta)}$ (see [13] for a variation or Appendix B). Since the density of the gas is much lower than that of the water, this relation implies that the bubble curtain has a characteristic specific acoustic impedance (ρc) much smaller than that of pure seawater. A large difference in acoustic impedance at an interface causes sound waves to mostly reflect at the outer interfaces of the bubble curtain.

[2] If the acoustic thermal boundary layer in the gas is large compared to the bubble size an isothermal assumption is appropriate, if the acoustic thermal boundary layer is small compared to the bubble size an adiabatic assumption is appropriate. In the work of Ainslie and Leighton [19] the concept of thermal diffusion ratio is introduced to help assess what the appropriate regime is.

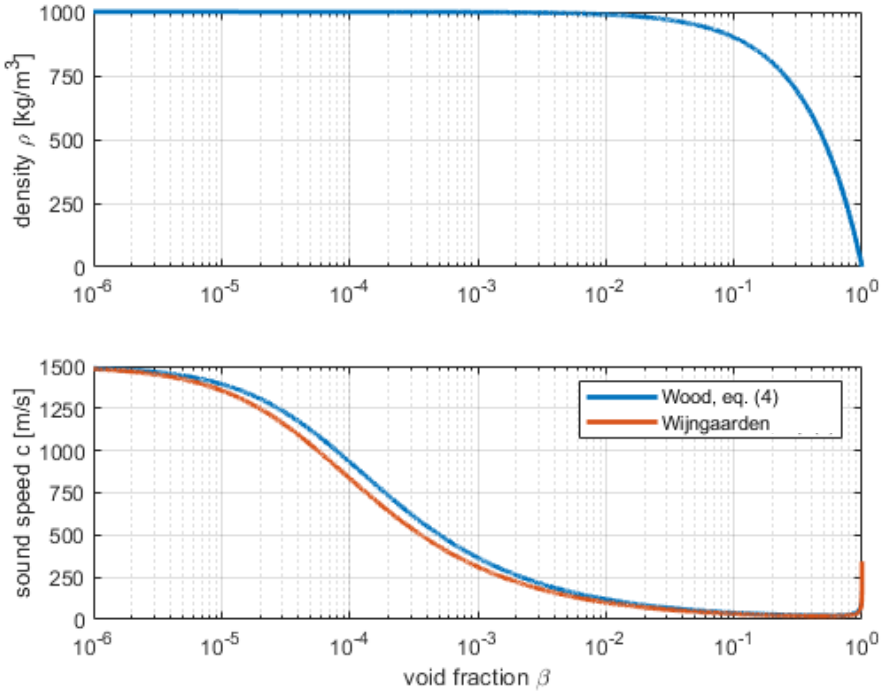

Figure 3.1: Effective density (upper) and sound speed (lower) of a homogeneous mixture of water and air bubbles (at 10°C and depth less than 100 m) for isothermal (Wijngaarden) and adiabatic conditions (Wood), as a function of void fraction β. Compared to the sound speed as predicted by Wood the predicted values by Wijngaarden differ a factor of ca. 0.85 for 10^(-3)<β<0.99 .

3.2.2 Commander and Prosperetti

In the work of Commander and Prosperetti [7] the sound field in a bubble cloud is modelled by treating the interaction of an incident wave with a bubble cloud as a multiple scattering problem (see [14] for a more elaborate derivation of essentially the same model). The model provides an average equivalent sound speed for an ensemble of bubble configurations that corresponds to a statistical description of the bubble curtain properties in the form of a bubble size and bubble position distribution. The individual interactions of an incident field with a bubble is described by a model including the effects of the compressibility of the gas, thermal effects due to transport of heat in the bubble and across the bubble boundary, radiation by the bubble to the surrounding water and viscous losses in the water.
The model results in an expression for the effective wavenumber k_m of the bubbly medium as function of the bubble size distribution $n(a)\mathrm{d}a$, representing the number of bubbles per unit volume with equilibrium radius between a and $a + \mathrm{d}a$.

$$k_{\mathrm{eff}}^2 = k_w^2 + 4\pi\omega^2 \int_0^\infty \frac{an(a)\mathrm{d}a}{\omega_0^2 - \omega^2 + 2\mathrm{i}\omega(b_v + b_t + b_a)} \tag{3.9}$$

where the terms b_v, b_t and b_a describe viscous losses[3], thermal losses and acoustic radiation losses associated with bubble oscillations, respectively. These damping terms are defined as

[3] In the work of Commander and Prosperity the damping terms are presented as a single term. Note that the denominator of the second term (associated with b_t) in [6] is incorrectly missing a term ω. This term was added here to Equation (3.11). Without this modification the results [6] cannot be reproduced suggesting this concerns a typographical error.

$$b_v = \frac{2\mu_w}{\rho_w a^2} \tag{3.10}$$

$$b_t = \frac{p_0}{2\rho_w a^2 \omega}\mathrm{Im}(\Phi) \tag{3.11}$$

$$b_a = \frac{\omega^2 a}{2c_w} \tag{3.12}$$

where μ_w denotes the dynamic viscosity of water, $p_0 = p_\infty + \frac{2\sigma}{a}$, with p_∞ the equilibrium pressure of the water, σ the surface tension between water and the air in the bubbles. The complex valued function Φ describes the transport of heat within the bubble[4] and is defined as

$$\Phi = \frac{3\gamma}{1-\mathrm{i}3(\gamma-1)\chi\{(\mathrm{i}/\chi)^{1/2}\coth[(\mathrm{i}/\chi)^{1/2}]-1\}} \tag{3.13}$$

with polytropic gas constant $\gamma = C_P/C_V$ and $\chi = D/\omega a^2$, where $D = (\gamma-1)K_T T/(\gamma p_0)$ the thermal diffusivity of the air, with T the temperature and K_T thermal conductivity.
Note that Commander and Prosperetti deliberately chose to cast the solution in a form describing a linear oscillator. The resonance frequency of the oscillator is given by

$$\omega_0^2 = \frac{1}{\rho_w a^2}\left[p_0\mathrm{Re}(\Phi) - \frac{2\sigma}{a}\right] \tag{3.14}$$

They note that the dependency of the damping terms and resonance frequency on the frequency of the incident field renders this similarity somewhat superficial. For a concise description of the similarities between the solution presented here and the equations describing a linear oscillator see Appendix C.
The bubble size distribution $n(a)\mathrm{d}a$ and the void fraction β are related via:

$$\beta = \frac{4}{3}\pi\int_0^\infty a^3 n(a)\mathrm{d}a \tag{3.15}$$

3.2.3 Kargl

Kargl [8] argued that higher-order multiple scattering, which is not included in the approximation by Commander and Prosperetti [7], becomes important for void fractions $\beta > 10^{-4}$. He proposes to include multiple scattering effects by using the equivalent properties of the medium in the definition of k_m the effective wavenumber of the mixture. His reasoning is that in this way, the response of a bubble is based on how it interacts with the effective medium which includes the effects of the presence of surrounding bubbles. The definition of k_m is thus

$$k_m^2 = k_w^2 + 4\pi\omega^2\int_0^\infty \frac{an(a)\mathrm{d}a}{\omega_{0m}^2-\omega^2+\mathrm{i}(b_{vm}+b_{tm}+b_{am})} \tag{3.16}$$

where the terms b_{vm}, b_{tm}, b_{am} and ω_{0m} represent the same quantities as before but are now defined in terms of the properties of the equivalent mixture

$$b_{vm} = \frac{2\mu_m}{\rho_m a^2} \tag{3.17}$$

[4] To first order $\Phi \approx 3\gamma$, so that eq.(3.20) predicts $\omega_0^2 \approx \frac{3\gamma p_0}{\rho a^2}$, yielding the Minnaert bubble resonance frequency [16]: $f_0 = \frac{1}{2\pi a}\sqrt{3\gamma p_0/\rho}$.

$$b_{tm} = \frac{p_0}{2\rho_m a^2 \omega}\mathrm{Im}(\Phi) \tag{3.18}$$

$$b_{am} = \frac{\omega^2 a}{2c_m} \tag{3.19}$$

$$\omega_{0m}^2 = \frac{1}{\rho_{wm} a^2}\left[p_0 \mathrm{Re}(\Phi) - \frac{2\sigma}{a}\right] \tag{3.20}$$

with the letter m in the subscripts of the different quantities indicating the properties of the equivalent mixture are to be taken. Kargl notes that in a dilute mixture, the approximate equalities $\omega_{0m} \approx \omega_0$, $b_{vm} \approx b_v$, and $b_{tm} \approx b_t$ hold because mixture laws for density and viscosity suggest that using $\rho_m = \rho_w$ and $\mu_m = \mu_w$ would have a negligible effect[5].
The term b_{am} however includes the speed of sound of the medium which is dependent on the wave number in the medium according to the definition

$$c_m = \frac{2\pi f}{k_m} \tag{3.21}$$

which makes the definition of k_m recursive. Kargl proposes to approximate the value of k_m iteratively. This can be done by repeatedly calculating k_m using the equation for k_m above, each time using the previous value for k_m to calculate the speed of sound. For the first evaluation of k_m the speed of sound in water is used.
It was found that the iterative process indeed seems to always converge (no cases of non-convergence were observed) and a stable solution (with a relative change in $|k_m| \leq 0.001$ between the last iteration steps) was always established within 50 iterations. All presented solutions using the method of Kargl used 50 iterations.

3.2.4 Feuillade

In the theory put forward by Feuillade [15] the total field incident on any bubble is defined as the sum of the external field plus the scattered fields from all the other bubbles, where these other bubbles are considered to have already experienced all of the interactions which affect them. The collective response of the whole system of bubbles may be fully represented by a complete set of coupled differential equations with the steady state volume oscillation amplitudes as dependent variables. The solution obtained by solving this system automatically and precisely incorporates all orders of multiple scattering between all the bubbles. Analogous to the models in the previous section an average solution is sought averaging over all possible configurations of the bubbles matching an associated statistic description. An analytic solution to the system of equations is presented that is derived by applying the concept of collective modes of oscillation (i.e. normal modes of oscillation of the ensemble). Under the assumption that the distribution of bubble radii is narrow compared to the mean radius with a bubble size distribution, a solution is obtained for a distribution of bubble radii

$$k_T^2 = k_w^2 + \frac{F}{1 - F\int_0^\infty re^{-ikr}dr} \tag{3.22}$$

with F defined as

$$F = 4\pi\omega^2 \int_0^\infty \frac{an(a)da}{\omega_0^2 - \omega^2 + 2i\omega(b_v + b_t + b_a)} \tag{3.23}$$

[5] For example, a void fraction of $\beta = 0.01$ produces a 1% decrease in ρ and Arrhenius's mixture rule for viscosity predicts an approximate 4% decrease in μ [7]. Additionally, the surface tension remains unchanged because it is a local property at the interface separating the gas within a bubble from the surrounding host fluid.

with $f(a)$, ω_0, b_v, b_t and b_a as defined in Section 3.2.2. Note that these equations are re-written versions of the expressions in the work of Feuillade to match the notation and form of the solutions presented in the previous subsection. If the distribution only includes a single radius, this approximate solution equals the exact solution for a single bubble radius that is also derived by Feuillade.
Feuillade explains that if the integral in denominator is taken from zero to infinity it will lead to an unbounded (unstable) growth of that term if k is real (i.e. in the case of no damping). He reasons that the effective k after a few bubble interactions will not be real-valued however, since interactions with bubbles adds damping according to the theory.
He continuous to state that for the first bubbles however, there is no interaction with other bubbles and k should have the value as that of water. At the same time, if the scattering and absorption cross-sections are large, only the first neighbors will respond strongly to the field scattered by a given bubble. Since every interaction with the scattered field will reduce the remaining sound field strongly, other bubbles that are present behind the direct neighbors are thus 'shielded'. His solution to the unbounded growth of the integral is therefore to change the higher bound of the integral thereby defining a 'range of influence' around a bubble with a finite radius within which bubbles are strongly coupled (the region is termed "region of collective interaction"). Feuillade assumes in his paper that this range is fixed for a given bubble distribution, leading to the expression

$$k_T^2 = k_w^2 + \frac{F}{1 - F\int_0^R re^{-ikr}dr} \tag{3.24}$$

For a couple of cases involving a single bubble radius he determines the range by fitting the predicted sound speed to measurement data. The fitting procedure involves adjusting R so as to minimize the least squares difference between the experimental determined attenuation measured at specific frequencies and the predicted values. This approach leads to favorable comparison of other measured data points (both attenuation and phase speed). It is shown that a less favorable comparison between measurement and predicted data is obtained for cases involving more complex bubble size distributions. Therefore, in the scope of this study the approach proposed by Feuillade is amended slightly. From the cases with a single bubble radius that were considered it is observed that a linear relation between average bubble distance r_0 and range of influence can be observed (at least within an interval of void fractions). The range of influence R is therefore made dependent on the average bubble distance r_0. Based on the presented data the relation that is established is

$$R = 1.272 r_0 \tag{3.25}$$

with the average bubble distance as a function of the void fraction β and bubble size a defined as

$$r_0 = \left(\frac{\beta}{\frac{4}{3}\pi a^3}\right)^{-\frac{1}{3}} \tag{3.26}$$

A consequence of making the bound of the integral dependent on the bubble radius is that the expression for the equivalent wave number should also be adjusted. The last step in obtaining this expression results from taking an integral over all bubble sizes, however, the integral of the denominator is now dependent on the bubble radius. The corrected expression which is used to produce all result of the Feuillade model in this study is

$$k_T^2 = k_w^2 + \int_0^\infty \frac{G(a)}{1 - \int_0^\infty G(a)da \int_0^{R(a)} re^{-ikr}dr} da \tag{3.27}$$

with

$$G(a) = 4\pi\omega^2 \frac{an(a)}{\omega_0^2 - \omega^2 + 2i\omega b} \tag{3.28}$$

3.2.5 Limitations

The main limitations of the model based on Wood's equation was already described in sub-Section 3.2.1. The implementation of the models based on the work of Commander and Prosperetti, Kargl and Feuillade used in this study do not suffer from these limitations. However, they do share certain other limitations due to the fact the scattering model for an individual bubble that is used is mostly identical.

The main limitations of this scattering model are related to linearization of the different equations describing the full behavior of the physical phenomena that are involved. The linearization steps imply the solution is valid only for the case of small oscillation amplitudes of the bubbles, and only when the incident field contains information of a single frequency[6]. Therefore, depending on both the amplitude and frequency content of the incident field the solutions may not provide accurate results, which can be especially problematic close to bubble resonance.
Another approximation of the scattering model is that only the so-called breathing mode is included. Besides not including higher order spherically symmetric modes (which are relevant to non-linear behavior) there are also non-spherical vibration modes. Although there is a coupling between such non-spherical modes and the breathing modes the consensus is that these modes do not contribute significantly unless they are significantly excited by an external source [4] (which requires an incident field that matches both resonance frequency and shape). Bubbles will also change in shape by their movement through the water. These changes are often slow compared to vibrations associated with the acoustic frequencies considered. From an acoustic perspective the bubbles will vibrate around a non-spherical rest state. This may have influence on the resonance behavior (resonance frequency, damping and radiation pattern). Such effects are also not included in the models that were implemented for the current study.

3.3 Modelling approaches

When the number of dimensions included in a model for the acoustic insertion loss of a bubble curtain is considered, the following breakdown of possible approaches can be made:

- 1D models
  - Representing the effects of depth dependent bubble curtain properties can only be approximated;
  - Representing the effects of an environment (waveguide) is not possible;
  - Efficient models, so useful for parameter studies.
- 2D models
  - Representing the effects of air-water interface possible, effects of side-walls can be included at the cost of additional computational efforts (for simple boundary conditions, such as acoustically hard walls);

[6] In [6] one of the assumptions is introduced by noting "This reduces to a simple proportionality only in the case of sinusoidal motion, to which we therefore confine the analysis from now on". A more elaborate derivation is given in [13] which adds that a gas bubble responds as a linear oscillator only when driven at a single frequency. Its response under "multiple-frequency or non-periodic excitation is far more complex and depends also on the past history of the motion."

  - Representing the effects of depth dependent bubble curtain properties is possible;
  - Less efficient, so unpractical for large parameter studies.
- 3D models
  - Effects of variation of parameters in all directions can be included;
  - Arbitrary 3D geometries can be described;
  - Very computationally intensive.

In the scope of this study only 1D and 2D models are considered. This next section discusses various models for the acoustic insertion loss with increasing complexity:

The following effects can be studied using a simple 1D case, i.e. an incident plane wave interacting with an infinite homogenous bubble screen in an infinite homogenous medium:
- The effects of bubbles on the compressibility and absorption of a water layer;
- The effects of bubble resonances added, without bubble-bubble interaction;
- The effects of bubble resonances added, with bubble-bubble interaction.

The following effects can be studied using a slightly altered 1D case, i.e. an incident plane wave interacting with an infinite, stratified inhomogeneous bubble screen in an infinite homogenous medium:
- The effects of variation of bubble distribution parameters over the thickness of the curtain.

Note that for all four cases above the effects can be studied without the need to define a specific environment, since the water surface, bottom or side walls of waveguide cannot be included. The effects below can be studied using a 2D case involving depth dependency:
- The effects of variation of bubble distribution parameters over the height of the curtain;
- The effects of the depth of the sound source and receivers;
- The effects of the distance of the bubble curtain to the sound source and receivers;
- Influence of the seabed on the insertion loss.

The current 2D model that was developed in the scope of this study is not suited for large-scale parameter studies and it is used here mainly for prediction of the insertion loss for the WP4 measurements that were carried out in the Concept Basin at MARIN (Chapter 6).

4 One-dimensional models for waveguides with a layer of water-bubble mixture

4.1 Insertion loss for 1D plane waves

The transmission of a plane sound wave with pressure amplitude p_{i} through the bubble curtain can be quantified in terms of the power transmission coefficient α_t, relating the amplitude p_t of the transmitted wave to the amplitude of the incident wave (see e.g. [16]). For a normal incident wave and identical fluid media on both sides of the bubble screen, the power transmission coefficient is related to the pressure amplitudes of the incident and transited wave by $\alpha_t = |p_t^2/p_i^2|$. In the second edition of Kinsler and Frey [16] this is expressed in terms of material properties of the fluids as

$$\alpha_t = \frac{4}{4\cos^2(k_{\mathrm{eff}}L)+\left(\frac{\rho_{\mathrm{eff}}c_{\mathrm{eff}}}{\rho_w c_w}+\frac{\rho_w c_w}{\rho_{\mathrm{eff}}c_{\mathrm{eff}}}\right)^2 \sin^2(k_{\mathrm{eff}}L)} \tag{4.1}$$

Here k_{eff} is the acoustic wavenumber in the curtain and L is the thickness of the curtain. The acoustic wave number is defined as $k = \omega/c$, with ω the angular frequency defined as $\omega = 2\pi f$, where f is the frequency in Hertz. This coefficient is found by solving a system of equation describing the waves traveling towards, away and in the bubble curtain as is schematically depicted in

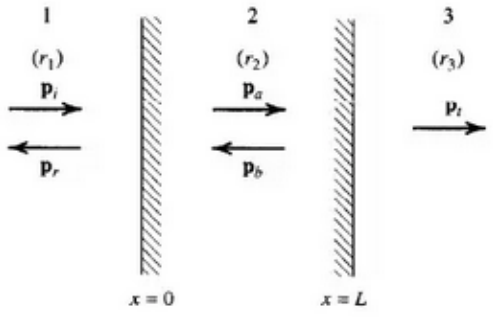

Figure 4.1: Reflection and transmission of a plane wave normally incident on a layer of uniform thickness.

In a later edition ([16], fourth edition) an analogue expression is provided for the intensity transmission coefficient

$$T_I = \frac{1}{1+\frac{1}{4}\left(\frac{\rho_{\mathrm{eff}}c_{\mathrm{eff}}}{\rho_w c_w}-\frac{\rho_w c_w}{\rho_{\mathrm{eff}}c_{\mathrm{eff}}}\right)^2 \sin^2(k_{\mathrm{eff}}L)} \tag{4.2}$$

which is equal to the power transmission coefficient for the case of normal incidence provided the fluids media on both sides of the screen are identical (i.e. in that case $\alpha_t = T_I$). This expression, although different in appearance, leads to the same numerical results obtained as using equation (4.1) for all cases considered in this report.
It was discovered that the expressions in equation (4.1) and (4.2) are not an exact solution to the present problem for the general case and gives significantly deviating results in the case damping is present in the screen, i.e. in case the speed of sound in the screen is complex valued. This may not come as a surprise since the expressions in Kinsler and Frey (both in the second and fourth edition) for the power transmission coefficient becomes complex valued as a complex sound speed is chosen for one of the media.
The exact solution was re-derived (see Appendix D) based on the theory set out in [16] and was found to be

$$\alpha_t = \left| \frac{2}{2\cos(kL)+i\left(\frac{r_2}{r_1}+\frac{r_1}{r_2}\right)\sin(kL)} \right|^2 \tag{4.3}$$

with $r_1 = \rho_{\mathrm{w}} c_w$ and $r_2 = \rho_{\mathrm{eff}} c_{\mathrm{eff}}$. It is observed that the denominator in the left hand side takes the form of a complex number, i.e. $z = x + iy$, as long as r_1, r_2 and k remain real-valued. In that case taking the square of the absolute value (also known as the squared norm) can be written as $|z|^2 = |x + iy|^2 = x^2 + y^2$. Under this assumption and using this relation equation (4.3) can be rewritten to yield equation (4.1), demonstrating that for this special case the equations give identical results. However, in the more general case where the speed of sound in one of the media becomes complex, r_1 or r_2 and k becomes complex and the denominator in equation (4.3) is not of the form $z = x + iy$. In that case equation (4.1) and 31 will not lead to identical results and equation (4.3), which is based on the more general case, is the appropriate expression. Since some of the models for bubble-water mixtures predict a complex valued speed of sound, the expression for the power transmission coefficient that is used in this report is that for the more general case provided in equation (4.3).
In the ideal case of one-dimensional plane sound waves, the insertion loss (IL, symbol ΔL) is related to the power transmission coefficient as

$$\Delta L = -10\log_{10}(|\alpha_t|)\ \mathrm{dB} \tag{4.4}$$

4.2 Homogenous layer of water using Wood's equation

Figure 4.2 provides examples of the calculated insertion loss as a function of void fraction and frequency. At lower frequencies, the insertion loss is reduced when the layer thickness is much smaller than the acoustic wavelength in the layer ($kL \ll 1$) and when the layer thickness is close to multiples of a half wavelength in the layer ($kL = \pi, 2\pi, 3\pi, \ldots$).

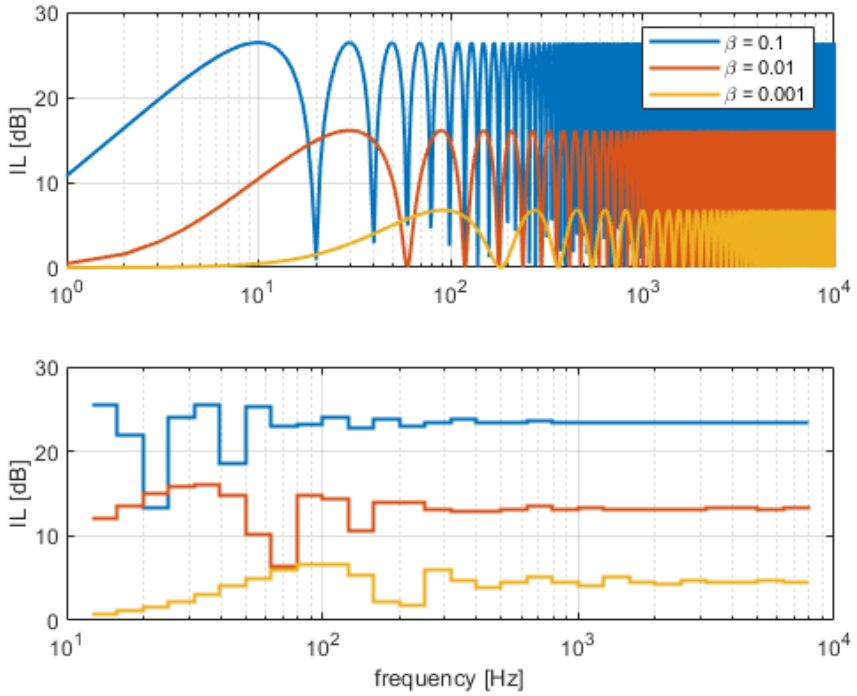

Figure 4.2: One-dimensional plane wave insertion loss of a 1 m thick layer of a homogeneous and isothermal mixture of water and air bubbles, without absorption, as a function of frequency for three values of the void fraction β. Both 1Hz band spectrum (upper) and decidecade band spectrum (lower) are plotted. The material parameters for water and air used are:
$\rho_w = 1000\ \mathrm{kg/m^3}$, $c_w = 1500\ \mathrm{m/s}$, $\rho_a = 1.2\ \mathrm{kg/m^3}$, $c_w = 344\ \mathrm{m/s}$, $\gamma = 1.4$.

Acoustic absorption in the mixture can be incorporated by adding an imaginary part to the sound speed

$$c_{\mathrm{eff}} = \frac{c_{\mathrm{r,eff}}}{(1+\mathrm{i}\alpha_{\mathrm{p}})} \tag{4.5}$$

where $c_{r,\mathrm{reff}}$ is the effective sound speed in absence of absorption, c_{eff} is the complex sound speed including damping, and α_p is the frequency independent damping coefficient expressed in dB/λ.
Hence, waves travelling in the mixture in positive direction propagate and decay as

$$\left|\mathrm{e}^{-\mathrm{i}k_{\mathrm{eff}}x}\right| = \left|\mathrm{e}^{-\mathrm{i}\frac{\omega}{c_{\mathrm{eff}}}x}\right| = \left|\mathrm{e}^{-i\frac{\omega}{c_{\mathrm{r,eff}}}x}\right| e^{-\frac{\omega\alpha_p}{c_{\mathrm{r,eff}}}x} \tag{4.6}$$

This will reduce the insertion loss at multiples of a half wavelength in the layer and it will significantly increase the insertion loss at higher frequencies, where the thickness of the layer supports multiple acoustic wavelengths, as illustrated in Figure 4.3 for a hypothetical damping coefficient $\alpha_p = 3$ dB/λ.

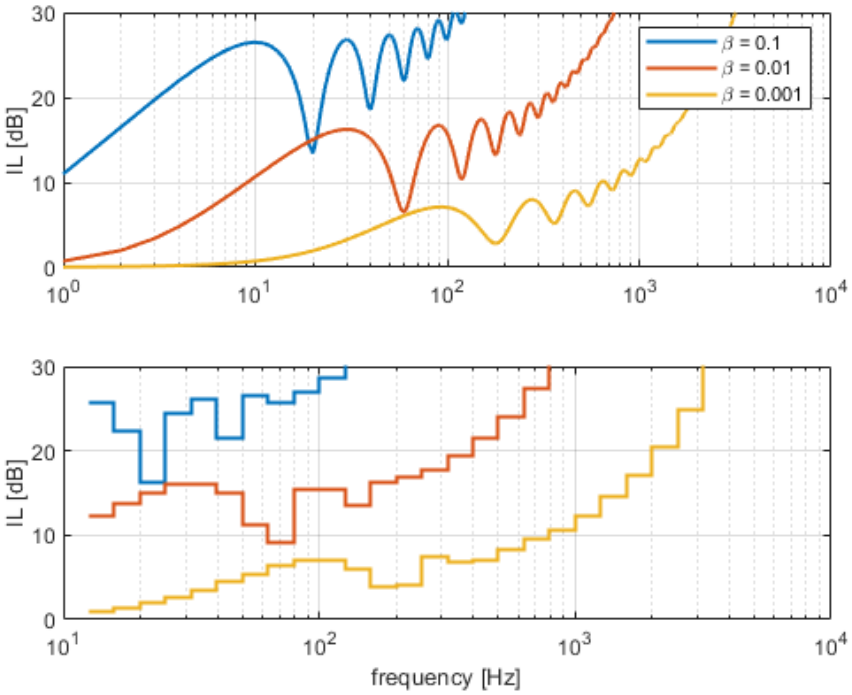

Figure 4.3: One-dimensional plane wave insertion loss for a of a 1 m thick layer of a homogeneous and isothermal mixture of water and air bubbles (at 10°C and depth less than 100 m), with hypothetical damping coefficient $\alpha_p = 3$ dB/λ, as a function of frequency for three values of the void fraction β. Both 1Hz band spectrum (upper) and decidecade band spectrum (lower) are plotted. The material parameters for water and air used are: $\rho_w = 1000\ \mathrm{kg/m^3}$, $c_w = 1500\ \mathrm{m/s}$, $\rho_a = 1.2\ \mathrm{kg/m^3}$, $c_w = 344\ \mathrm{m/s}$, $\gamma = 1.4$.

4.3 Homogeneous layer of water with resonant bubbles of equal bubble radius

The effect of damping due to the vibration of air bubbles in a fluid air mixture are demonstrated in the next two sections. The current section deals with bubble configurations having bubbles of identical radius. The effects of a configuration of bubbles with a bubble size distribution is explored in Section 4.4.
For the present example, air bubbles in seawater at 10°C are considered. The relevant properties are summarized in Table 4.1

Table 4.1: Material properties for air bubbles in seawater at 10°C.

property	symbol	value
Temperature	T	10°C = 283.15 K
Equilibrium pressure	P	1 atm = 101325 Pa
Sea water density	ρ_w	1027 kg/m^3
Sea water sound speed	c_w	1490 m/s
Sea water dynamic viscosity	μ_w	1.3076×10^{-3} Ns/m^2
Sea water surface tension	σ	74.2×10^{-3} N/m
Air density	ρ_g	1.25 kg/m^3
Air sound speed	c_g	337 m/s
Air dynamic viscosity	μ_g	18.03×10^{-6} Ns/m^2
Air ration of specific heats	γ	1.4
Air thermal conductivity	K_T	25.72×10^{-3} W/m/K

Note that the effect of the surface tension of the bubbles (defined as $2\sigma/a$) on the undisturbed pressure in the bubble p_0 is small (i.e. less than 1% for bubble radii larger than 0.15 mm for these conditions).

To illustrate the effect of damping due to the vibration of air bubbles in a fluid-air mixture, results for an example are presented here using the model of Commander and Prosperetti (see Section 3.2.2) and the model of Kargl (see Section 3.2.3).
A homogeneous distribution of equal bubbles with radius a is considered. The volume of a single bubble equals $V_a = \frac{4}{3}\pi a^3$, and using the void fraction β, the number of bubbles per cubic meter is defined as $n_a = \beta/V_a$. The approximate resonance frequency of individual bubbles is given by the so-called Minneart [17] frequency:

$$f_a = \frac{1}{2\pi a}\sqrt{3\gamma P/\rho_w}. \tag{4.7}$$

For a = {0.01,0.1,1} mm, the approximate resonance frequency equals f_a = {324,32.4,3.24} kHz respectively.

Figure 4.4 shows the relative contribution of the three loss mechanisms in the model of Commander and Prosperetti and Kargl for different bubble sizes and void fractions, as a function of frequency. The loss factor decreases with increasing void fraction and with decreasing bubble radius. Viscous losses are only relevant for very small bubbles (a<<0.01 mm), otherwise thermal losses dominate below the bubble resonance frequency and acoustic radiation losses dominate at and far above the resonance frequency.

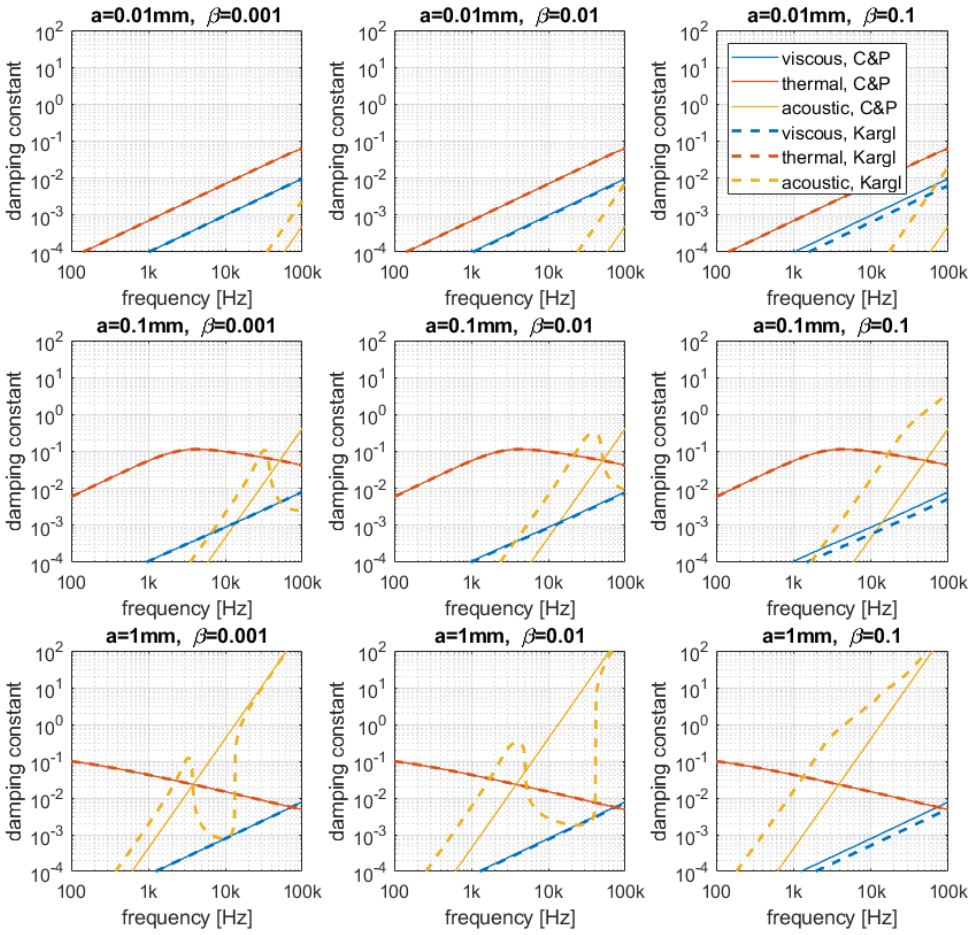

Figure 4.4: The three bubble oscillation loss contributions (viscous in blue, thermal in red and acoustic radiation in yellow) for different void fractions β of uniform distributions of equal bubble radii a, expressed as dimensionless loss factor $\delta_m = b_m/\omega_{0m}^2$ (see Appendix C). The solid lines are obtained using the model by Commander and Prosperetti (see Section 3.2.2); The dashed lines are obtained using the model by Kargl using 25 iterations (see Section 3.2.3).

Figure 4.5 shows the calculated effective sound speed in the mixture of water and single size gas bubbles, for the same void fractions and bubble radii. This illustrates that the approximation provided by Wood's equation (see Section 1), is quite accurate at predicting the equivalent sound speed below the bubble resonance frequency, e.g. at frequencies up to 10 kHz for bubble radii smaller than 0.1 mm. It can be observed that a small but significant damping component is already present below the resonant frequency, e.g. above frequencies above ca. 1 k Hz for bubble radii of 0.1 mm.

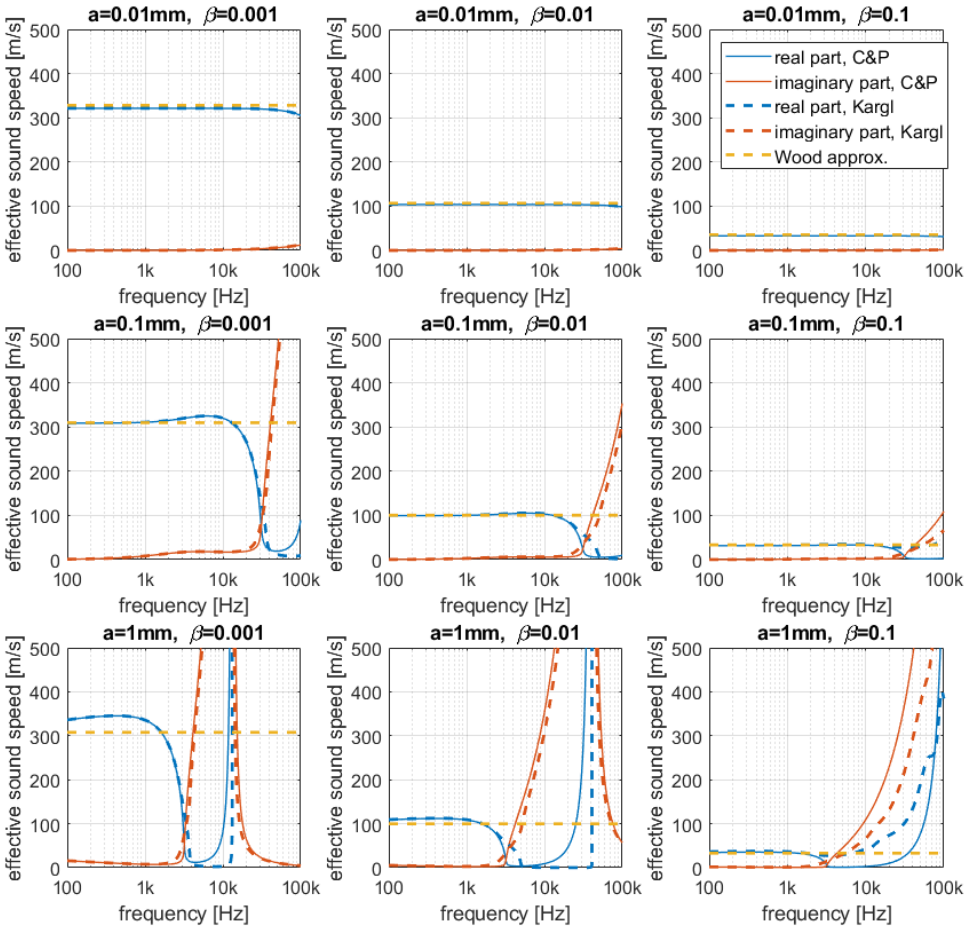

Figure 4.5: The real and imaginary parts of the effective sound speed $c_{\text{eff}} = \omega/k_{\text{eff}}$ for different void fractions β of uniform distributions of equal bubble radii $\overline{a}$. The solid blue and read lines are obtained using the model by Commander and Prosperetti (see Section 3.2.2); The dashed blue and red lines are obtained using the model by Kargl using 25 iterations (see Section 3.2.3). The yellow dashed line obtained using the model by Wood (see Section 3.2.1).

Figure 4.6 shows the calculated one-dimensional plane wave insertion loss (eq.4.4) of a 10 cm thick uniform distribution of equal bubbles, for the same void fractions and bubble radii. Besides the insertion loss as predicted by the model of Commander and Prosperity, the insertion loss as predicted by the model of Wood is also shown.
At frequencies well below the resonance frequency, the insertion loss is independent of the bubble radius and increases proportionally with $\mathbf{10}\log_{10}\beta$, as described in §4. In this regime the model of Wood predicts results very similar the results by the model of Commander and Prosperity and model of Kargl. For higher frequencies on the other hand the insertion loss predicted by the model of Commander and Prosperity and model of Kargl is very large around the bubble resonance frequency and above. For frequencies approaching the resonance frequency, the insertion loss predicted by these models already rises to significant higher values compared the model of Wood which more or less stabilizes to a constant IL for higher frequencies (in decidecade bands).
Note that the predicted amount of damping for a given bubble curtain will depend on the thickness of the curtain and the amount of damping per wavelength in the effective medium, but also on the sound speed of the effective medium. A higher void fraction will therefore not only lead to more damping by causing a higher damping per wavelength, but

also because the sound speed is in general lower for higher void fractions. This causes waves to travel more wavelengths in the curtain which leads to more damping. The dependence of the perceived onset and rate of increase of (the effect of) damping on the void fraction can also be seen in the various plots in Figure 4.6.

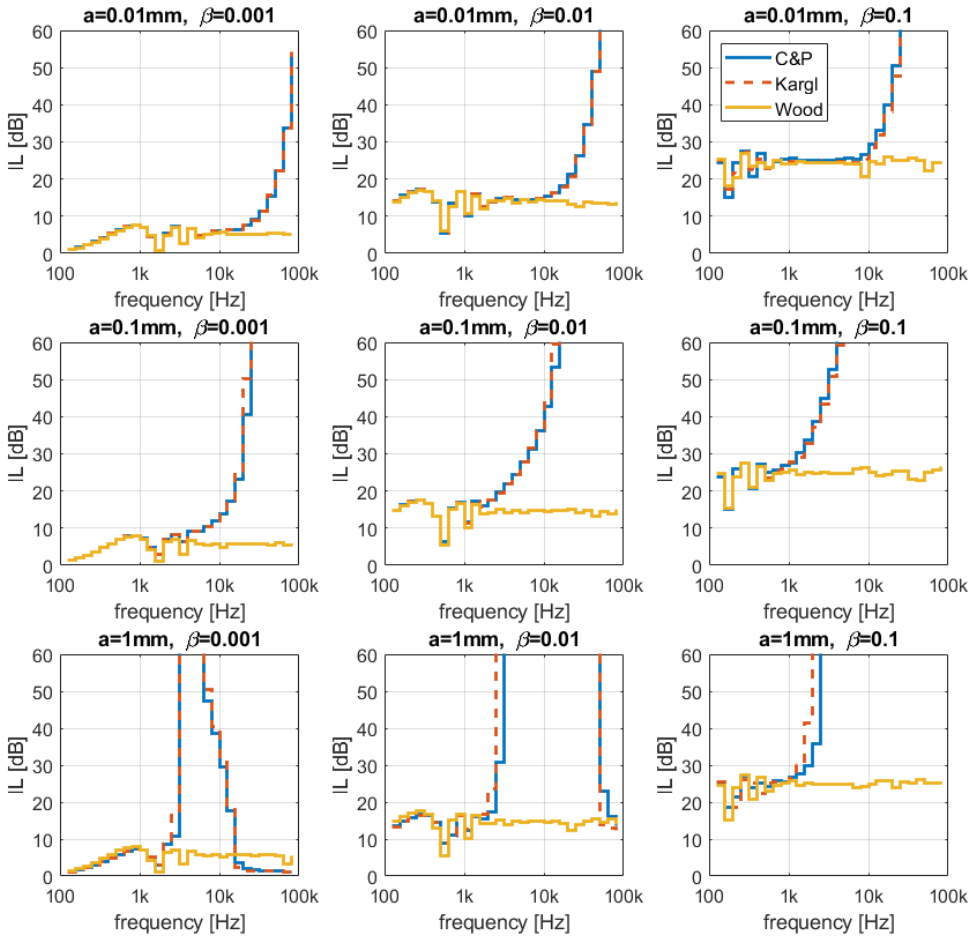

Figure 4.6: Decidecade spectra of the one-dimensional plane wave insertion loss of a 0.1 m thick bubble layer with a uniform distribution of equal bubbles, for different radius a and void fraction β. The blue line is obtained using the model by Commander and Prosperetti (see Section 3.2.2); The red line is obtained using the model by Kargl using 25 iterations (see Section 3.2.3). The yellow line is obtained using the model by Wood (see Section 3.2.1)

Note that the solutions for the Wood model differ slightly for the solutions with different bubble radii but identical void fraction. The difference in insertion loss is due to a slight difference in the isothermal speed of sound in the gas which is dependent on the pressure in the bubble which varies slightly with bubble radius due to the effect of surface tension.

4.4 Homogeneous layer of water with resonant bubbles and a bubble size distribution

In many cases involving a bubble water mixture the size of individual bubbles is not identical, and the bubble sizes encountered can be described statistically using a bubble size distribution. As suggested by Bohne et al. [18] (and reasonable well confirmed by experimental data from WP4) the bubble size distribution at a given position in a bubble curtain can be approximated by a log-normal distribution

$$f\left(a, \mu_{\ln(a)}, \sigma_{\ln(a)}\right) = \frac{1}{a\sigma_{\ln(a)}\sqrt{2\pi}} e^{-\left(\ln(a)-\mu_{\ln(a)}\right)^2/2\sigma^2_{\ln(a)}} \tag{4.8}$$

with $\mu_{\ln(a)}$ the mean of the logarithmic values of the bubble radius and $\sigma_{\ln(a)}$ the standard deviation. The associated probability density function (PDF) which by definition equals unity when integrated over all bubble sizes can thus obtained using

$$\mathrm{PDF}(a) = \frac{f(a)}{\int_0^\infty f(a)da} \tag{4.9}$$

Any probability density distribution for bubble size can be related to $n(a)$, which defines the distribution of the number of bubbles in the various models, by defining

$$n(a) = \mathrm{PDF}(a)N \tag{4.10}$$

Using equation (3.15) the following expression for N can be obtained it terms of the void fraction B and the probability density function

$$N = \frac{\beta}{\frac{4}{3}\pi \int_0^\infty a^3 \mathrm{PDF}(a)\mathrm{d}a} \tag{4.11}$$

Bohne et al. suggest using the values $\mu_{\ln(a)} = -6.70$ and $\sigma_{\ln(a)} = 0.67$ in the log-normal distribution which is based on fitting the parameters to measurement data for different flow rates and bubble screen configurations.

Results of the bubble size distribution measurements performed by MARIN in the Concept Basin (WP4) have been converted to probability density functions. These are plotted in Figure 4.7 for different depths together with a number of log-normal bubble size distribution. The solid lines (with the exclusion of the black line) correspond to measuring the bubble size distribution at different depths. The black solid curve corresponds to parameters for the log-normal distribution that were found by fitting the curve to measurement data as presented by Bohne [18]. The blue dashed curve corresponds to a fit of the log-normal distribution to the measurement data for the porous and nozzle configuration. The red dashed curve corresponds to a fit of the peak value of the log-normal distribution to that of the measurement data for the conventional configuration. The green dashed curve corresponds to a fit of the down slope of the log-normal distribution to that of the measurement results for the conventional configuration. The measurements are obtained in a freshwater environment at ambient temperature. The material properties used for all predictions that are compared against measurement in the MARIN Concept Basin are done assuming these material properties.

Table 4.2: Material properties for air bubbles in fresh water at 21°C.

property	symbol	Value
Temperature	T	21.15°C = 294.3 K
Equilibrium pressure	P	1 atm = 108.8 kPa
Freshwater density	ρ_w	998.201 kg/m^3
Freshwater sound speed	c_w	1481 m/s
Freshwater dynamic viscosity	μ_w	1.002×10^{-3} Ns/m^2
Freshwater surface tension	σ	72.75×10^{-3} N/m
Air density	ρ_g	1.25 kg/m^3
Air sound speed	c_g	343.9 m/s
Air dynamic viscosity	μ_g	18.18×10^{-6} Ns/m^2
Air ration of specific heats	γ	1.4
Air thermal conductivity	K_T	26.2×10^{-3} W/m/K

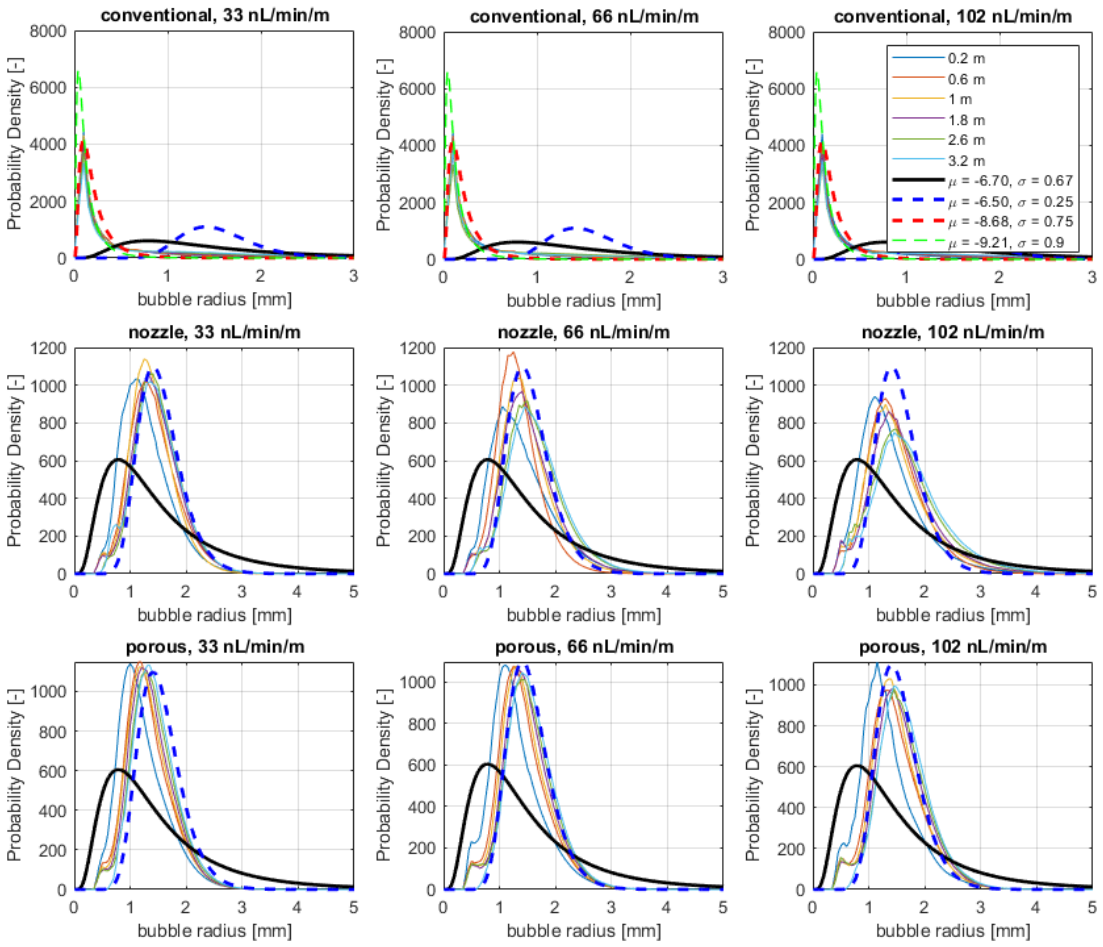

Figure 4.7: Probability Density Function for the bubble size based on measurements by MARIN at different depths in the Concept Basin and using a log-normal bubble size distribution as described in [18] for different parameter values. The black solid curve corresponds to values found by fitting measurement data by Bohne [18], the blue dashed curve corresponds to a fit of the log-normal distribution to the measurement data for the porous and nozzle configuration. The red dashed curve corresponds to a fit off the peak value to the conventional configuration data measured by MARIN. The green dashed curve corresponds to a fit of the down slope to the conventional configuration data measured by MARIN.

It can be observed that both the peak value and shape of the measurement data can be captured reasonably well with the log-normal model for the porous and nozzle configuration (using the same parameter values), while a single curve of the log-normal model cannot capture both the peak value and shape of the measured data for the conventional configuration. Note that the actual peak of the PDF could not be measured by the MARIN setup for the conventional configuration. The maximum value was observed at the minimum bubble radius that could be measured (0.25 mm) and the data was extrapolated by MARIN to smaller radii (a peak value at 0.1 mm was assumed).

Figure 4.8 shows the wave speed and attenuation in an air-water mixture as predicted by the models of Wood, Commander and Prosperetti, Kargl and Feuillade for a log-normal distribution with $\mu_{\ln(a)} = -6.5$ and $\sigma_{\ln(a)} = 0.25$ and void fraction $\beta = 0.1$.
Below 1 kHz, the attenuation in the bubbly medium predicted by the resonant bubble models is small and the main effect is the substantial reduction of the sound speed (phase velocity) due to the compressibility of the bubbles. At frequencies above about 1 kHz, the attenuation in the bubbly medium increases sharply. An indication of the most dominant

resonance frequency for the considered distribution may be obtained by calculating the Minnaert frequency for the median and mode of the bubble radius distribution ($a = 1.5$ mm and $a = 1.41$ mm, respectively). These radii correspond with a Minnaert frequency $f_0 \approx 2.27$ kHz and $f_0 \approx 2.42$ kHz, respectively. These frequencies indeed coincide with frequency regions where the attenuation has a maximum. Note that although the models seem to converge to the same values for attenuation and phase speed in the low and high frequency limit there are significant differences in both shape and absolute values of the curves for the three models that include the effects of resonances. Both the model of Kargl and Feuillade share similarities with the model of Commander and Prosperetti but include the effect of higher order interactions between bubbles. For low void fraction values the results for Kargl and Feuillade converge to the results for Commander and Prosperetti. What is striking is that even though they contain a correction for the same physical phenomena (higher order scattering) compared to the results for the model of Commander and Prosperetti, the models of Kargl and Feuillade seem to push the results in opposite directions for many features of the curves. The maximum phase speed for instance is higher and found at higher frequencies for the model of Kargl, while the maximum is lower and found at lower frequencies for the model of Feuillade. Similar statements can be made for the attenuation coefficient.

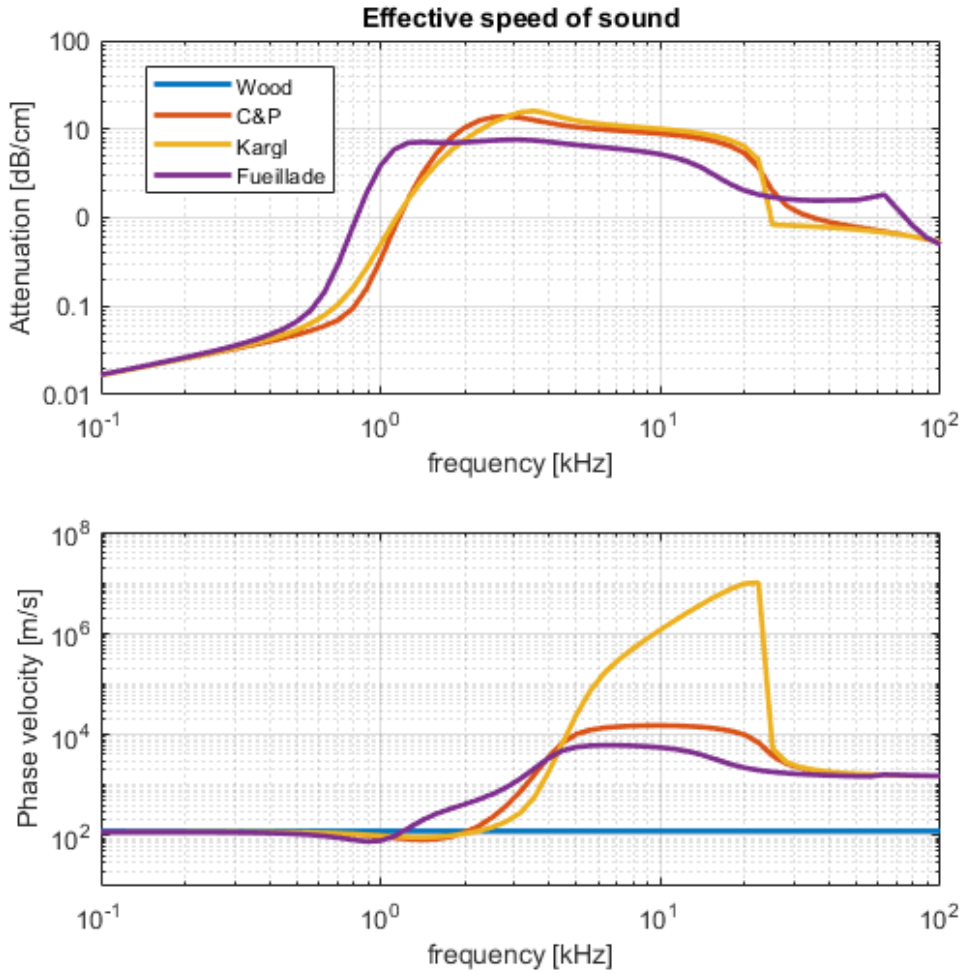

Figure 4.8: Effective wave propagation predicted by the models of Wood, Commander and Prosperetti, Kargl and Feuillade in an air-water mixture (Table 4.1), for a log-normal distribution with $\mu_{\ln(a)} = -6.5$ and $\sigma_{\ln(a)} = 0.25$ and void fraction $\beta = 0.01$.

The insertion loss of a 10 cm thick bubble curtain is shown in Figure 4.9 for a water bubble mixture with the same bubble size distribution and void fraction that are used to produce the results in Figure 4.8. Below 1 kHz all models predict an insertion loss of about 15 dB. While the predictions of the Wood model remain at that level, above 1 kHz the insertion loss rises sharply for the models including bubble resonance. The model of Feuillade rises to values around 80 dB, while the maximum values observed for the model of Commander and Prosperetti and Kargl reach peak values of ca.140 dB and 160 dB, respectively. Note that the onset of the sharp rise in IL occurs at much lower frequencies for the model of Feuillade, while the rate of the rise is slower for the model of Kargl.

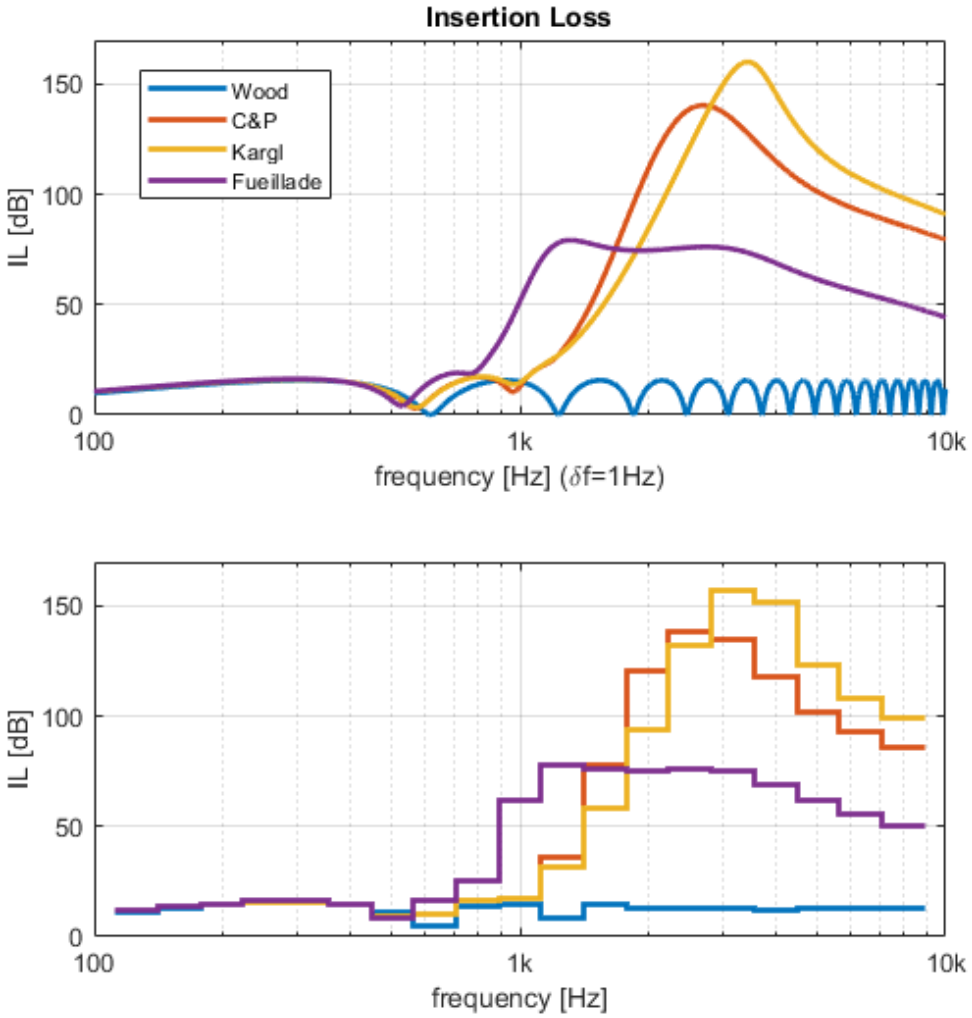

Figure 4.9: One-dimensional plane wave insertion loss of a 10 cm thick bubble layer for a log-normal distribution with $\mu_{\ln(a)} = -6.5$ and $\sigma_{\ln(a)} = 0.25$ and void fraction $\beta = 0.01$.

4.5 Range dependent void fraction

For all considered examples up to this point the bubble curtain is modelled as a bubble cloud with homogenous void fraction. This implies there is a clear transition from pure (bubble free) water to a bubbly liquid with a void fraction. In practice such a sharp demarcation between pure and bubbly water is not observed for bubble curtains. Instead the void fraction data provided by MARIN shows that the void fraction slowly grows from zero to a maximum around the middle of bubble curtain and gradually falls back to zero on the other side

forming a roughly symmetric profile. The void fraction as a function of range can be described reasonably well using a gaussian distribution

$$\beta(r) = N \frac{1}{\sigma_r \sqrt{2\pi}} e^{-\frac{1}{2}\left(\frac{r-\mu_r}{\sigma_r}\right)^2} \tag{4.12}$$

with μ_r the mean of the distribution/center of the bubble curtain and σ_r the standard deviation and N a scaling factor (so $\max(\beta(r)) = N/(\sigma_r\sqrt{2\pi})$. Void fraction values as a function of range as measured by MARIN for the concept basin are shown in Figure 4.10. A description of the associated measurement setup is given in Section 6. The figure also includes a fit of a gaussian distribution to one of the measured curves (z = 0.2m) suggesting a gaussian distribution is an appropriate approximation.

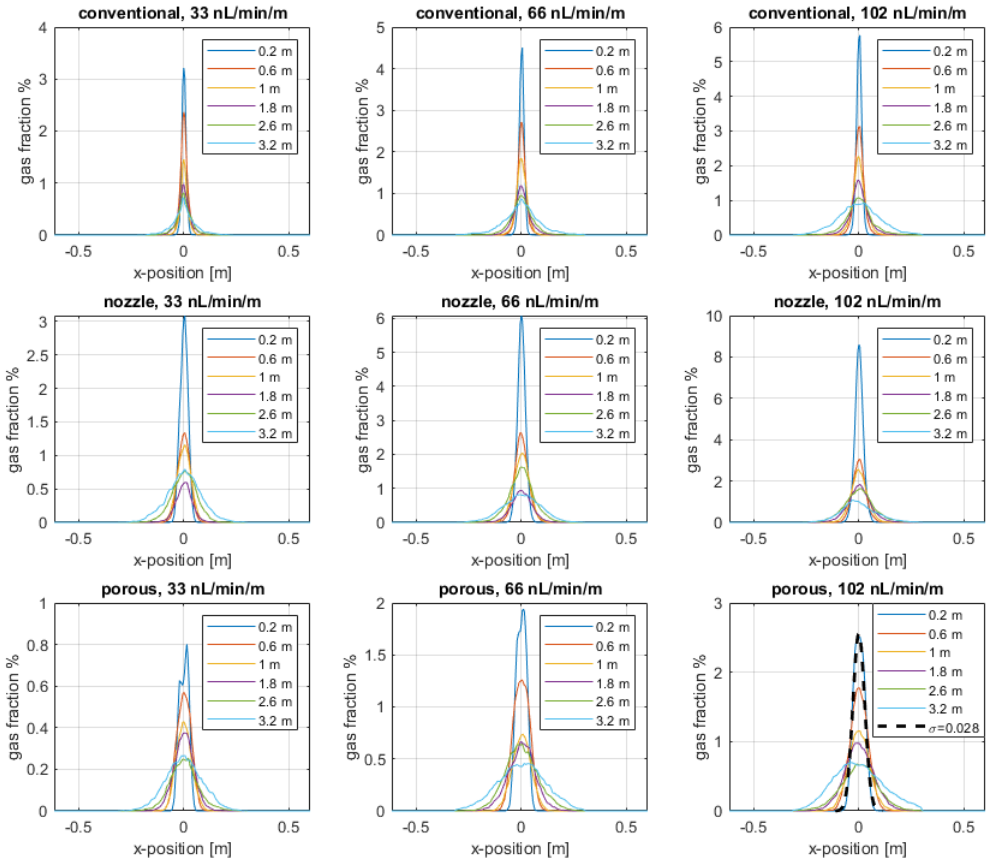

Figure 4.10: Void fraction as a function of range based on measurements by MARIN at different depths in the Concept Basin (see Section 6 for a description of the setup). The dashed black curve shows the results of a fit of gaussian distribution to one of the measured curves.

4.5.1 Effect of using a range dependent void fraction using gaussian distributions

To demonstrate the influence of using a range dependent void fraction instead of assuming a homogenous medium the insertion loss was calculated using the model of Wood for a number of scenarios. The case of a bubble curtain with homogenous properties used in the previous section (having a thickness of 0.1 mm and void fraction of $\beta = 0.01$ was) is used as a base line. Gaussian curves with various values of σ_r are discretized by approximating the

curve with sections of constant void fraction. The insertion loss for this system of coupled 1D layers is evaluated using the transfer matrix method [19]. Care is taken to use enough sections of constant void fraction such that further refinement does not change the resulting curves in a meaningful way for the frequency range of interest. In similar fashion, the curves are truncated at a range where extending the included range does not change the resulting curves in a meaningful way. The discretized curves are scaled such that the total area under each curve equals that of the curve for the case where the bubble curtain is approximated with a constant void fraction. In other words, the same amount of air is present in each bubble curtain, but it is distributed differently. The discretized curves that are considered are plotted in Figure 4.11.

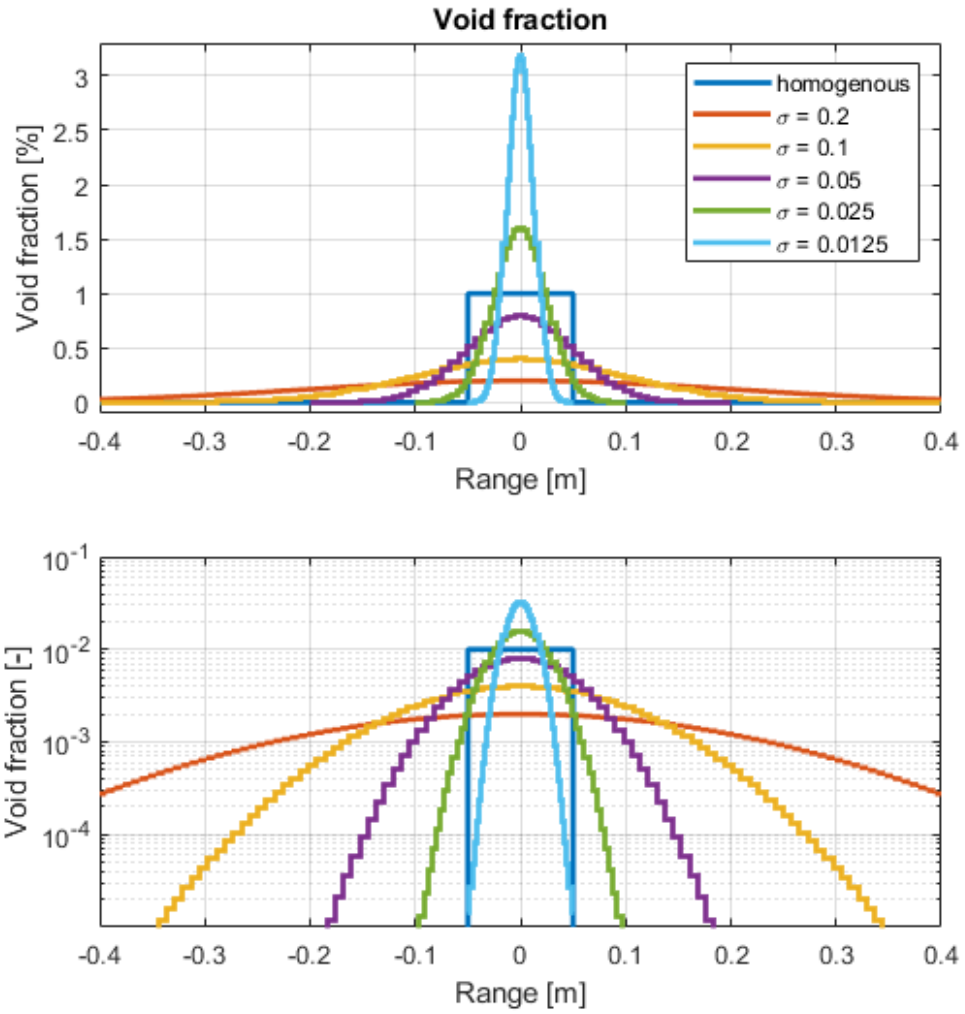

Figure 4.11: Void fraction as a function of range based on a gaussian distribution for various values of σ_r. The curves are discretized using sections of constant void fraction and are scaled such that the total area under each curve equals that of the curve where the void fraction is $\beta = 0.01$ over a continuous range of 0.1 m and zero elsewhere.

The insertion loss corresponding to these void fraction distributions with range as predicted by the model of Wood are shown in Figure 4.12.

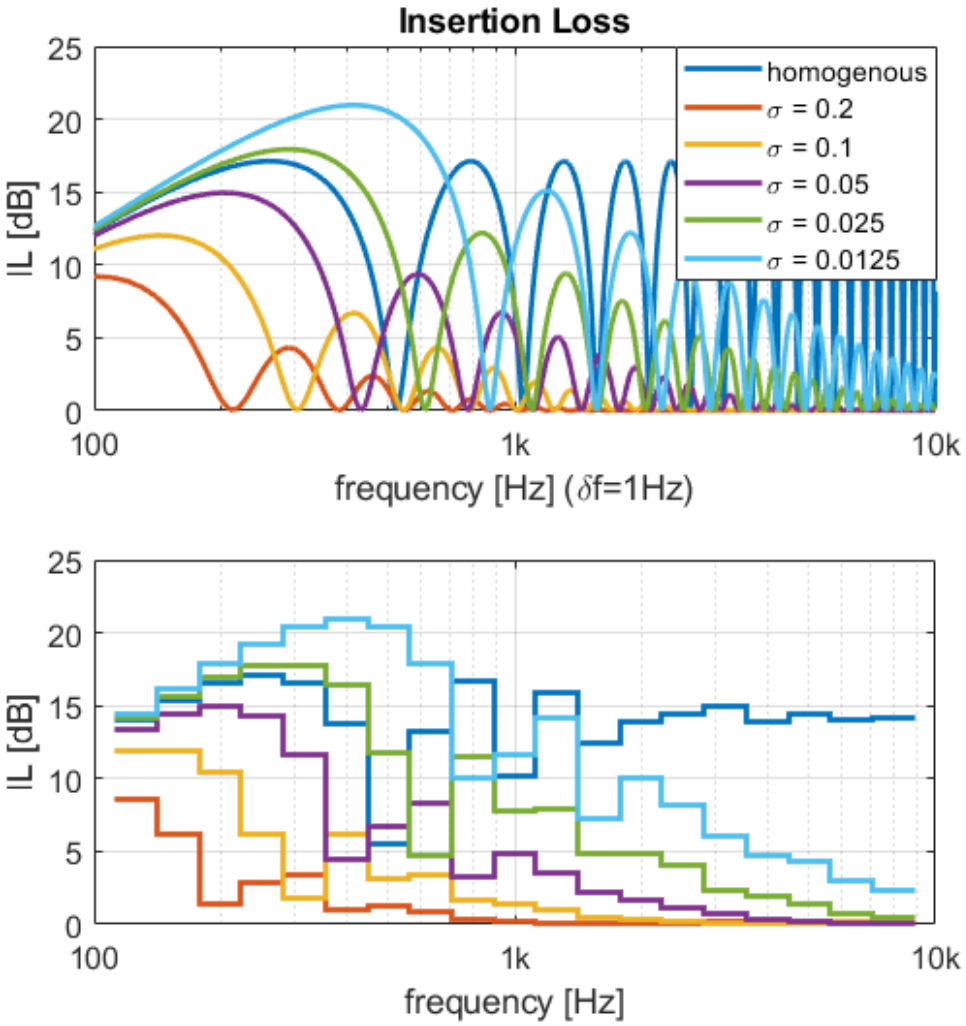

Figure 4.12: Insertion loss for bubble curtains having the same total amount of air but with different distributions. The associated plots for void fraction as a function of range for each curve is shown in Figure 4.11.

It is observed that only for the case where the void fraction is constant with range will the insertion loss in decidecades converge to a stable value in the high frequency limit. For all other considered distributions (with the same amount of air) the insertion loss ultimately decreases with frequency. This can be understood by considering that the model of Wood does not include damping and the only cause for transmission loss is by reflection. If the void fraction increases gradually, the equivalent sound speed will also increase gradually. If the rate of change in sound speed is small on the scale of a wavelength, the impedance mismatch is small at each location in the bubble curtain, and the amount of reflected energy will also be small, i.e. most sound will be transmitted. For any void fraction curve that is smooth this regime will be entered above a certain frequency. On the other hand, if the rate of change in sound speed is large on the scale of a wavelength, the impedance mismatch is large and most of the sound will be reflected (depending on the thickness compared to the wavelength). For all ‘compact’ void fraction curves (i.e. having non-zero values over a finite range) the rate of change will become large compared to the

wavelength below a certain frequency. In that regime the shape of the curve no longer matters, only the overall amount of encountered air influences the insertion loss. This is observed in in Figure 4.12 as all curves (all resulting in the same overall amount of air) converge toward one another in the low frequency limit.

4.5.2 Time averaged vs. instantaneous range dependent void fraction

The convergence of insertion loss at low frequency to a single curve irrespective of the precise distribution of air is also demonstrated by investigating the effect of modifying the distribution by making 'gaps' in the gaussian distribution. The modified curves considered here are intendent to resemble the instantaneous void fraction that may be encountered across the bubble screen at particular points in time. This in contrast to the void fraction curves in Figure 4.10, which are all time averaged values. An example of the raw void fraction data across the bubble screen width as a function of time is given in Figure 4.13. The position of the bubble screen is seen to modulate in width direction as time progresses. This data is 'straightened' so the void fraction profiles line up and the screen does not modulate in time. After this operation the time average of the void fraction profiles is taken over an extended time, yielding a curve such as shown in Figure 4.10.

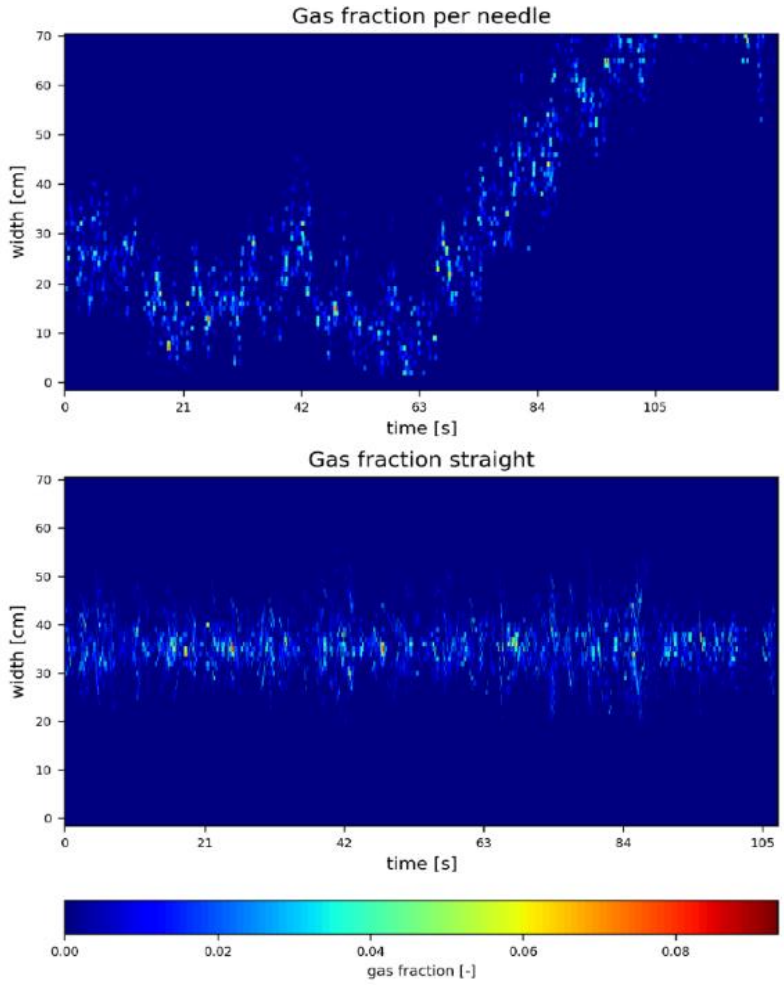

Figure 4.13: An example of raw measurement data for the void fraction across the width of the bubble screen in the concept basin as measured by MARIN.

To demonstrate the effect of averaging instantaneous void fraction curves, a representation of the instantaneous curves is needed. An abstract (non-exact) way of creating curves that together result in a time averaged curve that resembles a gaussian distribution and individually are representative of the instantaneous curves is by modifying a the distribution by making 'gaps' in the gaussian distribution. The curves labelled 'gaps A' and 'gaps B' in Figure 4.14 are examples of curves that are modified in the following way. The width of the curves (which are set at 0.1 m) is divided in ten sections of random width (with a minimum of 5 mm). For each section a Hann window is defined, and this window is multiplied with the values of the gaussian for that section. After a window is applied to all sections, the new curves with 'gaps' are scaled such that the total area under each curve is identical to the area of the unaugment gaussian. If these modified curves are averaged the resulting curve converges to the original gaussian distribution as more modified curves are used when averaging. An example of the resulting average void fraction curves for a set of 100 and 1000 modified curves with gaps are also plotted in Figure 4.14.

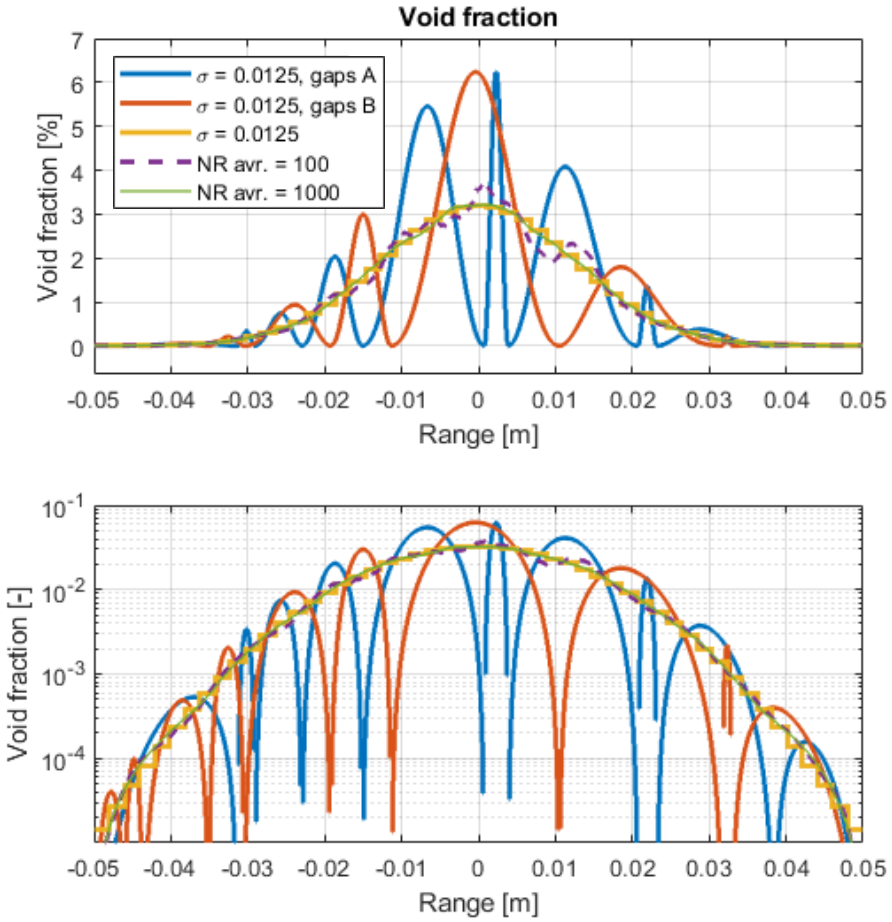

Figure 4.14: Gaussian distribution for the void fraction with $\sigma = 0.0125$ and modified curves with 'gaps' intended to resemble the instantaneous void fraction across a bubble curtain (an example of the measured instantaneous void fraction over the width of a bubble curtain is shown in Figure 4.13). The average taken over 100 and 1000 modified curves are also shown. It can be seen that the average curve converges to the original gaussian distribution as the number of modified curves that are averaged increases. The upper plot shows the data on a linear scale (in %) while the lower plot shows the same data on a logarithmic scale.

The insertion loss corresponding to the different curves for void fraction plotted in Figure 4.14 are shown in Figure 4.15. The insertion loss for the curves averaged over 100 and 1000 modified curves are not obtained by considering the averaged void fraction. Instead, the propagation loss (the change in pressure due to traveling across the curtain) is calculated for each modified curve which represent instantaneous states of the bubble curtain. The insertion loss is then calculated using the average (absolute) propagation loss. The reason for taking this approach is that at each port in time the sound waves interact with a different bubble screen configuration having a different effect on the amplitude of sound wave traversing the curtain. Secondly, in a system with a range dependent void fraction the relation between void fraction and insertion loss is complex and non-linear and taking the 'average of the insertion loss' of many void fraction curves is not necessarily identical to taking the insertion loss of the average acoustic transfer for the same set of void fraction curves. This distinction is illustrated by Figure 4.15. Depending on frequency, the insertion loss for the original gaussian distribution describing the void fraction is very different from the insertion loss based on the average propagation loss for many modified curves.

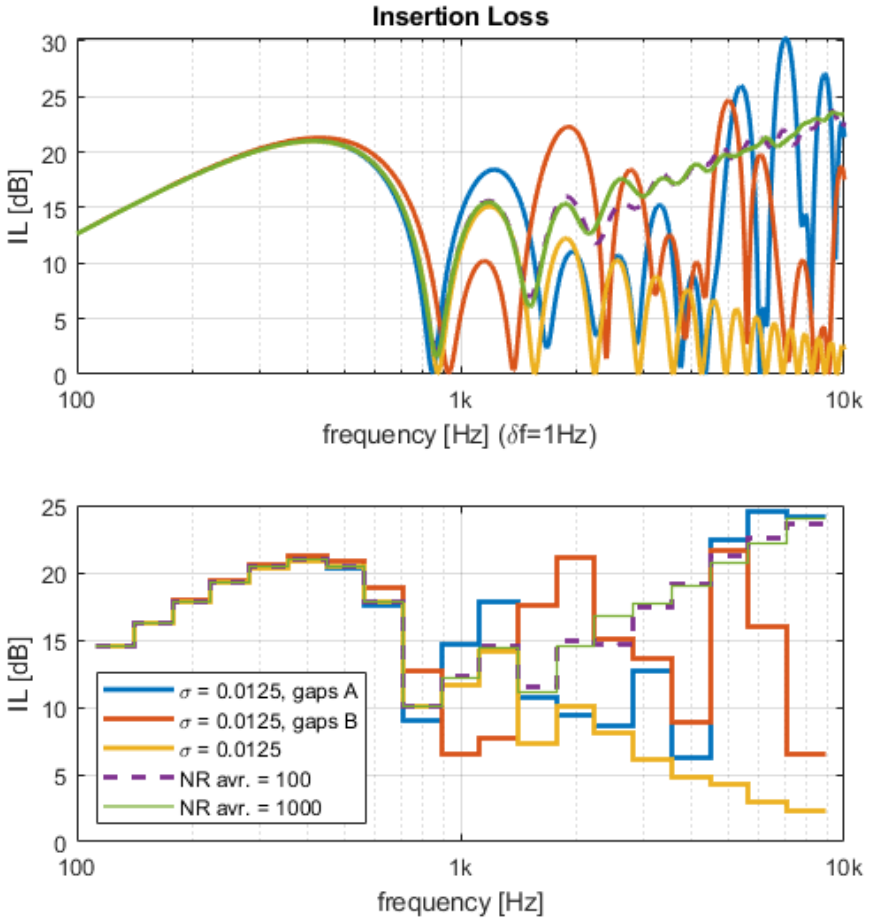

Figure 4.15: Insertion loss for the various void fraction curves shown in Figure 4.14. The insertion loss for the curves averaged over 100 and 1000 modified curves are not obtained by considering the averaged void fraction. Instead the value of the propagation loss (the change in pressure due to traveling across the curtain) is calculated for each modified void fraction curve and the insertion loss is calculated for the average propagation loss.

For low frequencies all curves have nearly identical insertion loss values. This illustrates again that if changes in void fraction happen on a scale much lower than the wavelength, the exact shape of the void fraction curve does not matter (only the area under the curve). On the other hand, above ca. 700 Hz the differences between the curves grow rapidly. Moreover, the trend of the insertion loss for the average void fraction (i.e. the unaugment gaussian distribution) is a reduction in insertion loss with frequency, while the curve based on the averaged propagation loss shows an increase of insertion loss with frequency.
Even though this simplified model includes many assumptions (e.g. the model is 1D, damping is not included, the modified curves with 'gaps' are only an abstract representation of the actual instantaneous void fraction curves) this is a strong signal that using the time averaged properties as input to acoustic models will not necessarily lead to correct predictions of time averaged acoustic properties. Moreover, the expectation is that using an averaged void fraction as input will lead to good predictions only for frequencies for which the instantaneous void fraction as a function of the spatial coordinates contains no structures on the scale of the wave length that are markedly different than what is observed for the average void fraction.
It is likely that similar behavior can be observed for bubble size distribution if it varies significantly with spatial coordinates. Based on the time averaged data the rate of change with depth seems to be small. It was not attempted to determine if the instantaneous bubble size distribution varies significantly with time/spatial coordinates. Note that the statistical concept of bubble size distribution breaks down if only an instantaneous state of the bubbles is taken and the region for which it is evaluated is small (i.e. enough bubbles should be included in a considered volume for a statistic approach to make since). This suggest the spatial structures that can ever be observed for bubble size distribution cannot be too small.

4.6 Depth dependence

In the examples presented above the bubble curtain is approximated with an 1D model. The previous section investigated the influence of varying void fraction with range which fits the 1D modelling approach. However, the measurement data for the void fraction in Figure 4.10 shows that the void fraction also changes significantly with depth which cannot be captured using a 1D model without additional assumptions. (The measurement data in Figure 4.7 suggest that the bubble size distribution is somewhat dependent on depth but to a lesser extent.)
An approach to capture the effect of depth dependence using 1D modelling techniques as described in the sections above is presented by Bohne et al. [18]. They propose to divide the waveguide in which the bubble curtain is positioned in a number of individual vertical slices, calculate the insertion loss per slice and combine these results using a procedure borrowed from the field of building acoustics for non-homogenous partitions.
This approach is not used here since the required assumptions (the incident, transmitted and internal sound waves are assumed to be plane waves traveling in direction normal to the center plane of the bubble curtain) are too limiting to model the measurement setup at MARIN (which include a point source and a reflective environment implying many relevant sound paths will not meet the assumptions). Secondly, it is not evident which physical phenomena can be examined using this type of model compared to modelling approaches used in previous sections.

4.7 Summary

The previous sections contain a number of examples demonstrating the physical phenomena at play in the interaction of sound waves with bubble curtains.
In Section 4.2 the relation between void fraction and insertion loss was investigated and the frequency-dependent effect of damping was demonstrated using the simplest representation of a bubble curtain. The effect and sources of damping due to the vibration of air bubbles in a fluid air mixture are described in Section 4.3 for a bubble configuration with bubbles having the same bubble radius. Section 4.4 introduced the concept of a bubble size distribution and demonstrates the effect of including higher order bubble-bubble interactions. The effect of varying the void fraction throughout the width of a bubble curtain is explored in Section 4.5. A model to include the effect of depth and range dependent bubble curtain properties is discussed shortly in Section 4.6.

Note that the 1D modelling approaches used in the sections above are all limited by the assumptions required for their validity and are unable to fully capture the physical phenomena at play in a real live bubble curtain setup.
Moreover, certain assumption may lead to an oversimplified view on the acoustics of bubble curtains and care should be taken when drawing conclusions using these approaches. For instance, the assumption of a constant void fraction throughout a bubble curtain is somewhat unnatural and combined with a model without damping may produce counter intuitive results. For very low frequencies (where the model predicts a continuous upslope in the IL) a doubling of the thickness of the screen results in an increase in insertion loss of ca 10 dB, which is in line with the earlier established relation between void fraction and insertion loss (see Section 4.2). However, the constant value for the insertion loss in decidecade bands that the solution approaches in the high frequency limit does not depend on the thickness of the bubble curtain (and therefore on the total amount of air in the bubble curtain). This is illustrated in Figure 4.16. The red and yellow curves are close in value above ca. 2 kHz, and the blue and yellow solutions are close in value above ca. 4 kHz despite the fact that they represent air volumes that differ by a factor 2 and 4, respectively.

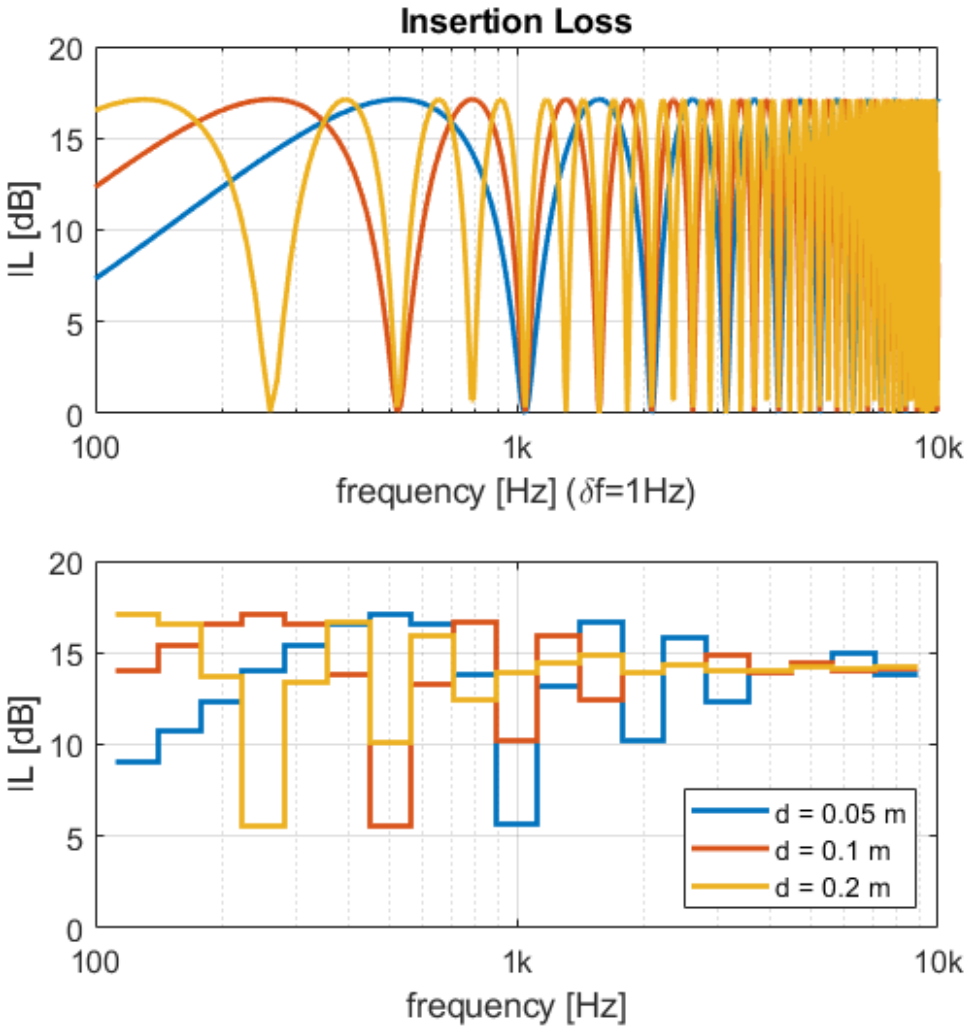

Figure 4.16: Insertion loss predicted by the model of Wood for bubble curtains of various thickness having a constant void fraction of $\beta = 0.01$.

Note that if damping due to bubble vibration is considered the effect of doubling the width of the bubble curtain is an increase in insertion loss which becomes more significant with increasing frequency. However, by introducing the effects of bubble vibrations, bubble resonance will also become relevant as frequencies rise, making the relation between frequency and insertion loss much more complex.
As mentioned above, the data in Figure 4.10 shows that the void fraction changes significantly with range and depth which cannot be captured properly using the 1D modelling. A 2D modelling approach which is used to predict the acoustic properties of the bubble curtains measured by MARIN is presented in the next chapter.

5 Two-dimensional models for a waveguide with a layer of water-bubble mixture

The 2D models used in this study are based on the Finite Element (FE) method. This FE method is known to work well for acoustic problems as long as a proper element mesh is used (see Section 5.4). The FE method is capable of describing arbitrary geometries. It can represent wave guides of infinite length using a perfectly matched layer (PML). Furthermore, the sound speed which varies continuously with position in the bubble curtain can be accounted for. In addition, FE models are capable of capturing arbitrary multi-layered, range dependent variations in a water waveguide and may include elastic behavior of the bottom which facilitates high fidelity modelling of bubble curtains in combination with impact pile driving. These features make the FE method an ideal choice for high fidelity modelling of bubble curtains.
In this section the implementation of the FE model and the decision process for certain design choices for the FE model are described.

5.1 Overview modeling approach

5.1.1 Calculated quantity

The most relevant quantity to validate is insertion loss in decidecade bands. Insertion loss is the de facto measure for performance of a bubble curtain, and a representation in decidecade bands allows to compare results without being side-tracked by details available in narrow band spectra (in general the narrow band curves for insertion loss show a lot of peaks and throughs at higher frequencies which are mostly averaged out in decidecade bands).

5.1.2 Frequency content

The FE method is widely applicable, but it can be computationally intensive. In particular, calculations for domains with many wave lengths are costly which implies that calculations at high frequencies are costly. Furthermore, doubling the frequency resolution of a calculation doubles the amount of calculation time. Since there is no desire to calculate the response of the bubble curtains in the time domain and the most relevant quantity to validate is insertion loss in decidecade bands it was decided to only calculate the solution at five sub-frequencies per decidecade band. The highest frequency for which a calculation is performed determines the mesh size required (see Section 5.4) which determines the

memory requirements and calculation time. It was chosen to calculate solutions up to the decidecade band with its center frequency at ca. 5 kHz.

5.1.3 Source

Use of insertion loss as a measure for performance makes having a representative excitation model less critical since only differences in sound levels are of importance for IL. The source used in the MARIN setup (see Chapter 6) can be considered an omnidirectional source by approximation. Since the details of source are not relevant the source is represented by a point source in the FE model.

5.1.4 Use of equivalent fluid models

It should be clear from the previous sections that acoustic modelling of individual bubbles for full size bubble curtains is not feasible. Instead, the influence of individual bubbles on the acoustics properties needs to be approximated. As described extensively in Sections 2.2 and 3.2 equivalent fluid models are an efficient way of representing the acoustic properties of bubbly liquids which can be used in combination with FE models. In this study the acoustic properties (speed of sound and density) are calculated prior to an FE calculation for many positions in the bubble curtain using equivalent models to populate a look up table. This look up table is used by the FE model to interpolate the appropriate equivalent fluid properties at the locations of the integration points when constructing the element stiffness and mass matrices. The speed of sound in the look up table is complex valued, and the appropriate damping of the equivalent fluid model is represented by the imaginary part of the associated complex valued wave number.

5.1.5 Extension for large ranges

FE models are capable of capturing arbitrary multi-layered, range dependent variations in the waveguide and may include elastic behavior of the bottom. These features allow modelling of bubble curtains in combination with offshore impact pile driving. Such models are however relatively computationally intensive and are limited to usage at relatively close ranges and low frequencies (depending on the case and hardware available, but in general less than ca. 1 km for frequencies up to ca. 1 kHz). If solutions are required at larger distances the solutions of FE models can for instance be used as input to normal mode models, which are very efficient and can be used up to any range[7].

5.1.6 Extension to three-dimensions

The main reason for pursuing a 2D modelling approach instead of using 3D models is the limitations posed by 3D FE models. The resources required for generating and solving the numerical systems associated with FE models grow rapidly if a third dimension is added. Assuming the same limitations on hardware and computation time apply as to 2D models only a fraction (the lower portion) of the frequency space can be evaluated.
Note that the 2D approach adopted allows correcting for 3D effects in the waveguide by considering a series of 2D calculations. This is described in more detail in the next section.

[7] These models will natively only allow range independent bathymetry (multiple sections having different properties can be linked though) and do not support elastic behavior of the bottom (requiring the use of an equivalent fluid).

5.1.7 FE software

The FE model is implemented in the commercially available software package COMSOL Multiphysics. This software suite contains all required features to easily setup, solve and post process data for acoustic problems in 2D (and 3D). The software allows the use of a lookup table to make material properties continuously dependent on spatial coordinates, includes perfectly matches layers (PML) which can be used to extend a waveguide to infinity and offers the choice to set up models in 2D Cartesian or 2D axisymmetric coordinates. The distinction between these coordinates is described in the next section.

5.2 Coordinate system

The 2D models considered in this section are an approximation of a 3D setup. An important choice when making this approximation is which coordinate system is being used to describe the model and how well it can represent the different features of the 3D setup. The 2D approximation is made by choosing a 3D coordinate system[8] and subsequently assuming no variations occur in any of the parameters or variables in one of the coordinate directions. The two most obvious choices for a 2D model in this context are based on a 3D Cartesian coordinate system where variations in one coordinate directions is not considered (usually referred to as a 2D model) or a 3D circular cylindrical coordinate system where variations in the circumferential directions are not considered. The latter option is usually referred to as an axially symmetric 2D model or axisymmetric 2D model.
The properties and limitations of both choices are shortly summarized below.

[8] This approach only works for a select number of orthogonal coordinate systems. A requirement is that the Helmholtz equation (which describes the relevant physical phenomena of acoustic wave propagation) and equations for linear elasticity (which are relevant if an elastic bottom needs to be modelled) can be rewritten using the techniques of separation of variables. After application of separation of variables, the solution for a chosen coordinate can be set to unity (i.e. no variations of the solution with that coordinate) and the general solution is now 2D, i.e. it is only dependent on the remaining coordinates.

5.2.1 Cartesian 2D model

This type of model is based on a solution in 3D Cartesian coordinates.

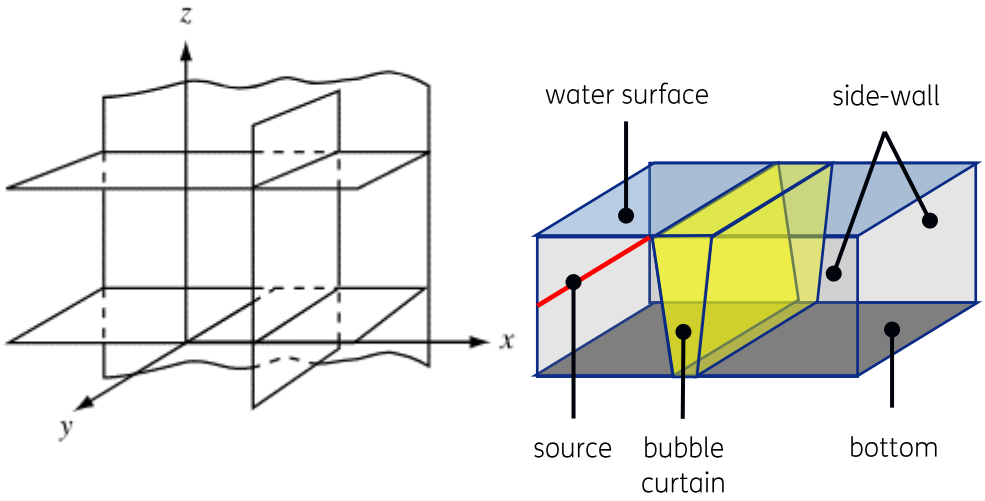

- The water surface and bottom of the waveguide are aligned with a plane having a constant z-coordinate.
- The straight parallel side-walls of the concept basin are aligned such that the y-coordinate, in which direction no variation occurs, has a constant value at these walls. Note that if the walls are perfectly reflective in the 3D case (both acoustically hard; or both pressure release surfaces) the propagation of waves that do not vary in y-direction can be described in 2D using this coordinate system without approximation. This is also true if the waveguide extends to infinite in positive and negative y-direction.
- The waveguide can be extended to infinite in negative and positive x-directions by using a PML on both sides of the 2D model.
- The volume containing the bubble screen is a prism in which the properties may vary in x and z-direction, but are constant in y-direction.
- The approximation that the solution has no variation in one coordinate direction also applies to the source. This implies a point source (which is used in the 3D setup) cannot be modelled in this coordinate system and the closest approximate is a line source. If the water surface, bottom and side-walls of the basin are described as above the line source would extend between the two side-walls. Note that this limitation implies that:
- The decay in amplitude is $1/\sqrt{r}$ for a line source and $1/r$ for a point source. Additional assumptions are needed to correct for this difference (such as the absence of diffraction in the bubble screen for directions involving the y-coordinate).
- The line source creates a cylindrical wave, implying the side-walls only interact with grazing sound waves (i.e. waves hitting the side walls at other angles are not included) and the bubble curtain only interacts with sound waves having a grazing angle in the xz-plane (i.e. the angle of incidence in the xy-plane is always normal).

The limitations due to modelling a line source can be overcome under certain conditions as is described below in Section 5.2.3.

5.2.2 Axisymmetric 2D model

This type of model is based on a solution in circular cylindrical coordinates.

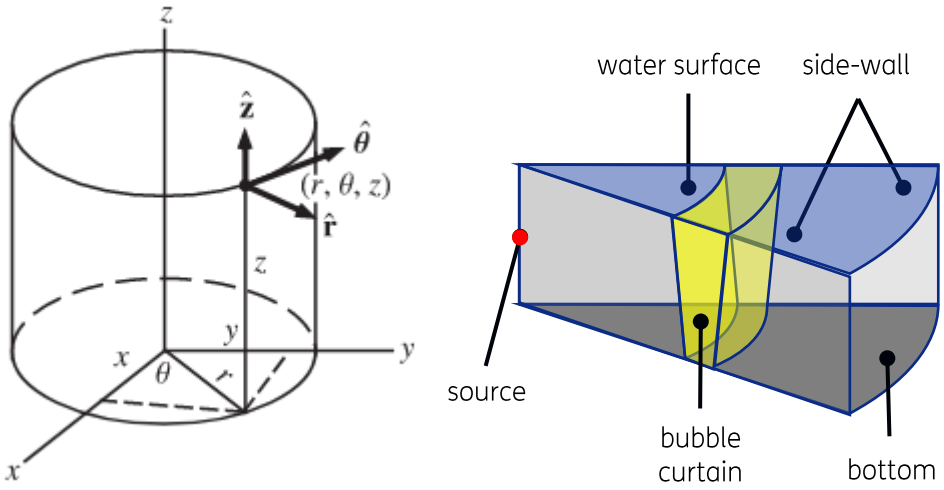

- The water surface and bottom of the waveguide can be aligned with a plane having a constant z-coordinate.
- The straight parallel side-walls of the concept basin are represented by planes for which the θ-coordinate does not change (and the solutions is assumed not to vary in θ-direction). In this coordinate system that means the basin walls are no longer parallel, but meet at the origin and grow farther apart width increasing range along the r-coordinate. Note that if the walls are perfectly reflective in the 3D case (both acoustically hard; or both pressure release surfaces) the propagation of waves that do not vary in y-direction can be described in 2D using this coordinate system without approximation. This is also true if the waveguide extends over 360 degrees to form a cylinder.
- The bubble screen has a curved shape in these coordinates and can be thought of as a bend prism. The properties may vary in r and z-direction, but are constant in θ-direction.
- The 3D point source can be modelled as a point source in 2D if it is situated on the axis of symmetry.

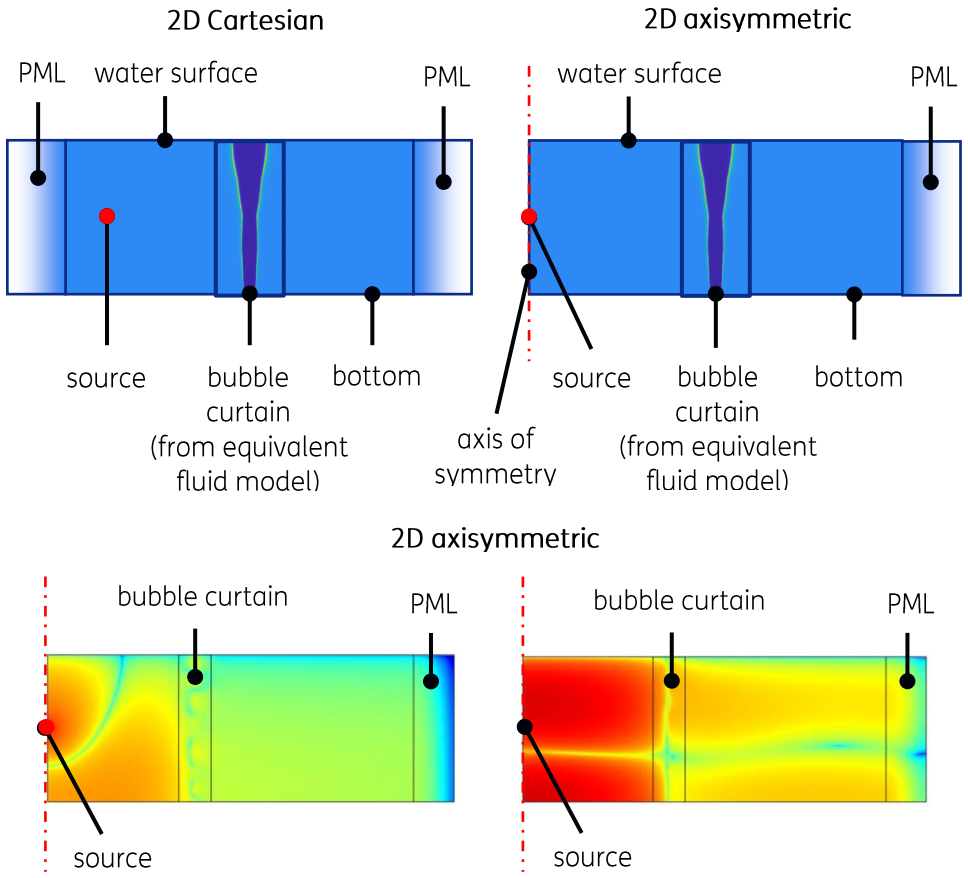

Figure 5.1: The top row shows a schematic representation of the FE domains for a 2D Cartesian and 2D axisymmetric model. The PMLs extend the wave guide to infinity in the positive and negative x-direction and positive r-direction. The axis of symmetry is by default an acoustically hard boundary. An example of the resonant behavior for the 2D axisymmetric model (which is not observed for the 2D Cartesian model) is shown in the bottom row. The left and right plots show solutions of an FE calculation for the concept basin (using preliminary data from MARIN) at frequency of ca. 300 Hz and 400Hz, respectively.

A potential issue with the 2D axisymmetric approach is that the axis of symmetry is by default an acoustically hard boundary. While the PMLs extend the wave guide to infinity in the positive and negative x-direction for the 2D Cartesian model a PML can only be used to extend the waveguide to positive r-direction for the 2D axisymmetric model. A schematic representation of the FE domains for a 2D Cartesian and 2D axisymmetric model is given in Figure 5.1. The acoustically hard axis of symmetry implies that sound waves that are reflected back to the source by the bubble curtain will be reflected again at the axis of symmetry. The sound waves can be 'trapped' this way, and this leads to resonances in the system associated with the 'trapped' volume. These additional resonances that are not encountered for a 2D Cartesian model with PMLs on both sides influence the predicted insertion loss. Note that while this effect will not happen in the MARIN setup which uses a straight bubble curtain in a rectangular basin, this effect will (to some extend) happen in practice for an actual bubble curtain if the setup is perfectly circular and the source (for instance a pile exited by impact pile driving) is positioned in its center. If the axial symmetry is broken, for instance because the curtain does not form a perfect circle, the source is not positioned in the center of the circle, or the properties of the bubble curtain are not constant along the length of the curtain, the effect will be there but it will be less pronounced.

An example of the resonant behavior for the 2D axisymmetric model (which is not observed for the 2D Cartesian model) is shown in the bottom row of Figure 5.1. The left and right plots show solutions of a FE calculation for the concept basin (using preliminary data from MARIN) at frequency of ca. 300 Hz and 400Hz, respectively. Since these resonant effects 'pollute' the calculated performance of the bubble curtain it was determined that using a 2D axisymmetric model is not appropriate for the present case (including a rectangular tank geometry with a bubble curtain on only one side).

5.2.3 Extension of Cartesian 2D model

It was already mentioned above that using a 2D Cartesian model the source in an equivalent 3D will take the form of a line source. For a 'standard' 2D Cartesian model this line source has a constant value, but the approach can be modified so this is no longer the case. The extension to other sources can be described as follows:
Instead of assuming the solution has no variation in y-direction (after the equation is re-written by separation of variables) another solution can be assumed. If the solution in y-direction takes the form of an exponential function (or sine or cosine) the equations for the solution in the remaining directions are very similar to the equations for the case where the solution in y-direction is constant. The only augmentation that is required is that an modified wave number k_a is used instead of the (unmodified) wave number k_{xz}, which is based on the material properties of each material. The modified wave number can be defined as[9]:

$$k_a^2 = k_{xz}^2 - k_y^2 \tag{5.1}$$

with k_y the wavenumber that is used for the solution in y-direction.
Considering the geometry of the concept basin it makes sense to choose the solution in y-direction such that it resembles a standing wave that fits between the basin walls and satisfies the boundary condition (i.e. acoustically hard). There are an infinite number of standing waves that fulfil this description. The associated solutions for the wave guide are often referred to as modes (as in 'modes of propagation'). The modes are orthogonal with respect to each other (i.e. multiplying two modes and integrating the result over the width of the basin results in zero, except if the two modes are identical), in fact they can be thought of as the components making up a discrete Fourier series. It should therefore not come as a surprise that a line source parallel to the y-axis that varies arbitrarily in strength (and phase) along the y-coordinate can be decomposed into the contributions of such modes. If the source is symmetric with respect to the centreline of the basin only the contributions of the even modes are needed to describe the source. The concept of the decomposition of a symmetrically placed point source and the shapes of the first few even modes are shown in Figure 5.2.

[9] Note that calculating k_a requires taking the square root of the difference between k_{xz} and k_a. Care must be taken to use the correct branch cut of the square root if this difference becomes negative or complex valued. One of the solutions will lead to waves that damp out (quickly) in xz-direction while the other solution will lead to waves that grow unboundedly as they propagate.

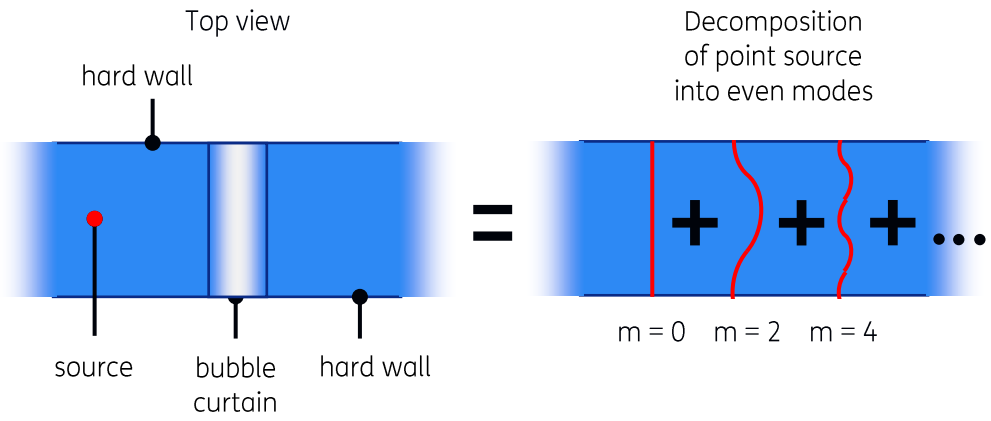

Figure 5.2 Decomposition of a symmetrically placed point source into its contributing waveguide modes.

It can be shown that the contributions of the even modes for the case of a symmetrically placed point source are all equal. In other words to obtain the 3D solution using modes, the 2D solution for each mode has to be calculated using the modified wave number (which is supported by default by COMSOL for acoustic calculations), the solution can be extended to 3D by multiplying it with the solution in y-direction for that the associated mode, and the solutions for each mode have to be simply summed. Note that if the receivers are also placed symmetrically with respect to the basin walls (which is the case for the current setup) the extension of the 2D solutions to 3D involves multiplying the 2D solution with unity.
Of course, not all terms of the infinite series can be included and a criterium has to be found to truncate the series. However, it was already mentioned that the contributions of all modes due to decomposing a point source are identical at the source. Fortunately, not all modes propagate equally well and only modes with a small wave number (and large wavelength) will propagate without attenuation in the waveguide. This is due to the fact that if k_y becomes larger than the real part of k_{xz} the imaginary part of the modified wave number k_a will become large compared to its real part (for real values of k_{xz} the modified wave number k_a will be purely imaginary if $k_y > k_{xz}$). So, if $k_y > \Re(k_{xz})$ the modified wavenumber in the FE solution is mostly imaginary and these waves will quickly attenuate after being emitted by the source. Modes that exhibit this behavior are called evanescent. After a few wavelengths of propagation (based on the unmodified wave number) only the non-evanescent modes contribute significantly. The so-called cut-off frequency for mode m above which the contribution of the mode is expected to become significant is reached when $k_y(m) = k_{xz}$. Using the width of the wave guide w and the speed of sound in water c_w the frequency cut-off frequency f_m for mode m can be expressed as

$$f_m = \frac{c}{2w} m \tag{5.2}$$

It was decided to include the first five even modes in the FE calculations (i.e. $m = [0,2,4,6,8]$. This number ensures the effect of higher order modes is correctly included up to frequencies of ca 1500 Hz. It was observed that including modes 6 and 8 does influence the results below 1500 Hz, but the overall trends are predicted correctly without their contributions. Therefore, the effects of higher order modes appear less visible in decidecade bands as the frequency increases. To keep the computational time manageable, it was therefore decided to not include modes above $m = 8$.

5.3 Implementation of the bubble screen in COMSOL

As is described above a 2D Cartesian model was implemented in the FE software package COMSOL. In the schematic below the 2D implementation of the measurement setup for the concept basin in COMSOL is shown again, this time including receiver positions.

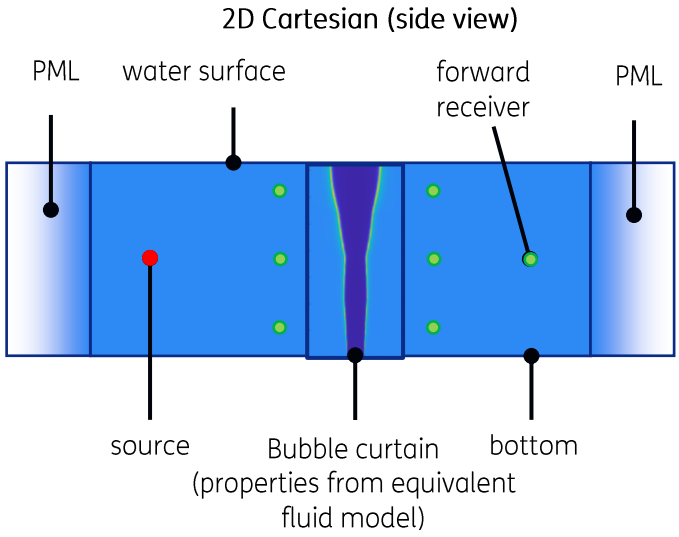

Figure 5.3: Schematic representation of the FE domains in the 2D Cartesian COMSOL model that was implemented. The PMLs extend the wave guide to infinity in the positive and negative x-direction. The properties of the bubble curtain are taken from a look up table which is populated with precalculated data based on the models of Wood, Commander and Prosperetti, Kargl and Feuillade.

The solutions of the FE calculations are extracted at the seven receiver locations used in the setup at MARIN (see Chapter 6). The most relevant receiver for determining the insertion loss as a means of characterizing the performance of the bubble curtain is the forward receiver (indicated in Figure 5.3). Results for the other receivers may useful for more extensive model validation or to probe the performance of sections of the bubble screen. In the present report only results from the forward receiver is considered.
As is explained in more detail in previous sections, the equivalent fluid properties of the bubble water mixture throughout bubble curtain are calculated by interpolating data from a look up table which is populated with precalculated data based on the models of Wood, Commander and Prosperetti, Kargl and Feuillade.

5.4 Notes on mesh size

An important step of the FE method is the discretization of the domain on which a solution is sought. The domains of interest are divided into elements which are connected and ideally describe the boundary of the domain accurately. The mesh size used in this discretization step should be such that the actual solution can be approximately described by the solutions space. For the Helmholtz equation this implies that ca. four elements per wavelength are needed to describe the actual solution with good accuracy when quadratic elements are used. The wavelength will depend on the frequency and the sound speed which is dependent on location and frequency for the equivalent fluid. Note that the dependency of

sound speed on location and frequency will be different for every bubble screen configuration.
A second criterion for a proper mesh is that it can describe the geometry of fluid medium accurately. For the cases considered (a bubble screen in a tank) the boundaries of the fluid domain are flat and do not have small features that require small element sizes to describe accurately. However, the sound speed in the bubble curtain changes quite rapidly with position depending on the equivalent fluid model and frequency. To capture the effects of reflection/diffraction and absorption accurately the mesh must also be able to describe the changes in equivalent sound speed. Given that at least four elements are used per wavelength the only additional requirement is that relatively sharp peaks and throughs in the sound speed that cannot be described by such a mesh are meshed finer. Considering the four elements per wavelength rule, such peaks/throughs would by definition be smaller than a wavelength. For such peaks/throughs to have a significant effect their prominence (i.e. how high/low the peak is compared to its immediate surroundings) must also be significant. Considering these criteria and the complex dependencies on frequency and position in the screen, it was decided to experimentally find a suitable element size by assuming a constant element size in the screen and checking for which size the criteria are satisfied everywhere. Based on this approach a minimum element size was chosen of 3.4 mm.

Note that the equivalent sound speed resulting from the Wood model is not dependent on frequency. It is known that this model only holds at lower frequencies and that for higher frequencies the actual equivalent sound speed (as determined from measurement) will return to that of water (independent of the void fraction or bubble distribution. This is the reason why high frequency sonars, such as depth sounders, are not disturbed by the bubbles that are always present near the ocean surface. The other equivalent fluid models are frequency-dependent and above ca. 500 Hz the minimum sound speed in the curtain rises with frequency, thus alleviating the mesh size requirements which become more stringent as frequency rises.
Since the Wood model is known to become inaccurate at high frequencies and including it in considerations for mesh size leads to small elements (and long computation times) at these frequencies, it is decided to not include data from the Wood model in the procedure to determine a suitable element size. This implies that when using the sound speed values predicted by the Wood model the mesh size requirements are met for lower frequencies, but are violated at higher frequencies (for the other models the mesh size requirements are met for all considered frequencies). Nevertheless, the Wood model is still evaluated at higher frequencies. However, for increasing portions of the screen the requirement of four elements per wavelength is violated as the frequency increases. Note that this only starts to become an issue for small parts of the screen for frequencies above ca. 900 Hz (below that frequency the mesh size requirements are met in the entire screen). The presented data for the Wood model should therefore not be considered above ca. 1000 Hz without asserting that the errors due to mesh size are small (for instance by refining the mesh and comparing results, which was not attempted in this study).

6 Results Concept Basin

6.1 Bubble curtain measurements at MARIN

Laboratory tests were performed in MARIN's facilities with bubble curtains in a controlled environment, as described in the WP4 report [20]. Three tests were carried out:

1. a test in September 2020 to characterize the acoustic conditions in MARIN's Offshore Basin, without a bubble curtain, in preparation for the upcoming bubble curtain tests.
2. a test in April 2021, in which different bubble curtain configurations were produced (three different hoses and three different air flow rates) in MARIN's Concept Basin. The acoustic insertion loss of the bubble curtains was measured by TNO in combination with measurements of the void fraction and the bubble distribution at selected locations in the bubble curtains, by MARIN and the Universiteit Twente (PhD candidate Simon Beelen, sponsored by the NOW AQUA project).
3. A test in July 2021 with a bubble hose in MARIN's Offshore Basin, varying both the air flow rate and current and waves in the basin. Again, the acoustic insertion loss of the bubble curtains was measured in combination with measurements of the void fraction and the bubble size distribution at selected locations in the bubble curtains.

The results of the April 2021 tests in the Concept Basin were used for the model validation study that is described in this report. The results from the Offshore Basin tests came too late to fit within the planning of the model validation in WP2C.

Table 6.1 provides an overview of the tested bubble curtain configurations and Figure 6.1 gives an impression of the 'nozzle' and 'porous' hose configurations.

Table 6.1: Different bubble curtain configurations tested in the Concept Basin (April 2021).

Hose description	Conventional configuration	Nozzle configuration	Porous configuration
Hose material	PVC pressure pipe	PVC pressure pipe	Porous hose
Hose diameter [mm]	15.4	15.4	25
Type of nozzle/gaps	Drilled gaps	Nozzles with silencers	Porous hose
Inner diameter of nozzle/gap [mm]	2	-	<< 1
Distance between nozzles/gaps [cm]	5	10	<< 1
Mass flow range [nL/min/m]	33, 66 and 102	33, 66 and 102	33, 66 and 102

MARIN's Concept Basin (CB) has a length of 220 m, a width of 4 m and a depth of 3.6 m. The bubble curtains were set up near to the center of the basin length.

Figure 6.1: Photo of the ‘nozzle’ and ‘porous’ hoses, next to MARIN’s Concept Basin.

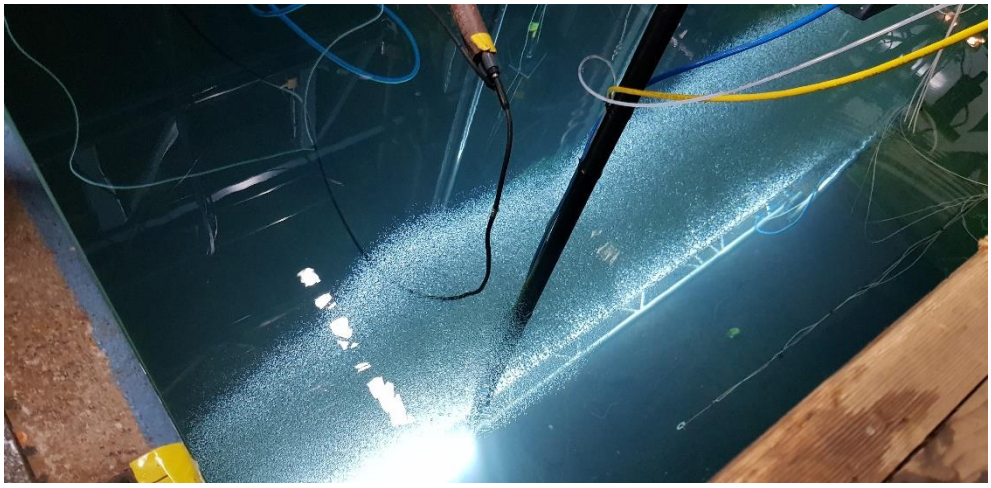

Figure 6.2: Photo of the conventional bubble curtain in MARIN’s Concept Basin, taken during the development of the curtain, just before the first bubbles hit the water surface.

Air void fractions and bubble size distributions were measured by MARIN, assisted by Twente University, at various locations across height and width of the bubble curtain. Because hydrodynamic modelling of the bubble curtain was not timely available, the input parameters for the acoustic models (void fraction and bubble size distribution as a function of position in the bubble screen) could not be generated using these models. Instead, the measurement data available at a limited set of positions was extrapolated across the curtain and then used as input for acoustic models. MARIN provided the results of the resulting distribution of void fraction and bubble size as a function of the position in the bubble curtain for the nine conditions (see Table 6.1) to TNO for the model-data comparison. The hydrodynamic analysis is described in [21].

Figure 6.3 provides an overview of the measurement configuration in the Concept Basin.

MARIN’s Data Physics/Gearing & Watson hydro-sounder model UW350 loudspeaker was used for the acoustic tests, transmitting logarithmic frequency sweep signals of 10 s, ranging from 100 Hz up to 10 kHz (velocity of 0.2 decade per second). The sound field on the source side, at 1.2 m before the bubble curtain, was measured with three RESON type 4032

hydrophones ('TOP1', 'MID1' and 'BOT1'). The sound field at 1 m and 4.3 m beyond the bubble curtain was measured by TNO's Brüel & Kjær (B&K) 8103 hydrophones ('TOP2','MID2', 'BOT2' and 'FWD').

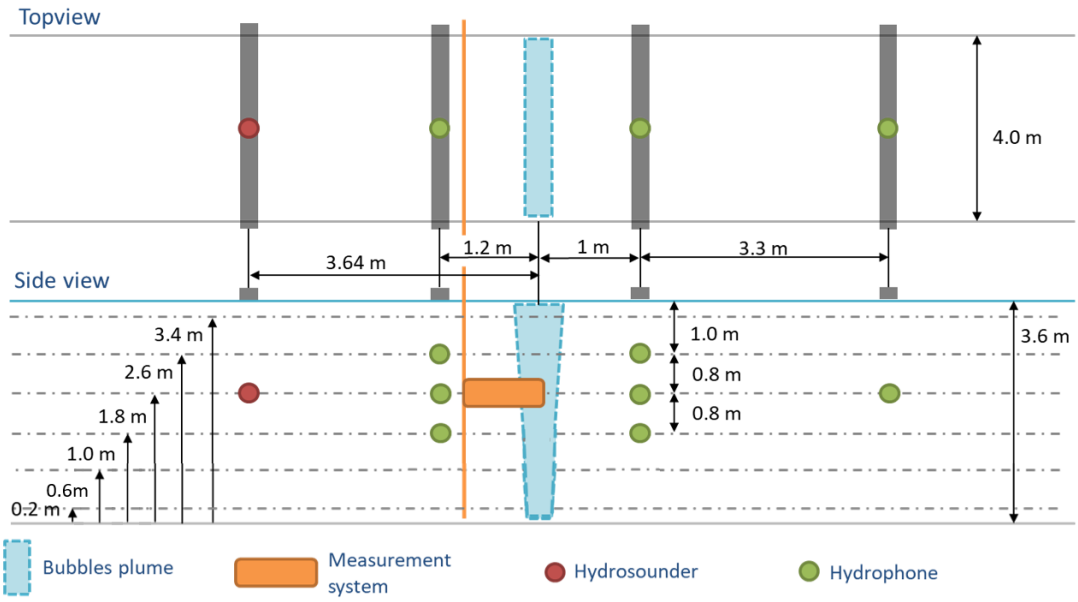

Figure 6.3: Sketch of top and side view of the measurement set-up in the Concept Basin (from measurement report [20]).

6.2 Effective speed of sound

An intermediate result of the model is the speed of sound and attenuation/damping as a function of position in the bubble curtain, predicted by the equivalent fluid models. An example of this intermediate output and the associated input (depth dependent bubble size distribution and void fraction as a function of range and depth) is given in Figure 6.4. The probability density function is interpolated/extrapolated to other depths based on the six curves shown.

Note that even though the void fraction as a function of range and depth as provided by MARIN looks smooth and the bubble size distribution as a function of depth which is also obtained by interpolation appears smooth (not shown here) the resulting speed of sound and damping plots appear to show interpolation artefacts. These rougher looking features are due to a combination of interpolation of the input quantities and the heavily non-linear relation between the input quantities (void fraction and bubble size distribution) and output quantities (speed of sound and damping) of the equivalent fluid model. It is unknown what the effects of these artefacts is on the predicted insertion loss. The artefacts appear to be largest for regions where the speed of sound is relatively high. At the frequency considered in Figure 6.4 (i.e. 1 kHz) the wave length is 1.5 m and the length scales of the artefacts are small compared to the wave length, suggesting their influence will be insignificant. At significantly higher frequencies (i.e.10 kHz and higher) the length scales may become similar.

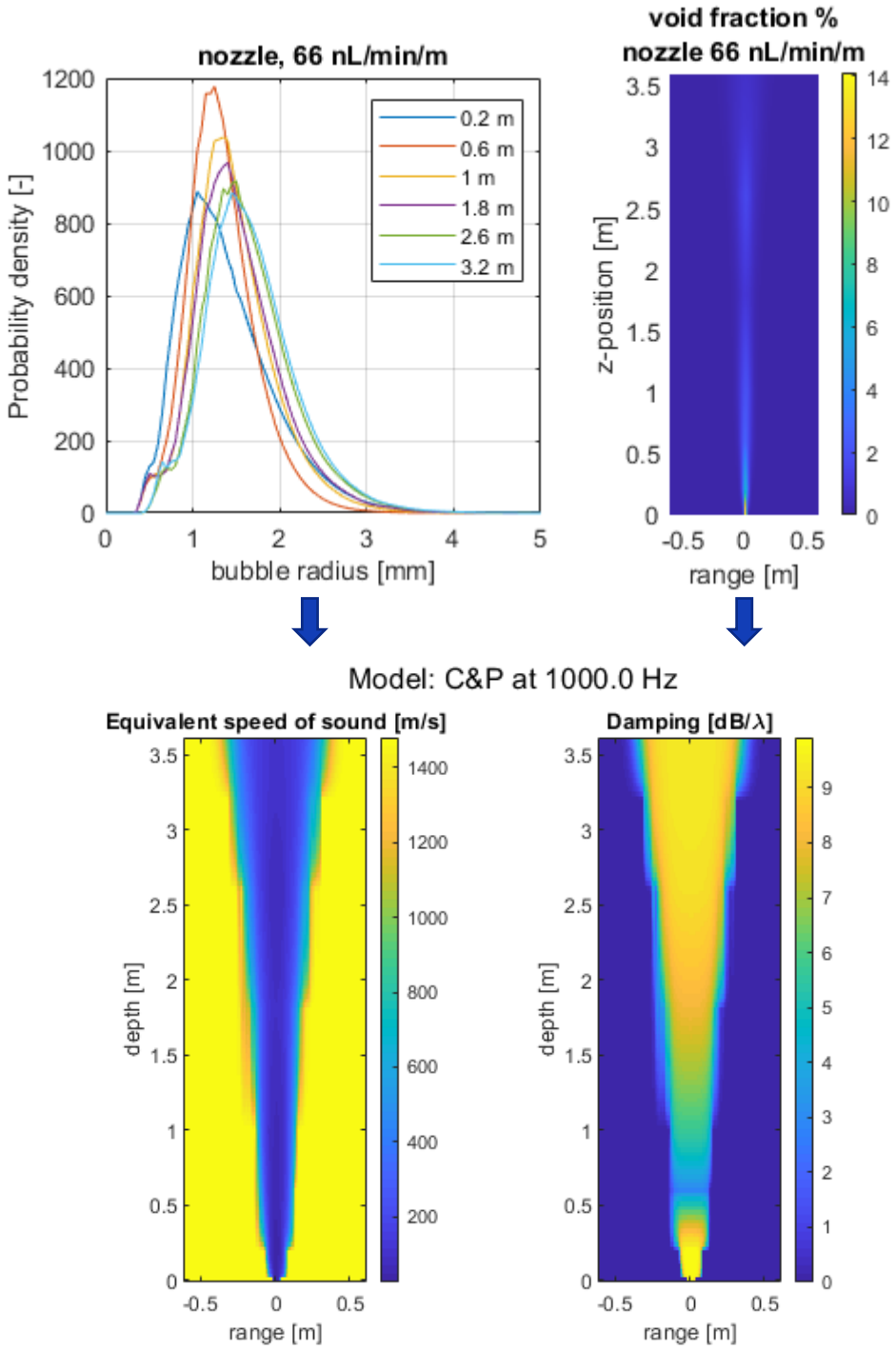

Figure 6.4: Bubble size distribution (top left), void fraction (top right), the equivalent speed of sound (bottom left) and the damping (bottom right) for the Nozzle bubble curtain with flow rate 66 nL/min/m. The speed of sound and damping are calculated with the model of Commander and Prosperetti at a frequency of 1000 Hz.

6.3 Insertion loss

The predicted and measured insertion loss at the forward receiver is plotted in Figure 6.5 for all bubble screen configurations measured in the concept basin at MARIN.
The processing of the measurement data was adjusted slightly compared to an earlier Memo [22] to remove 50 Hz noise and an altered reference set (i.e. data for the case without a bubble curtain) was used[10]. Another difference with the previously produced plots is the frequency range for which data is shown. In relation to this it is worth noting that even though the source was driven with a sweep signal between 100 Hz and 10 kHz during the experiments the setup was also excited below 100 Hz. Moreover, for a considerable frequency range below 100 Hz enough energy was put into the water by the source to have a signal to noise ratio (SNR) at the receiver greater than 0 dB. Since the models predict interesting features below 100 Hz it was decided to include measurement data for the frequency interval for which the SNR was consistently above 3 dB. The starting frequency of this interval is different for each bubble screen configuration, which explains the difference in plotted frequency range for the measured results in the following figures.

A striking observation that can be made by observing all plots is that while all equivalent fluid models lead to insertion loss values that are similar to the measured values for the conventional bubble curtain configurations for all frequencies, the three equivalent fluid models including the effects of bubble resonance dramatically overpredict the insertion loss for the nozzle and porous bubble curtain configurations above ca. 800-1000 Hz (depending on the model). In this same frequency region, the model of Wood consistently underpredicts the measurement results for all bubble curtain configurations. The underprediction by the model of Wood is easily explained by the lack of a way to represent damping due to bubble vibrations in the model. In other words, the model is used outside its expected range of validity. Moreover, it was explained in Section 5.4 that the results for the Wood model may be unreliable above ca 1 kHz due to (local) violation of the mesh size criteria for accurate results.
It is also worth mentioning that from the three equivalent fluid models including the effects of bubble resonance the model by Feuillade introduces the least damping and shows the lowest insertion loss values. The model by Kargl produces the highest peak in insertion loss for the nozzle and porous bubble curtain configurations. This can be seen for the porous configuration with a flow speed of 33 nL/min/m in Figure 6.5. For the other configurations the peaks fall outside the plotting area.

To provide a better view of the results below 1 kHz the same data is plotted again in Figure 6.6.

[10] Removal of the 50 Hz noise only resulted in minor changes compared to the earlier produced plots (<2dB at bands including 50, 100,150 and 200 Hz, and <1 dB for other bands). The reference that was taken in the current processing is based on the average of three measurements for the case without bubble curtain. In the earlier produced plots, the reference case for each bubble curtain was a single (but different) measurement for the case without bubble curtain. The differences fluctuate between 0 and 4 dB depending on frequency, flow rate and bubble curtain type.

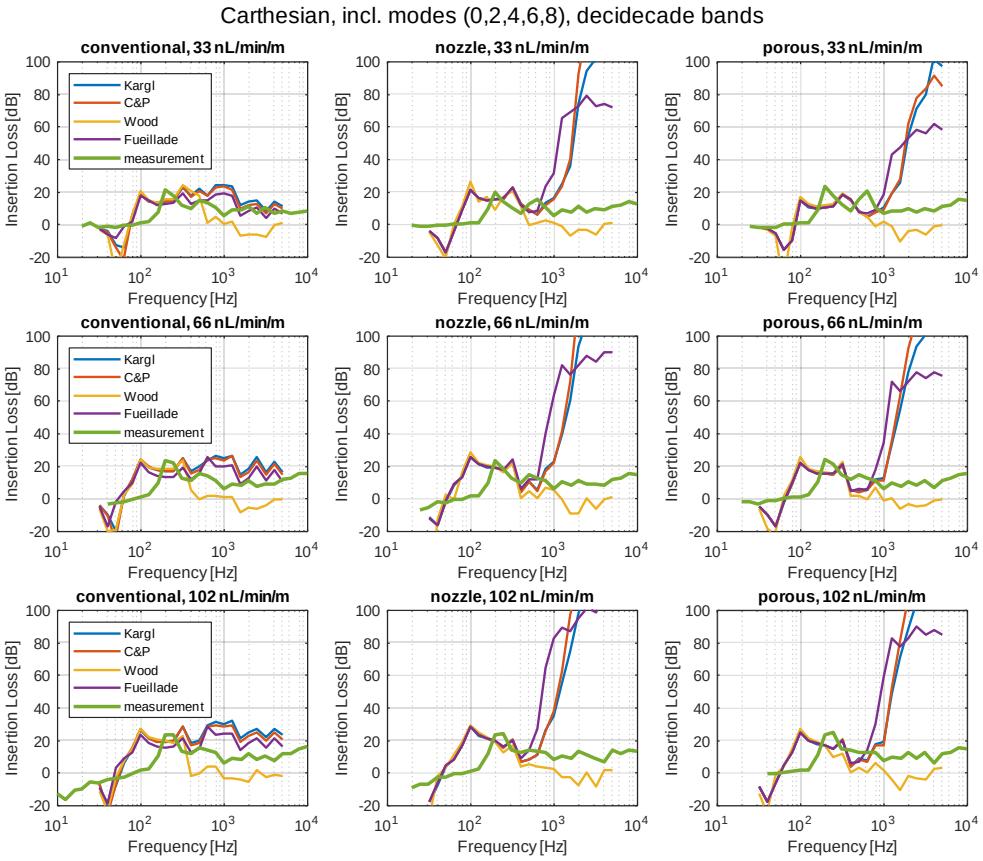

Figure 6.5: The predicted and measured insertion loss at the forward receiver for all bubble screen configurations measured in the concept basin at MARIN. The label C&P refers to the model by Commander and Prosperetti. The measurement data is plotted for all frequencies where the signal to noise ratio is larger than 3 dB. The threshold above which this is condition depends on the bubble screen configuration, explain the difference in plotted frequency range for the measured results.

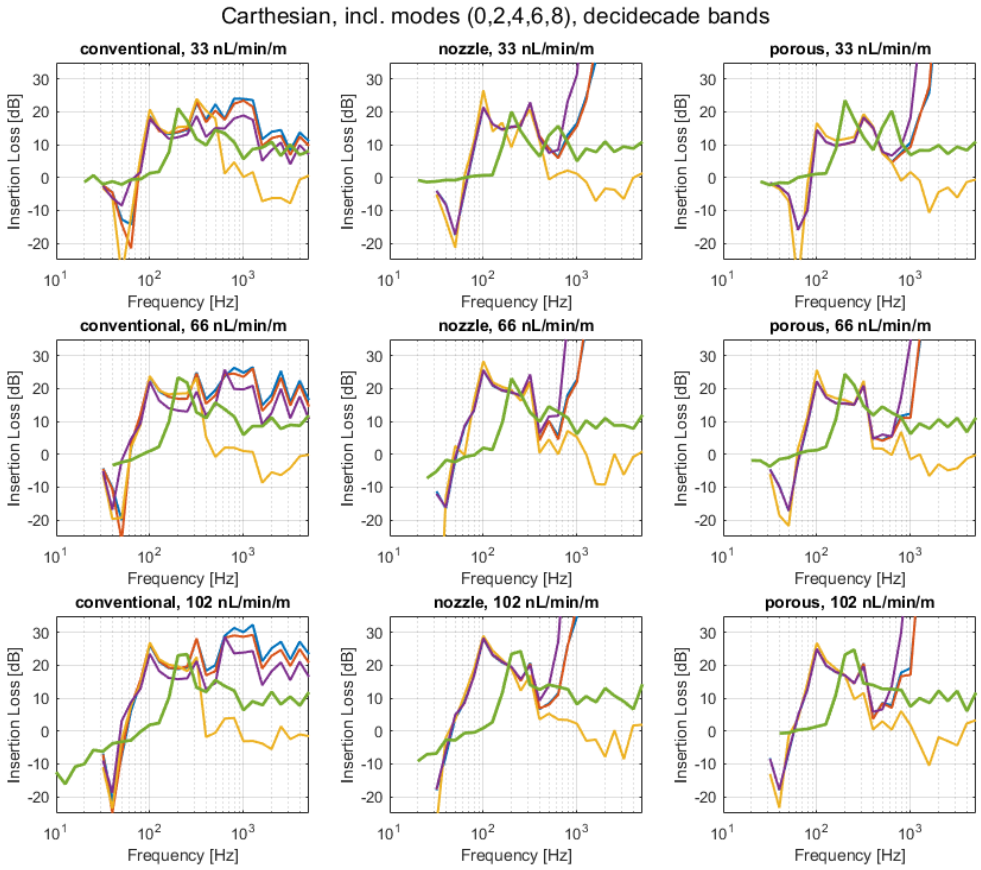

Figure 6.6: The same data as plotted in Figure 6.5 but with different extents of the frequency and insertion loss axes.

It can be observed that all model results are very similar at low frequencies. For the nozzle and porous bubble curtain configurations the results are very close up to ca. 400 Hz with the results by the model of Wood being most different from the other results. The difference between model results increases as the frequency increases.
For the conventional bubble curtain configurations, the spread in predicted insertion loss values is somewhat bigger, but all model results are very similar at 100Hz. Above this frequency the results start to differ more as frequency increases.
For all bubble curtain configurations, the results of the model by Wood start to differ significantly from results by the other models for frequencies above ca 400 Hz. The insertion loss predicted by the model of Wood drops below zero from that point (the results dip well below zero for frequencies above 1 kHz which could be related to the violation of the mesh size criteria as discussed in Section 5.4). Based on these observations of the predicted insertion loss it can be concluded that for the nozzle and porous bubble curtain configurations the insertion loss is dominated by the effects of a mismatch in acoustic impedance in the bubble curtain for frequencies up to ca. 400 Hz, while the insertion loss is dominated by the effects of damping above frequencies of ca. 400 Hz. A similar statement can be made for the conventional bubble curtain configurations; however, the region of transition seems to involve lower frequencies and seems to occur over a wider frequency range.
For the conventional bubble curtain configurations, it can also be observed (for almost all frequencies) that from the three models that include bubble resonances the model by

Feuillade predicts the lowest insertion loss values while the model by Kargl tends to predict the highest losses.

An important observation is that there is no consistent match between the measurement and modeling results. The predicted and measured values coincide for certain frequencies for each bubble curtain configuration, but the features of the different curves do not match. Nevertheless, some of the predicted trends do follow the trends observed in the measurements.
For instance, at very low frequencies the predicted and measured insertion loss may become negative suggesting a reduction in propagation loss is achieved by inserting the bubble curtain. At the frequencies where this occurs the wavelength in the water is large compared to the combined system of source and bubble curtain, and the source and bubble curtain act as a single system. In such a situation the bubble curtain may actually lower the radiation impedance felt by the source (i.e. it becomes easier for the source to output energy into the water at these frequencies), resulting in larger sound pressures at the receiver compared to the situation where the bubble curtain is not present.
Above this region the insertion loss shows a quick rise to a peak for both modeling and measurement results. Although the location of the peaks is different between prediction and measurement, the height of the peaks is very similar for almost all bubble curtain configurations.
After the peak the insertion loss slowly drops for both modeling and measurement results. For the measurement results the insertion loss decreases up to ca. 1000 Hz for all bubble configurations (with a small second peak between ca. 400 Hz and 600 Hz) and then rises again slowly until the end of the considered frequency range. For the model of Wood, the insertion loss is predicted to drop to ca. zero around 400 Hz. The three models that include bubble resonance predict a small peak followed by a sharp drop and successive sharp rise in insertion loss somewhere between ca. 400 Hz and 600 Hz for the nozzle and porous configuration. For the conventional configuration after the second small peak and successive drop, these models predict a slow rise in insertion loss to a plateau between ca. 700 Hz and 1000 Hz which is followed by a second plateau which is ca 10 dB lower.

Based on the results for the nozzle and porous bubble curtain configurations it is clear that the models including the effects of bubble resonance predict too much damping close to the resonance frequency associated with the bubble radius at the peak of the bubble size distribution. The peaks for the bubble size distribution are found between 1 mm and 1.5 mm depending on depth and correspond to a Minnaert frequency between 3.4 kHz and 2.3 kHz respectively. On the other hand, it is also clear that a model that does not account for damping due to bubble vibration is not adequate for frequencies above ca. 400 Hz.
For the conventional bubble curtain configurations, the overall match between model predictions and measurement is much closer (especially for the lowest flow speed). This is due to the fact that the bubble size distributions for the conventional bubble curtain configurations is very different from those for the other configurations (as can be seen in Figure 4.7). The peak of the distribution is found at much smaller radii (ca. 0.1 mm) causing the Minnaert frequency (at 34 kHz) to be much higher than the highest considered frequency. However, a frequency range where a relatively large overestimation of the insertion loss is observed is found between ca 700 and 1000 Hz. This peak cannot be explained by a peak in the bubble size distribution.

The bubble size distribution for the conventional and nozzle bubble curtain configurations with a flow rate of 33 nL/min/m are shown in Figure 6.7 on a logarithmic scale.

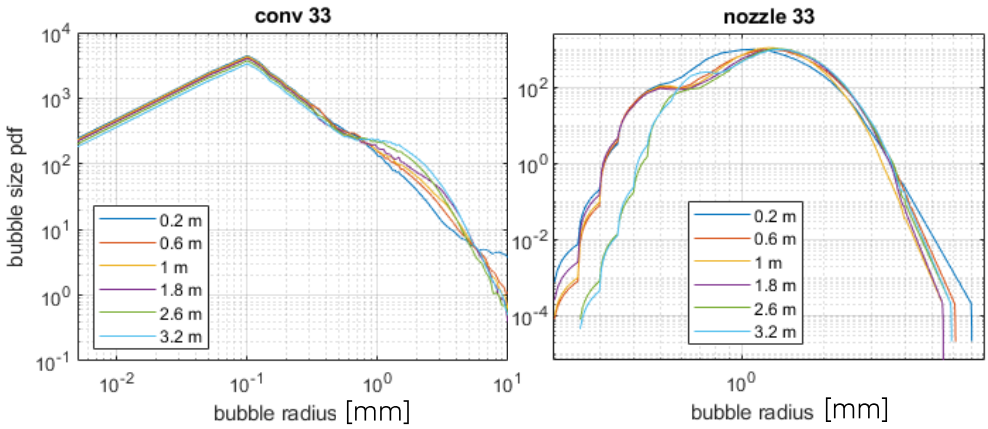

Figure 6.7: Bubble size distribution for the conventional (left) and nozzle (right) bubble curtain configurations with a flow rate of 33 nL/min/m.

It can be observed that the overall shapes of the curves are very different. It can also be seen for the curves of the conventional configuration that besides the main peak a bulge that almost makes a secondary peak is seen[11] for radii of ca. 1-1.5 mm. The Minnaert frequency for such radii is between 3.4 kHz and 2.3 kHz, so this feature may explain the second plateau of elevated insertion loss. The higher plateau found between 700 and 1000Hz would require a peak in the distribution around 3.5-5 mm which is not observed.

6.4 Difference in insertion loss between model and measurement results

The difference between the modeled and measured insertion loss is plotted in Figure 6.8 for all considered bubble curtain configurations. The large peaks and through observed in all plots at low frequencies (below about 1 kHz) are the result of the fact that the peaks observed in the insertion loss do not occur at the same frequency in the model and measurement results.

[11] For the nozzle configuration there are also many bulges observed but for radii smaller than the main peak. These are the result of linear extrapolation of the curves for smaller radii. These bulges will have a Minnaert frequency associated with them that are at the edge or outside of the frequency range that is considered.

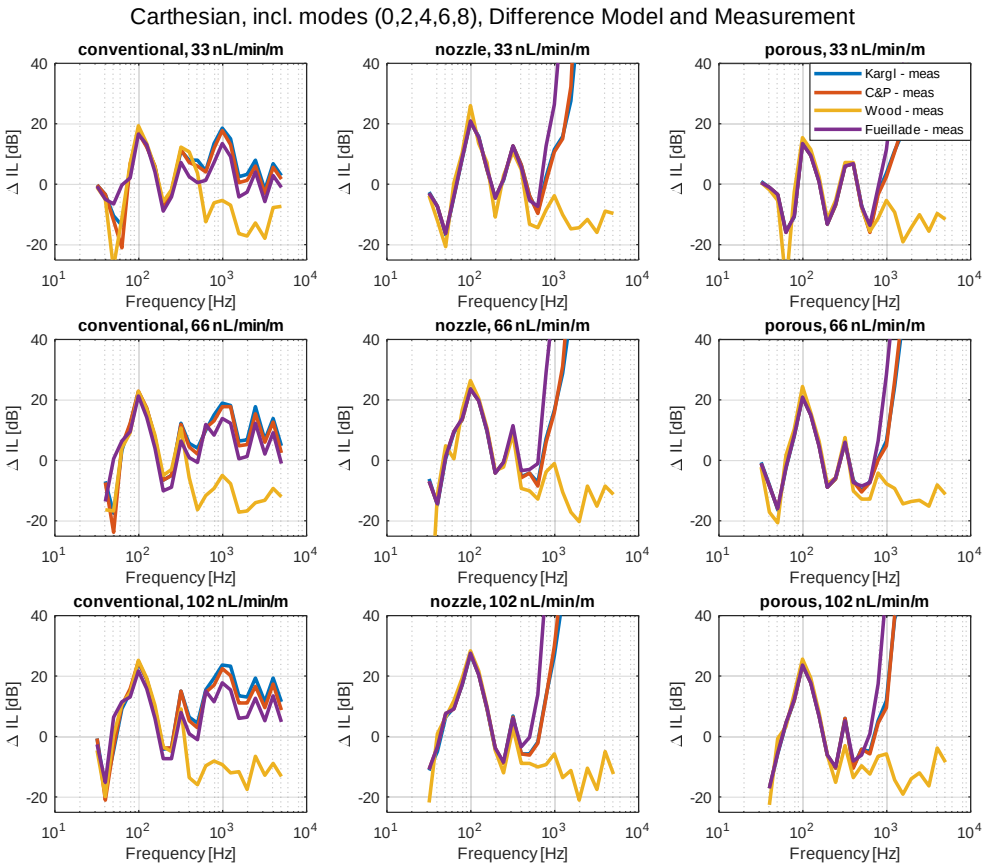

Figure 6.8: Difference between the modeled and measured insertion loss for all considered bubble curtain configurations.

6.5 Difference in insertion loss between flow speeds

The differences in insertion loss for the same bubble curtain type but different flow speeds are plotted in Figure 6.9 for all model and measurement results. It can be observed from the measurement results that for the considered cases flow speed has a limited effect on insertion loss. In contrast, the models predict that the amount of damping (for the models that include damping) is greatly dependent on the flow speed for most frequencies (through the influence of void fraction and bubble size distribution). The peak of the insertion loss grows with increasing flow speed for the three models than include the effect of bubble vibration, in the frequency range where bubble resonance is dominating.
It is also observed that all models predict a dependence of the insertion loss on flow speed at low frequencies (below ca. 100Hz and around ca. 300 Hz).

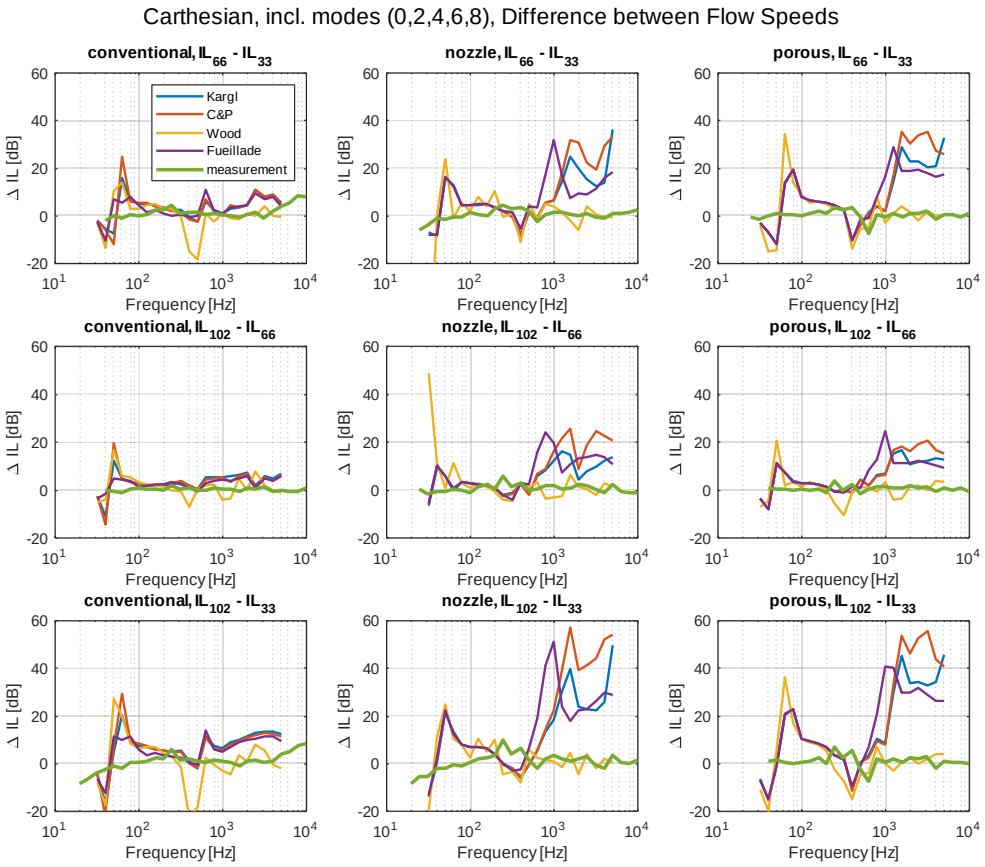

Figure 6.9: Difference in insertion loss for the same bubble curtain type but different flow speeds.

To get a better understanding of the influence of flow rate on insertion loss, based on the measurement data, the insertion loss for the measurement data is replotted in two different groupings in Figure 6.10.

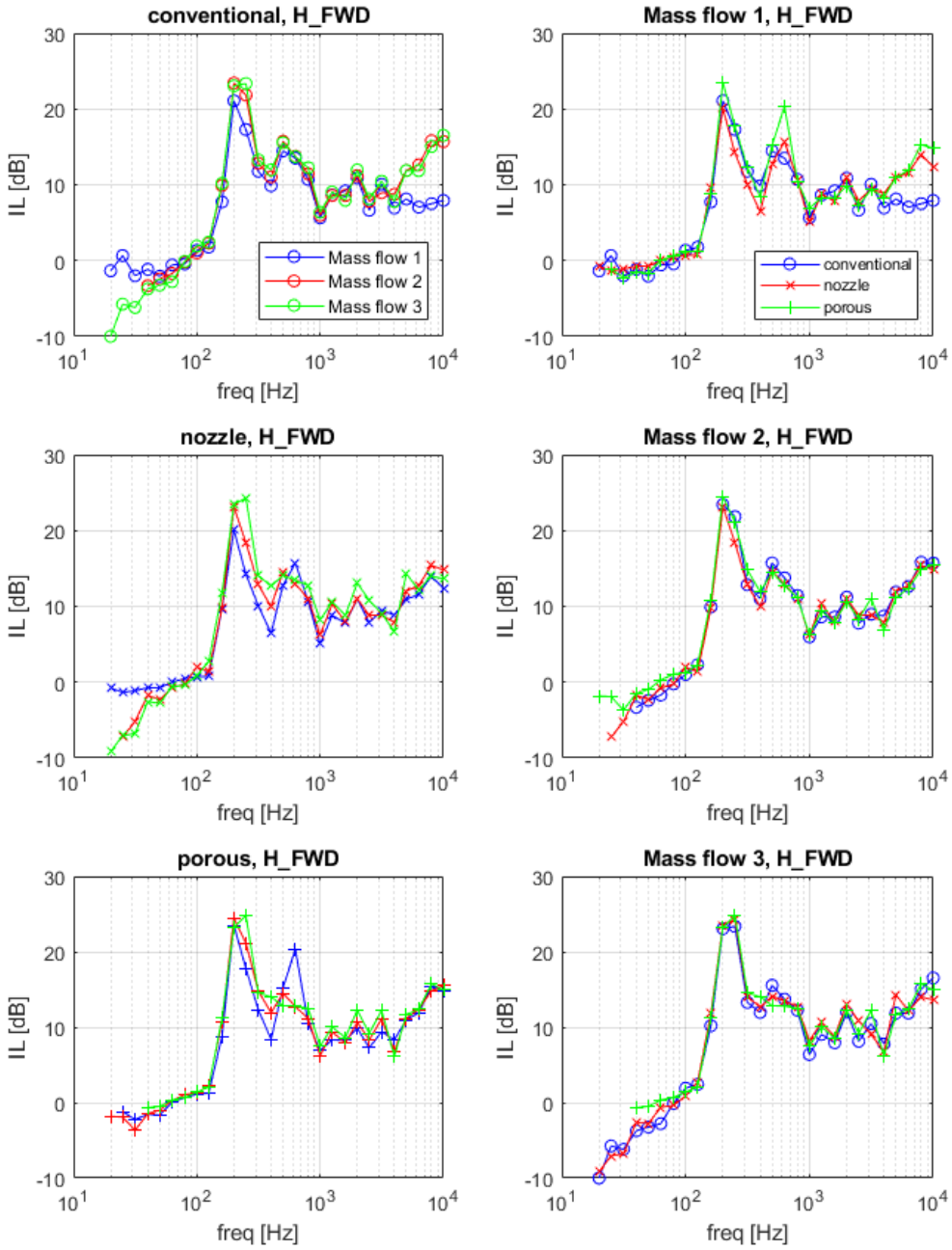

Figure 6.10 Measured insertion loss. The plots in the left column show data for the same bubble curtain type in a single graph (one plot per bubble curtain type). The plots in the right column show the same data but now data with the same flow speed are depicted in a single graph (one plot per flow speed). Flow rate 1 is 33 nL/min/m, flow rate 2 is 66 nL/min/m, and flow rate 3 is 102 nL/min/m.

If the results are grouped by flow rate (the right column of plots in Figure 6.10), it becomes clear that the difference in insertion loss between the different bubble curtain types is small, especially for flow rate 2 and 3 (66 nL/min/m and 66 nL/min/m, respectively). For flow rate 1 (33 nL/min/m) the differences are larger for certain frequencies and the porous bubble curtain seems to offer the highest overall insertion loss. For the conventional and nozzle bubble curtains it is frequency dependent which curtain has the highest insertion loss.

If the results are grouped by bubble curtain type (the left column of plots in Figure 6.10) the following observations can be made: For the conventional bubble curtain configuration an increase in flow rate increases the insertion loss somewhat between 100 and 1200 Hz (increases between 0 and 6 dB) and between 4 and 10 kHz (increases between 0 and 8.5 dB). The observed increase happens mostly between flow rate 1 and 2.
For the nozzle bubble curtain configuration an increase in flow speed increases the insertion loss between 100 and 500 Hz (increases between 0 and 10 dB), between 800 Hz and 4 kHz (increases between 0 and 8.5 dB), and above 5 kHz (between 1.5 and 3.5 dB). For the first frequency interval the increase observed between flow rate 1 and 2 is similar to the increase between flow rate 2 and 3. For the other two intervals the magnitude of the increase between flow rates is more erratic (for some frequencies there is only an increase between flow rate 1 and 2 or between 2 and 3 and at some frequencies there is an increase between 1 and 2 but a decrease between 2 and 3)
For the porous bubble curtain configuration an increase in flow speed increases the insertion loss between 40 and 500 Hz (increases between 0 and 7 dB), between 800 Hz and 4 kHz (increases between 0 and 3 dB), and between 5 kHz and 10 kHz (increases between 0 and 1 dB). For large sections of the first two frequency intervals the increase observed between flow rate 1 and 2 is similar to the increase between flow rate 2 and 3 (but for some frequencies a reduction in insertion loss is observed between flow rate 1 and 2). For the third interval the magnitude of the increase between flow rates is more erratic.
The overall observation is that increasing the flow rate will lead to an increase in insertion loss for most frequencies. However, the increase is not uniform, implying that depending on the bubble curtain and current flow rate an increase in flow rate may lead to only a small increase in insertion loss or even a decrease at specific frequencies. In other words, based on the current dataset a simple guideline for expected increase in insertion loss based on increase in flow rate cannot be given.

6.6 Difference in insertion loss between bubble curtain types

The difference in insertion loss for the same flow speed but different bubble screen types are plotted in Figure 6.11 for all model and measurement results. It can be observed from the measurement results that for the considered cases the bubble screen type does not have a consistent effect on insertion loss. For low flow speed the insertion loss seems to be higher for the nozzle and porous configuration at frequencies above ca. 3000 Hz. The model results suggest the dependency on bubble curtain type is much larger, especially around 100 Hz and above ca. 600 Hz large differences are observed for all combinations of screen types and at all flow rates.

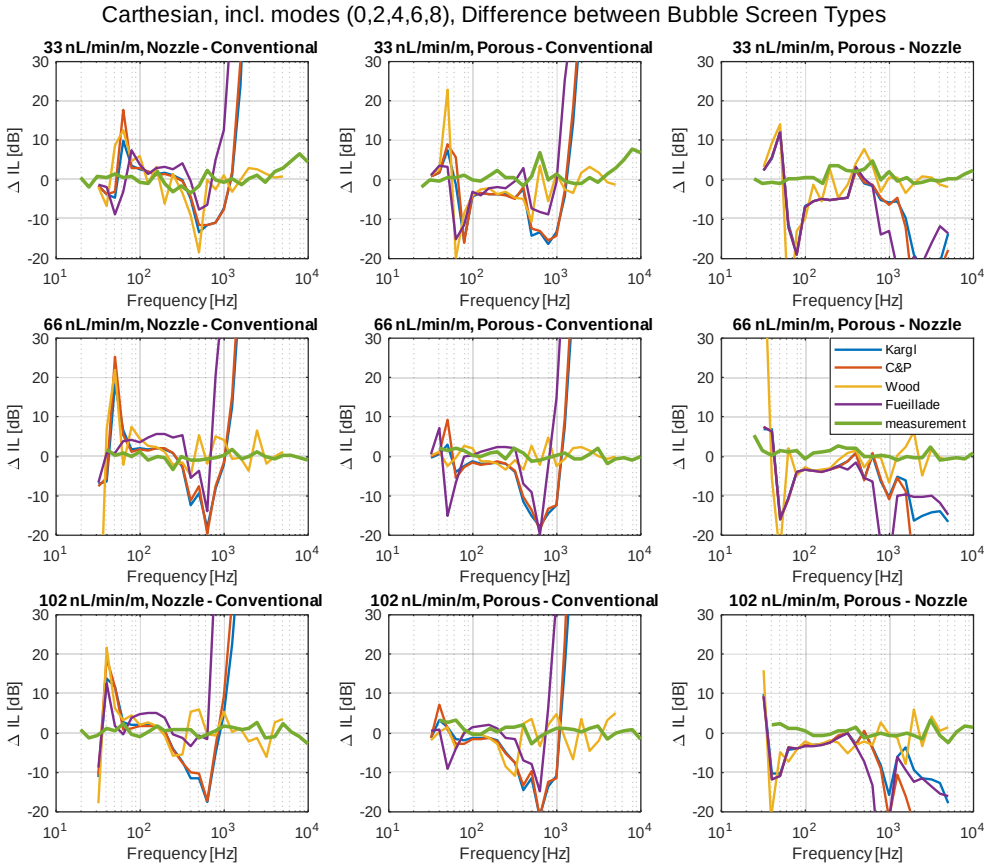

Figure 6.11: Difference in insertion loss for the same flow speed but different bubble screen type.

6.7 Discussion

The observed lack of agreement between model predictions and measured insertion loss of the different bubble curtain configurations in the MARIN Concept Basin model indicates that there are significant uncertainties in both measurements (of the void fraction and bubble size distribution) and modelling (of the acoustic properties). Some of these uncertainties are discussed in this section. The quality of acoustic predictions depends on the quality of the acoustic models as well as on the quality of the input to these models.

6.7.1 Use of time averaged void fraction measurement data

The measured profiles for void fraction and bubble size distribution are not exact. They are based on extrapolation of measuring on only a few depths (and in the case of bubble size distribution only in the approximate center of the width of the curtain). In addition, the profiles provided by MARIN are representative of the time averaged properties of the bubble curtains. The instantaneous values of void fraction (and bubble size distribution) vary with position differently than the average. It was demonstrated in Section 4.5 that the same amount of air may lead to a different insertion loss depending on how it is distributed. Furthermore it was shown that a collection of void fraction curves that on average match a

gaussian distribution will have an average insertion loss (based on calculating the insertion loss from the average propagation loss of the different instances) that is different than the insertion loss for that gaussian distribution (i.e. the average void fraction).
The time averaged void fraction as a function of space is based on measurement data that is 'straightened' before it is averaged. An example of the raw measurement data for void fraction obtained by MARIN and the 'straightened' version that is used to calculate the time average void fraction as a function of range are shown in Figure 4.13. In a 1D application the effect of 'straightening' the movement of a water-bubble layer prior to calculating the insertion loss is minor if the velocity at which the bubble cloud moves is small compared to the sound speed. As the water-bubble layer moves back and forward in the same direction as the wave propagation the phase information of the transfer function from the source signal to the receiver signal will change, but its amplitude will be unaffected. For the 2D case the effects are more complex. As the bubble cloud waves back and forward depending on the considered frequency the movement can create structures with a length scale comparable or larger to the wavelength. If such structures are present in the shape of the bubble curtain incident sound will scatter and refract differently at each instance in time. The reflection and transmission depend on how the sound scatters and refracts in the 2D setup in a non-linear way. Therefore, a similar effect as was described for the instantaneous values of void fraction vs. the time averaged void fraction (based on the 'straightened' data) will occur. It is not necessarily true that the average acoustic performance for many instantaneous shapes of the bubble curtain will match the acoustic performance of the average of the time averaged (i.e. 'straightened') shape of the bubble curtain.

6.7.2 Rate of change of void fraction and bubble size distribution with position

In the literature study in Appendix A (Section A.3.9) it is briefly mentioned that when using theories that include bubble-bubble interaction for the prediction of equivalent fluid media care must be taken when the collective response of the bubbles or the equivalent wavenumber change with position. In the paper of Henyey [10] guidance is given on if and when the approaches including bubble resonance[12] are valid for media that are not uniform in space. He states "equation (11) is derived in a uniform medium. Clearly, one cannot use [the] evaluation of the integral when F and K are functions of position. Since the integral is dominated by r on the order of $1/(k+K)$, presumably one should use averages over such a sphere in the correction. If F and K vary little on the scale of $1/(k+K)$, then equation (11), evaluated locally, should be correct."
In other words, if the collective bubble response or the equivalent speed of sound varies significantly over a distance $1/(k+K)$ the approach will not produce accurate results. It is not made fully clear what is meant by "presumably one should use averages over such a sphere" but it likely implies the average of the values for the collective bubble response and the equivalent speed of sound should be taken over a sphere with radius $1/(k+K)$ in the expression. It is not mentioned how to implement this or if and how this changes the solution.
Since the collective response of the bubbles and the equivalent wavenumber depend on the void fraction and bubble size distribution, changes in these properties may lead to situations where the criteria proposed by Henyey are violated. Since the relation between void fraction

[12] It is shown by Henyey that the solution by Commander and Prosperetti [6] includes first order bubble interaction. This suggests the criteria on when the theory may be expected to be valid for inhomogeneous media properties also applies to that theory and by extension to that of Kargl.

and bubble size distribution and the collective response of the bubbles and the equivalent wavenumber are complex it cannot be assessed a priori if the criteria will be violated.
For frequencies where bubbles having a radius that dominates the bubble distribution are close to resonance it is observed that the values for the speed of sound can vary very rapidly with range. An example is given in Figure 6.13 which depicts the speed of sound and attenuation as function of position in the bubble curtain for the nozzle configuration with a flow rate of 66 nL/min/m as predicted by the model of Feuillade.

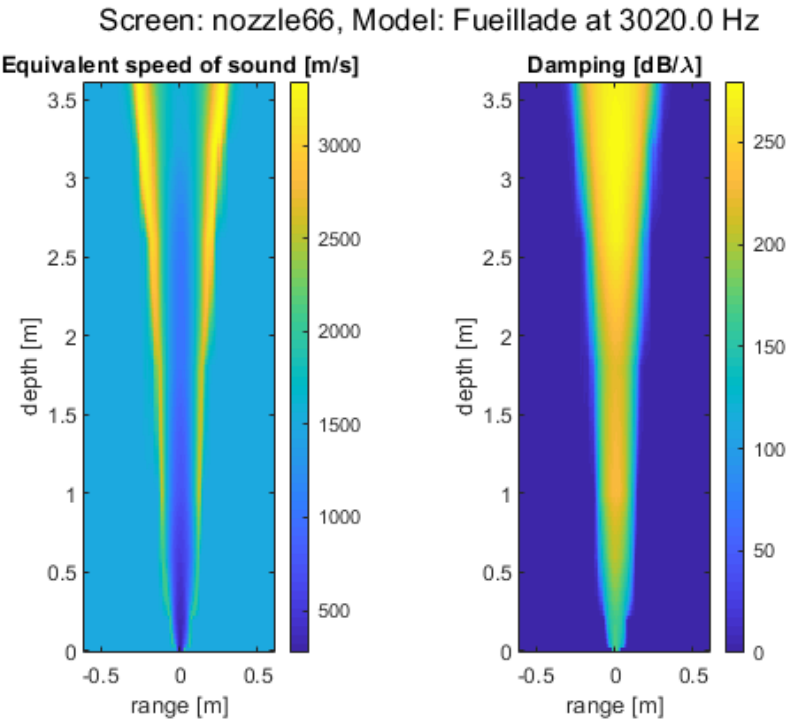

Figure 6.12: Speed of sound and attenuation as function of position in the bubble curtain for the nozzle configuration with a flow rate of 66 nL/min/m as predicted by the model of Feuillade.

For this example, using the average sound speed observed in Figure 6.12 the distance over which the rate of change in the equivalent wavenumber should be small is found to be 0.038 m. The same figure shows that within that length scale the sound speed changes from the value in water to values 2 times higher, implying the criteria for a low rate of change set by Henyey are not met. Note that in some sense this is a best case scenario in the sense that using the average sound speed observed in Figure 6.12 causes the considered length-scale to be twice as small compared to using the maximum sound speed and using results from the Feuillade model causes the length-scale and maximum observed change in sound speed to be small (compare to results from the other models including the effect of bubble vibration).
Based on these considerations it should not be a surprise that the results produced by the models of Commander and Prosperetti, Kargl and Feuillade do not match the measurement data for frequencies at which bubbles with a radius close to the maximum of the distribution are at resonance (i.e. for frequencies where bubble resonance is very important). Note however that this does not automatically imply that if averaging as proposed by Henyey is implemented correctly this will lead to correct prediction of the results in this frequency region. It is likely that non-linear effects play an important role in the observed differences

between model and measurement. In other words, the solution proposed by Henyey are likely to be necessary to get a good match but are also likely to not be sufficient.

6.7.3 Total air volume in curtain

A relevant metric for the (low-frequency) performance of a bubble curtain is how much air is needed to achieve a certain impedance level. If two bubble curtains achieve the same amount of insertion loss but one requires a significant lower flow rate this curtain is preferable from an operational/cost perspective. When optimizing for air flow rate it can be useful to consider the total amount of air that is in the water at any given moment for different bubble curtain configurations given a fixed inflow rate and investigate how this effects performance.

Based on the measured time averaged void fraction as a function of range that was gathered at 6 depths, the time averaged void fraction as function of range and depth was reconstructed using interpolation and extrapolation by MARIN. An example of such a data set is depicted in Figure 6.4. This data was integrated over the full width and depth of the extent of the bubble curtain to obtain the total volume of air in the curtain (per meter of bubble curtain length). The total air volume for each bubble curtain configuration is shown in Figure 6.13.

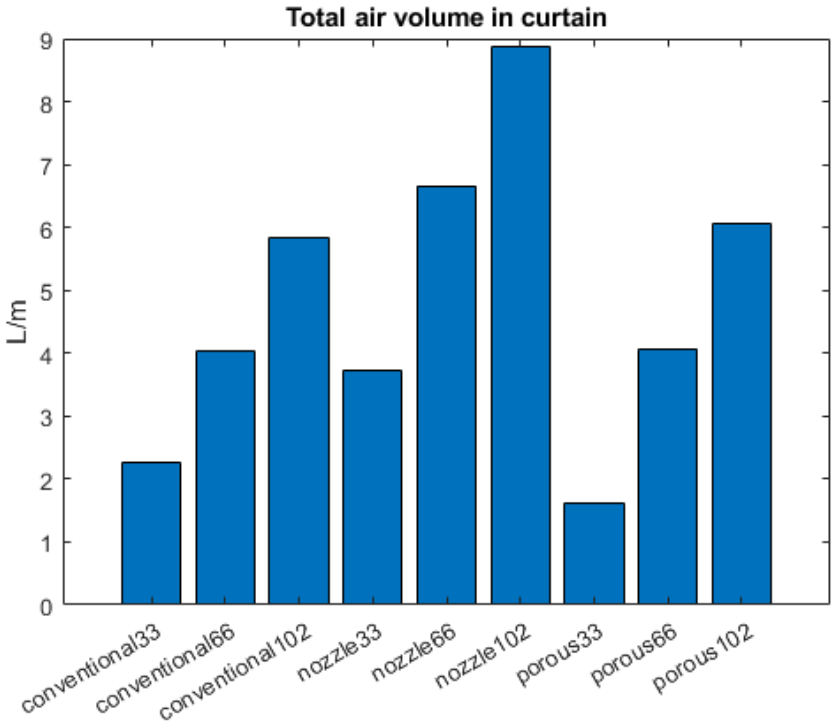

Figure 6.13: Total air volume in the water (per unit hose length) at every instance for different bubble screen types and air flow rates. The number in the labels on the horizontal axis indicates the flow rate in nL/min/m.

As may be expected, the total air volume for each bubble curtain type increases as the flow rate of air provided to the curtain increases. Furthermore, it can be seen that using the same inflow rates the curtains of different type contain a different total amount of air, which may seem counterintuitive. This paradox is resolved by considering the amount of time the air spends in the curtain before reaching the surface also influences the total amount of air in the curtain.

For each flow rate the nozzle configuration contains the most air. The total amount of air is much closer for the conventional and porous configuration. For the lowest flow rate, the total air volume is lower for the porous configuration, while for the highest flow rate it is lowest for the conventional configuration. The air volume data in Figure 6.13 combined with the measured acoustic performance as depicted in Figure 6.10 shows that the total amount of air in the curtain is not a direct measure for acoustic performance. It matters how the air is distributed, i.e. which bubble sizes are present and how the air is distributed across range and depth.

6.7.4 Boundary conditions

An important aspect of the 2D acoustic models that are used are the boundary conditions. For the present case the FE domain is bounded by the concrete walls of the basin. In the models these walls are assumed to be acoustically hard, i.e. a velocity boundary condition is employed setting the normal velocity of the sound field to zero at the walls of the basin. This boundary condition determines if and how acoustic waves incident on the basin walls reflect. Waves reflected by the basin walls lead to interference patterns in the basin. These patterns influence the location and height of the peaks and throughs observed in the insertion loss plots presented in this section. If decidecade bands are considered the influence of such interference patterns is only observed in the lower frequency bands (at higher frequencies the peaks and throughs within a single band mostly cancel each other out). In other words, if the assumption of acoustically hard walls is not suitable this can have an effect on the location and height of the peaks and throughs in the insertion loss that are observed at low frequencies. The difference between measurement and model observed at low frequencies may be due to the assumption of acoustically hard basin walls. Below it is investigated (with increasing complexity) to which extend the assumption of acoustic hard walls is expected to be appropriate (and an alternative is discussed shortly).

The reported (longitudinal) speed of sound for concrete falls somewhere in the range 3200 m/s and 3700 m/s, while a typical reported density is 2400 $\mathbf{kg/m^3}$. This implies the difference in characteristic impedance between concrete and water is a factor of ca. 5.1-5.9, which is not that big (by comparison, using for instance the typical reported values for the density and speed of sound for steel results in an impedance difference of a factor 26.7).
If a plane wave is normally incident on an interface of two half spaces of a homogenous medium the intensity reflection coefficient is given by [16]

$$R_I = \left(\frac{r_2 - r_1}{r_2 + r_1}\right)^2 \tag{6.1}$$

with r_1 and r_2 the characteristic impedance (product of sound speed and density) in each media. Plugging in the values for water and concrete (using 3700 m/s for the speed of sound in concrete) implies only ca. 50% of the energy is reflected while 50% is transmitted into the other medium (for steel the reflected amount of energy is ca. 86%).
If the concrete wall has a finite thickness the material on the other side of the wall has an influence on the reflected amount of energy. In that case the intensity reflection coefficient is given by [16]

$$R_I = \left|\frac{(1 - r_1/r_3)\cos(kL) + i\left(\frac{r_2}{r_3} - \frac{r_1}{r_2}\right)\sin(kL)}{(1 + r_1/r_3)\cos(kL) + i\left(\frac{r_2}{r_3} + \frac{r_1}{r_2}\right)\sin(kL)}\right|^2 \tag{6.2}$$

with r_1 and r_3 the characteristic impedance in the media on each side of the layer, and r_2 and k the characteristic impedance and wavenumber in the layer. This expression implies

that the reflection coefficient becomes frequency dependent (through the involvement of the wavenumber k). See Figure 6.14 for an example of the intensity reflection coefficient as a function of frequency for a normally incident wave on a concrete wall of 0.5 m thickness. The behavior is related to that of power transmission coefficient introduced in Section 4.1 in the sense that the reflection coefficient will experience a dip for frequencies where the power transmission coefficient has a maximum (i.e. when the width of the concrete wall matches a multiple of half a wavelength). These frequencies correspond with the resonance frequencies of the wall. For frequencies in between the transmission is low and the reflection coefficient has a maximum. While for low frequencies (below the first resonance frequency of the wall) transmission loss experiences a maximum, the reflection loss has a minimum (i.e. at low frequencies almost all sound is transmitted). For a wall thickness of 0.1 m, 0.2 m, 0.5 m and 1 m the first resonances for a concrete wall with sound speed 3700 m/s are 18.5 kHz, 9.25 kHz, 3.70 kHz and 1.85 kHz, respectively. This suggests the minimum values of the reflection coefficient are relevant for a large section (the lower frequencies) of the region where the equivalent fluid models produce meaningful results.
At very low frequencies the intensity reflection coefficient for the case of a concrete wall reduces to the intensity reflection coefficient for the case of two half spaces (where the concrete is absent). So the minimum values of the reflection coefficient are determined by the impedance contrast between water and the medium on the other side of the concrete wall, also referred to as the backing material. An example of the intensity reflection coefficient as a function of frequency is given in Figure 6.14 for a normally incident wave impinging on a concrete wall of 0.5 m thickness with different backing materials.

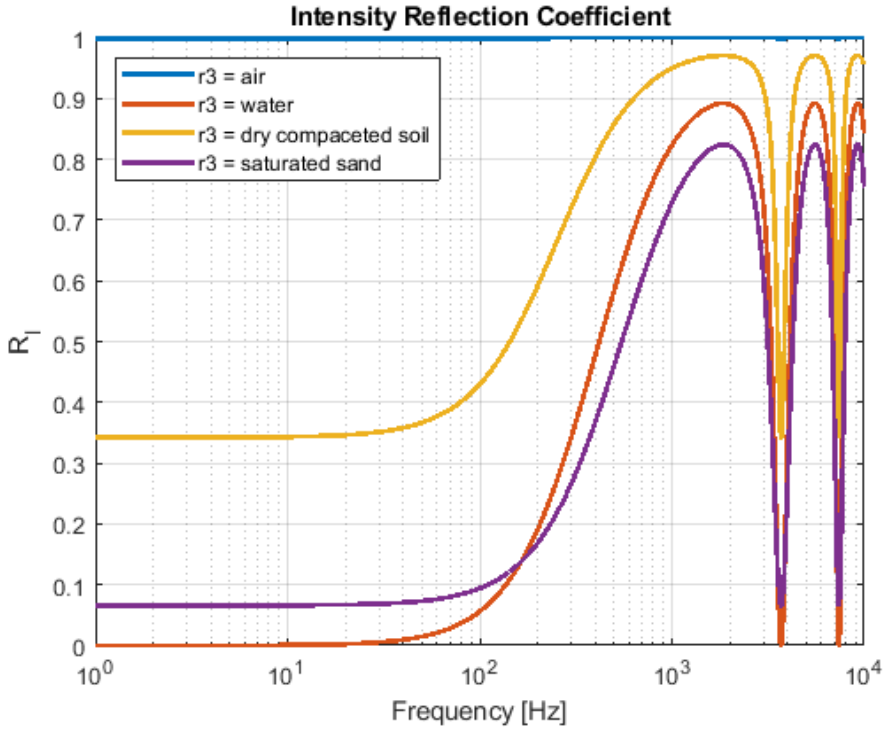

Figure 6.14: Intensity reflection coefficient as a function of frequency for a wave in water ($c = 1500$ m/s, $\rho = 1000$ kg/m^3) normally incident on a concrete wall of 0.5 m ($c = 3700$ m/s, $\rho = 2400$ kg/m^3) with different media on the other side: air ($c = 1500$ m/s, $\rho = 1000$ kg/m^3), water, dry compacted soil ($c = 260$ m/s, $\rho = 1510$ kg/m^3) and saturated sand ($c = 1275$ m/s, $\rho = 1990$ kg/m^3).

The values for the material properties of water and air are common values found in the literature. The material properties for the dry compacted soil were taken from

Oelze et al. [23] (air dry, dense, Plainfield soil). The material properties for the saturated sand were taken from Williams [24] (density was calculated using the listed density of sand grains and water and the porosity, the speed of sound was approximately set to the high frequency, infinite density result). The work of Williams indicates that the speed of sound in saturated sand-like sediment is frequency dependent below 100 Hz. This was not included when calculating the results in Figure 6.14, suggesting that in reality the behavior below 100 Hz is different. It is not known what the actual backing is behind the basin wall in the MARIN setup. Figure 6.14 suggest that depending on the backing and considered frequency the assumption of a hard wall can be good or not suitable.

For waves incident at oblique angles the relation between reflection coefficient and material properties and frequency becomes more complex. Diffraction will occur at the interfaces of the concrete wall if the sound speeds are different and part of the energy of incident waves will be converted to shear waves at the interfaces between concrete and water (and concrete and backing material). If the angle of incidence is larger than $\mathbf{asin}(c_w/c_c)$, with c_c the speed of sound in concrete, total internal reflection will occur at the water concrete interface. In that case, the only (longitudinal) acoustic waves that propagate in the concrete are evanescent waves which attenuate as they travel (the amount of attenuation is dependent on the ratio of the sound speeds and the angle of incidence). The thickness of the wall determine how much the evanescent wave attenuates before it reaches the other interface, which determines how much acoustic energy can be transported to the medium on the other side of the concrete wall. So, provided the wall is thick enough most of the energy will be reflected.
Note however that even if almost all acoustic energy is reflected, this does not automatically imply that the assumption of an acoustically hard surface is appropriate. The phase of the reflected wave also depends on the specifics of the situation. For an acoustically hard surface the reflection coefficient equals unity and the phase of the reflected wave is equal to that of the incident wave at the surface. However, for the case of reflection on an interface, the absolute value of the reflection coefficient may be unity (or close to it) but its value may be complex implying that the reflected wave has a different phase than the incident wave at the interface. The phase information also influences the interference pattern between direct and reflected waves in the basin and therefore also influence the location and height of the peaks and throughs observed in the insertion loss plots presented in this section.

None of the complexity described above is currently included in the 2D FE model. If information on the basin structure is available (in the form of thickness and material properties of the basin wall and material properties of the backing material) this can be included in the model. Note that calculating and prescribing a single reflection coefficient for the entire wall surface would not suffice. The theory used above requires plane incident waves, however the source in the setup can be regarded as a point source and does not produce plane waves. So, a more refined approach is needed to include the effect of the wall and backing material. The most straightforward approach would be to include the concrete layer and part of the backing material in the FE domain, using a PML to remove unwanted reflections at the end of the FE domain. Considering the current size of the FE domain this would not increase the calculation times and memory requires to unreasonable levels.
Note that the current approach to include reflections of the side walls also uses the assumption of acoustically hard walls. This assumption allowed to determine a finite number of propagating modes that will ‘fit’ in the waveguide (i.e. match the boundary conditions). If the backing material which extends to infinity has to be represented, the sum over a countable infinite set of modes (from which only the propagating modes are included) is replaced by an integral over an uncountable infinite range of modes, with each

value of the integrant requiring an FE calculation. It is not immediately clear how such a representation should be evaluated.

6.7.5 Bubble curtain shape

It was already stated in Section 5.2.2 that sound waves can be ‘trapped’ inside an axisymmetric circular bubble curtain which can lead to resonances in the source-mitigation system associated with the volume of water that is ‘trapped’ by the curtain. These additional resonances may significantly influence the insertion loss. While the effect will not happen in the MARIN setup (which uses a single straight bubble curtain in a rectangular basin) the effect will to some extent happen in practice for an actual circular bubble curtain centered around a sound source such as a pile exited by impact pile driving. The influence of the effect depends on many parameters: the nature of the sound source, the way the bubble curtain reflects/absorbs/transmits incident sound, the water depth, the condition of the sediment (sub-bottom layering and material properties), the degree to which the setup is axial symmetric (to what extend does the curtain form a perfect circle, is the source positioned in the center, can the properties of the bubble curtain be regarded as constant along the length of the curtain). Imperfections in the axial symmetry of the setup (curtain shape and properties and source location) may also lead to differences in the observed performance of the curtain depending on the direction of propagation from the source (in the plane of the waveguide), even if the source itself radiates sounds homogenously in all directions.

7 Summary and conclusions

7.1 Literature

The literature study (Appendix A) suggests that research on the subject of acoustic interaction with bubbles is not settled. In particular, it was observed that

- The models for equivalent fluid properties are only successfully validated for limited cases (i.e. distributions with a single bubble radius and small void fraction ($\beta \leq 0.01$) or distributions with a range of bubble radii but for very low void fractions ($\beta \ll 0.01$) which are not representative for the application of sound mitigation using bubble curtains. The models are also only successfully validated away from bubble resonance (criteria to assess if this assumption is satisfied are not provided).
- It is still debated what the best approach is for the inclusion of bubble-bubble interaction in the predictions of equivalent fluid properties. Bubble-bubble interaction is known to be important for accurate predictions when bubbles are at or approach resonance.
- Non-linear effects are expected to be important at or close to bubble resonance. A main source of non-linear behavior are large amplitude vibration of bubbles. However, there are no criteria available describing when non-linear effects become important for the prediction of the equivalent properties of bubble-fluid mixtures. There is also no consensus on the best suited non-linear model for prediction of equivalent fluid properties or on an approach to use such models in the context of broad band excitation (which is relevant for instance for impact pile driving).

Notable extensions of work presented in the literature include:

- It was discovered that the solution for the transmission coefficient (used to calculate the insertion loss for a uniform layer in a medium) given by Kinsler and Frey [16] is incorrect in case medium in the layer has damping (i.e. a complex valued speed of sound). The correct equations are derived based on the original theory. Note that this new solution gives identical results to expression given by Kinsler and Frey for the case of zero damping.
- The model of Henyey which includes the effect of bubble-bubble interaction was not used yet in the literature to produce results. The model was implemented and the expressions for the equivalent speed of sound where evaluated. From the three branches of solutions that are produced, none was found to consistently produce physically meaningful results and converge to the correct solution for low and high frequencies.

7.2 1D models

- It was demonstrated in Section 4.5 (for the case of no damping) that the way void fraction changes across the width of the bubble curtain influences the overall shape of the insertion loss curve. Besides the overall shape, the location of the peaks and throughs observed in insertion loss spectra can also change.
- It was also shown that using (an abstract representation of) the instantaneous void fraction as a function of position may lead to different insertion loss curves compared to using the time averaged void fraction as function of position.

- Using the average of the propagation loss of many instances of the instantaneous void fraction to calculate the insertion loss also leads to different results than calculating the insertion loss based on the time averaged void fraction.
  - Significant differences are only observed if the instantaneous void fraction as a function of position includes features that are not present in the time average void fraction and have a length-scale that is equal to or larger than the wavelength considered.
  - In other words, using the time-averaged void fraction as a function of position will lead to acceptable results at low frequencies, but may lead to significant deviations at higher frequencies.

7.2.1 Equivalent fluid models and insertion loss

- At low frequencies, the insertion loss result for the considered equivalent fluid models converge to the same solution. In this regime for which damping due to bubbles is very low, the model of Wood, which is the simplest model, is adequate to describe the equivalent fluid properties.
- Above frequencies where the insertion loss predicted by the model of Wood starts to drop to zero (but well below bubbles with the most encountered radius reach resonance), a model including the effects of bubble resonances seems best suited to predict the equivalent properties of water-bubble mixtures.
- The models of Commander and Prosperetti, Kargl, and Feuillade, which include the effects of bubble resonances, all predict very high values for the phase velocity and attenuation around the bubble resonance of bubbles with a radius dominating the bubble size distribution.
- Even though the models of Kargl and Feuillade contain a correction for the same physical phenomena (i.e. higher order scattering) compared to the results for the model of Commander and Prosperetti they seem to push the predicted values (and features of the curve) of the predicted phase velocity and attenuation in opposite directions.

7.3 2D models

The conclusions below are drawn based on the results from evaluating 2D FE models and the measurement data from the tests in the Concept Basin at MARIN.

- There are significant differences in the locations of the first peaks and throughs in the insertion loss curves between measurement and prediction. These differences may be related to the assumption of acoustically hard basin walls which may not be an appropriate assumption (using decidecade bands the effect would be most apparent at low frequencies).
- All three models including the effects of bubble resonances overpredict the insertion loss by many dB's in the region where the effect of bubble resonance is dominant (i.e. around the resonance frequency of bubbles that have a radius equal to the peak of the bubble size distribution).
- The model by Feuillade predicts the lowest insertion loss values in the region where the effect of bubble resonance is dominant and therefore approximates the measured data the best, while still too high.
- The modeling results show an overall increase of the insertion loss with increasing flow rate. The increase in insertion loss is especially large for the nozzle and porous configuration. The overall trend is that the difference in insertion loss between flow rate 1 and 2 is larger than between flow rate 2 and 3. The measurement results also mostly show an increase in insertion loss with increasing flow rate, but the relation is less consistent depending on bubble curtain type and frequency.

- The model results suggest that insertion loss will depend significantly on the bubble curtain type. In contrast, the measurement results show that roughly the same insertion loss is obtained independent of the bubble curtain type.
- Regarding the measured bubble size distribution and void fraction as a function of range:
  - The bubble size distribution for the nozzle and porous bubble curtain configurations are very similar, also for different flow rates. The bubble size distributions for the conventional bubble curtain are similar to each other at different flow speeds, but have bubbles of much smaller radii compared to the two other configuration.
  - The void fraction distribution as a function of width across the different bubble curtain configurations is similar in shape for the different air flow rates. As expected, the peak values for void fraction increase with air flow rate, reflecting that the total volume of air in the curtain grows with increasing flow rates.
  - All the bubble distribution curves resemble gaussian distributions. The width of the distributions for the nozzle and porous configuration are also relatively similar (with those for the porous configuration marginally wider but the peaks much lower), while the width for the conventional configurations is somewhat narrower (with the peak heights similar to the nozzle configurations).

The similarities and differences in the bubble size distribution and the void fraction across the curtain width that are observed between the different bubble curtain configurations can explain most of the observed differences in the modelled insertion loss curves.

7.4 Conclusions regarding bubble curtain performance

- In the frequency region where bubble curtain performance is mainly due to impedance contrast between pure water and bubbly water the performance may be increased by selecting a bubble curtain that results in a narrower curtain with a sharp changes in local void fraction (instead of a wide curtain with gradual changes in void fraction).
- The overall trend that is observed in measurement data is that increasing the flow rate will lead to an increase in insertion loss for most frequencies. However, the increase is not uniform and based on the current dataset a simple guideline for expected increase in insertion loss based on increase in flow rate cannot yet be given.
  - For the conventional bubble curtain, the overall trend is that the difference in insertion loss between flow rate 1 (33 nL/min/m) and 2 (66 nL/min/m) is larger than between flow rate 2 and 3 (102 nL/min/m). This suggests that a further increase in flow rate may yield only a small increase in performance.
  - For the nozzle and porous bubble curtain there are regions where the difference in insertion loss between flow rate 1 and 2 is larger than between flow rate 2 and 3 and there are regions where this difference is similar. This suggest that a further increase in flow may yield a significant increase in insertion loss.

The model data suggest that an increase in flow rate will lead to an overall increase in insertion loss and a further increase in flow rate will lead to additional increase in insertion loss. It must be noted however that the considered range of flow rates is relatively small and not necessarily representative of the intendent use case. In addition, if the bubble curtains are allowed to develop in a water column of larger height, a different trend in performance may be observed.

- The difference in insertion loss between the different bubble curtain types is small.
  - The differences are especially small for flow rate 2 and 3 (66 nL/min/m and 102 nL/min/m, respectively).

- For flow rate 1 (33 nL/min/m) the differences are larger for certain frequencies. The porous bubble curtain seems to offer the highest overall insertion loss. For the conventional and nozzle bubble curtains it is frequency dependent which curtain has the highest insertion loss.
- The observations are remarkable, since the measured void fraction and bubble size distributions do vary for the different bubble curtain types and the models using these as input suggest that these differences should have a significant effect.

In general, it can be concluded that insertion loss of bubble curtains increases with increasing void fraction, which can be achieved by increasing the air flow rate and limiting the dispersion of the bubbles. This effect can be predicted by models that describe the distribution of compressibility in the curtain. This is a dominant effect at the lower frequencies where unmitigated impact piling sound has the highest contributions to the unweighted broadband SELss. Effects of bubbles size distribution on the insertion loss at higher frequencies remain unclear.

7.5 Recommendations for further research

The considered equivalent fluid models are only successfully validated well below frequencies where bubbles having the most dominant bubble radius in a given distribution are at resonance. Interpretation of data from acoustical modeling at higher frequencies using these equivalent fluid models does not seem warranted.

Variation in hose type was expected to influence the insertion loss due to the different bubble size distributions the hose types create. However, the measurements in the MARIN CB do not confirm the expected relationship between hose type and bubble size distribution (with the conventional hose producing the smallest bubbles) and the measured influence of bubble size distribution on insertion loss appears to be small. Furthermore, the considered equivalent fluid models appear to overestimate insertion loss due to damping of bubble vibrations ate frequencies where these are resonating.
However, different hose types lead to a different distribution of void fraction through the width of the bubble curtain which influences the insertion loss in the frequency region below bubble resonances, where impedance contrast (between pure and bubbly water) dominates the insertion loss. The modelled insertion loss in this frequency range is closer to the measurements. The models should be further validated with full-scale measurements.

The air flow rates achieved in the scale model tests may not be representative for the final use case (sound mitigation of offshore pile driving using bubble curtains). In future measurements of the performance of bubble curtains under lab condition the full range of flow rates that are foreseen to be available for the final application should be sampled. To limit the effect of the zones where bubble behavior may be different compared to the rest of the curtain (i.e. where bubbles emerge from the hose and close to the surface), the trends should be investigated for larger water depths.

Given the uncertainty in the input parameters (void fraction and bubble size distribution) and limited knowledge on the validity of the models for the equivalent sound speed for the case of interest the complexity of the test setup for validating the acoustic models is challenging. A number of steps could be taken to increase the knowledge on the validity of the models for the equivalent sound speed in bubbly water:

- For validation and development of suitable equivalent fluid models, to test the validity of the available equivalent fluid models for relevant void fractions and bubble size distributions, it would be highly useful to carry out measurements on water-bubble

mixtures in a more controlled setting (e.g. a flow tube/bubble tube) so void fractions, bubble size distribution and the acoustic field can be better controlled (and the setup can be represented by 1D models).
- It would also be useful to find the transition between linear and non-linear behavior of the bubble clouds experimentally (for relevant void fractions and bubble size distributions, at different frequencies using a single frequency source) and asses if the sound levels during sound mitigation with bubble curtains surpass this transition point.
- It could also be useful to investigate experimentally if the applied broad band sweep signals are sufficiently representative of sound from impact pile driving, particularly above the threshold for non-linear behavior.
- These effects could also be studied by implementing a non-linear model.
- If non-linear effects are potentially important, the absolute level of the incident field becomes an important input parameter (even for insertion loss measurements). In that case, bubble curtain measurements as carried out in the scope of this project require a calibration of the source level.

The modeling results in this report show that the relation between the performance of bubble curtains and the way void fraction varies across the width of the curtain can be studied using 1D models. More knowledge on the effectiveness of bubble curtains at higher frequencies can be gained if the model that includes void fraction as a function of width is extended to equivalent fluids with damping.

There are significant differences in the insertion loss curves between measurement and prediction also well below bubble resonance frequencies. These differences may be related to the assumption of acoustically hard basin walls which may not be an appropriate assumption. The current FE model can be extended to include wave propagation in the basin wall and backing material to get a more representative reflection behavior. This approach requires knowledge on the (acoustic) material parameters of the basin wall and backing material (soil) and the basin wall thickness.

It is not expected that the acoustic performance of the considered bubble curtains change much when switching to salt water. The sound speed will change somewhat and the bubble size distribution and void fraction may also experience small changes by changing the salinity (due to differences in surface tension). It would be good to do a small parameter study to assess the expected influence of these changes in sound speed, bubble size distribution and void fraction due to changes in salinity. For instance, the current models could be re-run for values obtained with hydrodynamic model developed by MARIN for sweet and salt water (also adjusting the sound speed accordingly) with the aim of tracking the difference in acoustic performance.

References

[1] C. de Jong, B. Binnerts, M. Prior, M. Colin, M. Ainslie, I. Mulder & I. Hartstra, „Wozep – WP2: update of the Aquarius models for marine pile driving sound predictions," report TNO 2018 R11671, 2019.

[2] J. Wood, A textbook of sound, London: G. Bell and Sons Ltd, 1941.

[3] S.H. Medwin, Fundamentals of Ocean Acoustics, London: Acedemic Press Limited, 1998.

[4] T. Leighton, The Acoustic Bubble, London: Academic Press, 1994.

[5] L. Foldy, „The multiple scattering of waves. I. General theory of," *Phys. Rev.,* vol. 67, nr. 3-4, pp. 107-119, 1945.

[6] A. Mallock, „The damping of sound by frothy liquids," *Proc. R. Soc. A,* vol. 84, pp. 391-395, 1910.

[7] K. Commander & A. Prosperetti, „Linear pressure waves in bubbly liquids: Comparison between theory and experiments," *J. Acoust. Soc. Am.,* vol. 85, pp. 732-746, 1989.

[8] S. Kargl, „Effective medium approach to linear acoustics in bubbly liquids," *J. Acoust. Soc. Am.,* vol. 111, nr. 1, pp. 168-173, 2002.

[9] Z. Ye & L. Ding, „Acoustic dispersion and attenuation relations in bubbly mixture," *J. Acoust. Soc. Am.,* vol. 98, pp. 1629-1636, 1995.

[10] F. S. Henyey, „Corrections to Foldy's effective medium theory for propagation in bubble clouds and other collections of very small scatterers," *J. Acoust. Soc. Am.,* vol. 105, pp. 2149-2154, 1999.

[11] C. Feuillade, „The attenuation and dispersion of sound in water containing multiply interacting air bubbles," *J. Acoust. Soc. Am.,* vol. 99, pp. 3412-3430, 1996.

[12] P.A. Martin, „Acoustic scattering by one bubble before 1950: Spitzer, Willis, and Division 6," *J. Acoust. Soc. Am.,* vol. 146, pp. 920-926, 2019.

[13] L. van Wijngaarden, „One-Dimensional Flow of Liquids Containing Small Gas Bubbles," *Annual review of fluid mechanics,* vol. 4, pp. 369-396, 1972.

[14] A. Prosperetti, L.A. Crum & K.W. Commander, „Nonlinear bubble dynamics," *J. Acoust. Soc. Am.,* vol. 83, pp. 502-514, 1988.

[15] C. Feuillade, R.W. Nero & R.H. Love, „A low-frequency acoustic scattering model for small schools of fish," *J. Acoust. Soc. Am.,* vol. 99, pp. 196-208, 1996.

[16] L. Kinsler & A. Frey, Fundamentals of Acoustics, 2nd, Red., New York: John Wiley & Sons, 1962.

[17] M. Minnaert, „On musical air-bubbles and the sound of running water," *Philosophical Magazine,* vol. 16, nr. 104, pp. 235-248, 1933.

[18] T. Bohne, T. Grießmann & R. Rolfes, „Modeling the noise mitigation of a bubble curtain," *J. Acoust. Soc. Am.,* vol. 146, nr. 4, pp. 2212-2223, 2019.

[19] Brekhovskikh, Waves in Layered Media, New York: Academic Press, 1960.

[20] L. Kemp, M. van Rijsbergen & C. de Jong, „Bubbles JIP, Laboratory Tests, Model tests on a bubble curtain.," MARIN Draft report 31610 , 2023.

[21] M. van Rijsbergen, „Bubbles JIP | Hydrodynamic model of a bubble curtain (to be published),” MARIN, Wageningen, 2023.

[22] L. Kemp, M. van Rijsbergen & C. de Jong, „Bubbles JIP | Laboratory tests (to be published),” MARIN, Wageningen, 2023.

[23] M.L. Oelze, W.D. O’Brien & R.G. Darmody, „Measurement of Attenuation and Speed of Sound in Soils,” *Soil Sci. Soc. Am. J.,* vol. 66, pp. 788-796, 2002.

[24] K.L. Williams, „Sand acoustics: The effective density fluid model, Pierce/Carey expressions, and inferences for porous media modeling,” *J. Acoust. Soc. Am.,* vol. 125, pp. 164-170, 2009.

[25] M.A. Ainslie & T. G. Leighton, „Review of scattering and extinction cross-sections, damping factors, and resonance frequencies of a spherical gas bubble,” *J. Acoust. Soc. Am.,* vol. 130, pp. 3184-3208, 2011.

[26] M.S. Plesset, „The dynamics of Cavitation bubbles,” *J. Appl. Mech.,* vol. 16, nr. 3, pp. 277-282, 1949.

[27] E. Silberman, „Sound Velocity and Attenuation in Bubbly Mixtures Measured in Standing Wave Tubes,” *J. Acoust. Soc. Am.,* vol. 29, pp. 925-933, 1957.

[28] C. Feuillade, „Acoustically coupled gas bubbles in fluids: Time-domain phenomena,” *J. Acoust. Soc. Am.,* vol. 109, pp. 2606-2615, 2001.

[29] F.E. Fox, S.R. Curley & G.S. Larson, „Phase velocity and absorption measurements in water containing air bubbles,” *J. Acoust. Soc. Am.,* vol. 27, p. 534–539, 1955.

[30] W. Lauterborn & T. Kurz, „Physics of bubble oscillations,” *Reports on Progress in Physics,* vol. 73, pp. 1-88, 2010.

[31] T. D. Rossing, Springer Handbook of Acoustics, New York: Springer, 2007.

Appendix A

Literature overview

The main interest in this study is on models describing the effect of bubbles on the perceived macroscopic acoustic properties of bubbly liquids. Papers that exclusively describe work based on measurement data or are mainly focused on measurement data are only of interest in as much they contribute to the understanding and or validation of the theories underlying the models considered here. The overview of literature presented below is therefore focused on papers dealing with or related to modelling of the acoustic properties of bubbles in liquids. In paragraph X an overview was presented on the sub-models that can be identified in a bubble screen model. The considered literature can be grouped based on the focus each work puts on a sub-model.

- Papers on the acoustic properties of individual bubbles. The focus is on the describing the vibration behavior of the bubble surface and the resulting radiation or damping
- Papers on the sound speed of sound in liquid with bubbles. The focus is on the macroscopic effects of the bubbles on the acoustic properties, such as the speed of sound, of the bubbly liquid.
- Papers on the acoustic properties of bubble screens. These involve a bubble screen, a connected body of water without bubbles and an environment. The focus is on the interaction of sound waves with the bubble screen while traveling through the environment. Such models also require description of the distribution of bubbles in the screen and their size. These models are not related to acoustics and a description of the available literature on that topic is part of WPX.

The history of research on sound propagation involving bubbly liquids is long (the first papers date more than 100 years back) and the body of available work is fast. There is too much work to address all contributions. Therefore the following approach is adopted to report on the literature study that was carried out in the scope of the Bubble JIP.

- References to existing overview papers and books are provided;
- References to often sited papers that featuring key ingredients that are relevant to current models are provided;
- A more comprehensive overview and discussion of more recent work is presented.

A.1 Overview papers and books

The book of Leighton [4] contains an extensive summary of the fast body of available literature on the interaction of bubbles with acoustic fields. Besides many other topics the book coffers a number of topics that are relevant to the current study including non-linear effects, vibration of bubbles in shapes other than its breathing modes, and the relation between scattering cross section and transfer function between incident and scattered field (see Section A.3.5 for a short discussion on the information used from this publication).
A second work containing useful background information on some of the theory addressed in this report is the book of Medwin and Clay [3]. The topic of the book ocean acoustics and chapter eight is devoted to everything related to bubbles.
Two useful papers that give an overview of literature on the response of individual bubbles are the work of Martin [12] and the work of Ainslie and Leighton [25]. The work of Martin focuses on the history of the development of models for the response of individual bubbles and includes papers up to 1950. The work of Ainslie and Leighton includes more recent

work and focuses on the different definitions of extinction cross-sections, damping factors, and resonance frequencies used by various researchers and how these may be reconciled. Ainslie and Leighton cast the response of a bubble in terms of a scattering cross-section, while most of the other cited sources in this report regard the response of a bubble as a transfer function between the pressure of the incident field at the bubble and the pressure of the scattered field (at a reference distance). The relation between scattering cross section and transfer function between incident and scattered field for a damped forced oscillator is for instance given in the book of Leighton[13] [4]. This relation allows to re-interpret work done on scattering cross-section (for instance the overview of Ainslie and Leighton) in terms of a transfer function between incident and scattered field which is necessary to calculate equivalent fluid properties for bubble liquids.

A.2 Highlights of relevant developments

- A paper by Mallock [6] seems to be the earliest cited source for the effects of bubbles on the speed of sound and damping in a liquid. The citation is found in the book of Wood and the equation provided for the speed of sound in the mixture is the same (although in a different form) to that presented by Wood [2] (see the section on Absorption of Sound Waves in Turbid Media). The equivalent fluid model described in these sources is based on averaging the density and elasticity of the liquid and gas.
- An important ingredient of the models for the acoustic response of a single bubble is the relation between instantaneous bubble radius and pressure (at the bubble surface and at infinity). An early version of this relation is given by the so-called Rayleigh–Plesset equation which is based on the assumption of a spherical bubble in an infinite body of incompressible liquid. The initial equation was derived (without terms for surface tension or viscosity) by Besant but solved by Rayleigh [1917]. Plesset applied the equation to cavitation bubbles including the effects of surface tension [26]. The equations were extended to include (approximately) the effects of liquid compressibility by Keller and Herring (see [14] for references).
- Foldy [5] introduced an alternative averaging concept for modelling the contribution of scatters (such as bubbles) in a medium to its acoustic properties. He proposed to calculate the average response of a collection of scatters in a fluid by averaging over an ensemble of configurations of scatterers that correspond to a statistical description of the collection of bubbles.
  - The seminal paper of Commander and Prosperetti [7] merges a number of concepts put forward by earlier works. These include:
  - The model by Keller relating the change of the radius of a single bubble and the change in pressure at the bubble surface. The model includes:
  - the effect of surface tension and the effect of viscosity due to motion in the fluid surrounding the bubble.
  - A relation between the pressure on the outside of the bubble and the inside of the bubble involving surface tension.
  - A relation between the pressure in the bubble, the bubble surface velocity and the temperature field in the bubble including the effect of heat transfer into the fluid.
  - The statistical approach of Foldy to allow to theory to be applied to ensembles of bubbles with varying radii .
- The model proposed by Commander and Prosperetti only account for interaction of the incident field with individual bubbles. A model accounting for (multiple) interaction between bubbles in the form of group resonance was proposed by Feuillade [11].
- In the work of Bohne [18] the model of Commander and Prosperetti for the equivalent speed of sound is combined with a model for the void fraction and an model for the

[13] The relation is established by Equations 4.10 through 4.13 and Equations 4.20 through 4.27.

bubble size distribution in a bubble plume. Missing input parameters for the models for void fraction and bubble size are obtained by fitting the results of these models to data found in literature and obtained from measurement, respectively. The approach was used in combination with a transfer matrix method (in which the power transmission coefficient is calculated for horizontal slices of the bubble curtain which is averaged over depth) and in combination with a 2D hybrid FE/PE model (i.e. a short range FE model that is coupled to a PE model for predictions at larger ranges).

A.3 Discussion

In the scope of this study a large body of literature on acoustic properties of bubbles and bubbly liquids spanning many decades was consulted. It is perhaps unsurprising that some of these papers contain errors (of typographical nature, or other kind). What is somewhat surprising is that some of these errors have been passed on to later publications or fail to acknowledge errors in cited sources. Besides actual errors some papers contain phrases that are multi interpretable (worsened by the fact some texts are less accessible due to use of different jargon), fail to mention crucial assumptions or omit crucial steps in derivation of important expressions. Furthermore, at certain times conclusions from a source are used stripped from the nuance of the original context to justify approaches in later publications.

With this in mind, the discussion of work below aims to:

- Highlight the importance of certain pieces of work in the context of this study;
- Indicate if errors are present (and present a correction);
- Give an interpretation of phrasing that is multi interpretable;
- Add relevant statements on missing assumptions or key steps in the derivation;
- Evaluate the conclusions of a text in the context of that text and other publications;
- Accentuate the link between certain papers if relevant to the present study.

Publications are presented below in chronological order.

A.3.1 1941 Wood, A textbook of sound

The part of the book most relevant to the present study is the section on Absorption of sound in Turbid Media. The presented model is valid for non-resonant air bubbles in water. It is assumed that “the velocity of sound in a mixture of two fluid media” is “the same as that in a homogenous fluid of the same mean density and mean elasticity as in the mixture”. Although not mentioned explicitly, from the presented equations it becomes clear that the arithmetic mean of the density of both media is taken while the harmonic mean of elasticity is taken (accounting for the proportion of the constituents by volume in both cases). The velocity/speed of sound is taken as the square root of the elasticity over the density.
It is not explicitly mentioned if the elasticity is based on isothermal or adiabatic assumptions. Sadly, the units are not provided for the numerical example that is presented. The density of water is given as 1.0 which leads to the conclusion the units for density should be in kg per liter. The number provided for the density of air also makes sense in this unit. On the other hand, the stiffness is listed as 2.25e10 (again without units), which is problematic, since the typical value listed for water is 2.2 GPa. It seems that the value for stiffness should be divided by 10 to obtain a value of 2.2GPa. Under these assumptions, the sound speed for water in the example turns out to be 1500 m/s which is an often stated value. If these assumptions are applied to the value for air a sound speed of 316 m/s is found. This value is too low for the adiabatic sound speed in air under atmospheric conditions (ca. 344 m/s) but too high for the speed of sound in air under isothermal conditions (ca. 298 m/s). The value for the speed of sound that is taken approximately

equals the average value of the adiabatic and isothermal limits. It is not mentioned explicitly if this is a conscious decision and if so, why this is done.
Furthermore, the curve for the speed of sound as a function of void fraction shown in the book could not be recreated successfully using the provided equations and input parameters. The curve shown in the book (retraced) and obtained by evaluating the equations provided in the book are shown in Figure A.1. The values for the effective speed of sound of the curve in the book do seem to match the values predicted by the equations for the limits where the void fraction goes to zero and unity. Furthermore, the minimum value of the curve in the book and the equation are very similar, however the overall shape of the curve is different. Moreover, the curve in the book suggest the minimum is found for $\beta \approx 0.1$, while the minimum for the re-created curve based on the provided equations is found for $\beta \approx 0.5$. The latter of these values matches the value of the void fraction for the minimum found in other references (such as for instance van Wijngaarden [13]), suggesting the curve in the book is perhaps (inadvertently) created using an alternative expression for the effective speed of sound.

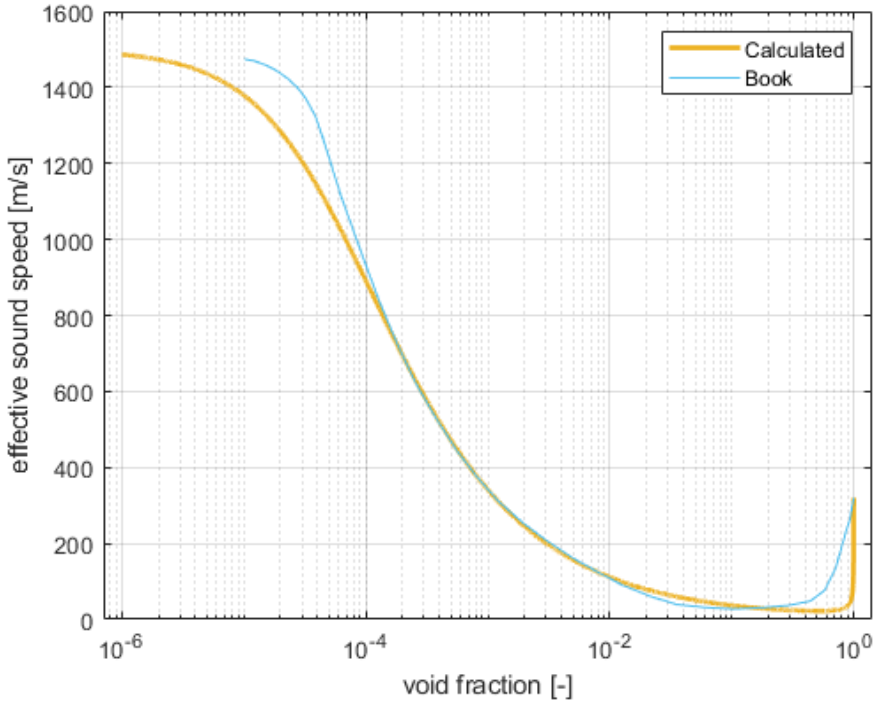

Figure A.1: The effective speed of sound as a function of void fraction for the example shown in the book of Wood [2] (retraced) and obtained by evaluating the associated equation for the input parameters provided in the book.

The book of Wood suggest that damping is provided by the large volume variations in the liquid surrounding each bubble. Later publications show that the viscous losses associated with the change in volume of the water surrounding the bubble do contribute to the damping but thermal and radiation losses are in general more significant (see for instance [4]). Note that in this approximation it is not relevant how the gas is distributed over the fluid other than that the distribution is in some sense homogenous (there are no specific patterns or concentrations of air) and the assumption holds that the volumes of gas are not at resonance.

A.3.2 1933 Foldy, The multiple scattering of Waves

The work of Foldy [5] concerns a wave propagation theory for multiple scattering of sound waves which are isotopically scattered by a random distribution of scatters. The interest is

in the averaged value of physical quantities, with the average being taken over a statistical ensemble of collections of scatterers. It is shown that the average of the wave function satisfies a wave equation for a continuous medium without scatters with a wave speed that is complex (and depending on the input, a function of position). The difference between the square of the average wave form and the average of the square of the waveform is usually referred to as the incoherent scattering term.

$$p_{sq,av} = \left|\frac{1}{\mathrm{n}}\sum_{n}^{i=1}\mathrm{p_i}\right|^2 \quad p_{av,sq} = \frac{1}{\mathrm{n}}\sum_{n}^{i=1}|\mathrm{p_i}|^2$$

The term ‘incoherent’ in this context is referring not to a lack of definite phase relationship between the incident wave and the wave scattered by a particular scatterer, but to the statistical superposition of these scattered waves when propagated to the point of observation because of the random distribution of the scatterers. The average of the square of the wave function at any point is equal to the square of the average wave function at the point plus a contribution representing scattering from all other portions of the medium.

Note that although the theory of Foldy allows the statistic properties of the ensemble of bubble collections to vary with distance (continuous or sectionally continuous) there may be limits to the suitability of position dependent statistical properties when the theory is combined with certain scattering models. One of the assumptions required by the theory of Foldy is that the response of the scatterers are independent. This is for instance not the case in the model proposed by Kargl [8]. In that model the expression for the damping due to radiation is depend on the sound speed of the effective medium, which is influenced by the surrounding bubbles. If the statistical properties of the ensemble do not vary, this does not lead to complications since the effective speed of sound is identical everywhere (the effect that neighboring bubbles have is independent of positions). On the other hand, if the statistical properties change with position, the influence of neighboring bubbles (experienced through the effective sound speed) becomes dependent on their position, which is not supported by the theory proposed by Foldy.
A similar issue is encountered when the statistical approach proposed by Foldy is combined with the scattering model proposed by Feuillade [11]. In the model of Feuillade the interaction between bubbles is fully accounted for, however positional dependence is not explicitly incorporated in the theory. In Feuillade’s theory bubbles have a limited area of influence which he calls the ‘region of collective interaction‘ “beyond which no multiple scattering interactions take place”. This suggest that if changes in statistical properties are small on the length scale of the ‘region of collective interaction‘ the resulting errors due to assuming they are constant locally are probably negligible. Feuillade himself does not discuss the possibility of position dependence and a threshold below which a rate of change in statistical properties leads to acceptable errors is not available.

A.3.3 1957 Silberman, Sound Velocity and Attenuation in Bubbly Mixtures Measured in Standing Wave Tubes

The work of Silberman [27] includes an important source of measurement data used by other papers (for instance [7] [8] [11]) to validate their models.
Silberman uses an expression for the effective speed of sound in a mixture of fluids that is not equal to equation (3.8), stating “Woods formula may be written”

$$\left(\frac{c_w}{c}\right)^2 = \left(1-\beta+\frac{\beta E_w}{P_0}\right)\left(1-\beta+\frac{\beta\rho_g}{\rho}\right) \tag{A.1}$$

The expression is re-written here using the symbols introduced earlier in this document. Similar to the work of van Wijngaarden [13] (See Appendix B), the formula presented is actually not found in the book of Wood that is referenced [2]. Silberman also states: “The formula is derived under the assumption that the bubbles pulsate isothermally”, which is not explicitly mentioned in the book of Wood. The expression given by Wood can be made identical to that of Silberman under the assumption that the following approximation holds for the bulk modulus of the gas and the pressure in the bubble

$$E_g = P_0 \tag{A.2}$$

which is valid if the bubbles are assumed to pulsates isothermally, **and** if the approximation is made that the density of the mixture equals that of water

$$\rho = \rho_w \tag{A.3}$$

which only holds for $\beta \ll 1$. This assumption is not mentioned explicitly in the work of Silberman. See Appendix B for a discussion of the difference between the expressions used by van Wijngaarden and Wood.

A.3.4 1989 Commander and Prosperetti, Linear pressure waves in bubbly liquids: Comparison between theory and experiments

In the work of Commander and Prosperetti [7] the following features are combined for the first time in a model for the behavior of liquids with bubbles

- Expression for the average response of a field of point scatterers (bubbles);
- Expression for the response of individual bubbles;
- Expression for frequency dependent damping terms accounting for the effects of radiation of bubbles to the fluid, heat flow in the gas, and viscosity of the fluid surrounding the bubbles;
- Expression for frequency dependent stiffness accounting for the effects of heat flow in the gas;
- Expression for damping and stiffness at frequencies away from resonance;
- Expressions derived from ‘first principle’ equations, i.e. conservation equations for mass, impulse and energy combined with suitable equations of state.

Work in the literature prior to the work Commander and Prosperetti may include one or more of these features but does not include them all.

It was already mentioned that the second term in the expression for the damping term b (equation (33)) in [7] appears to be missing a factor 1/ω. This factor is included in the work of Kargl [8] that builds on and references the work of Commander and Prosperetti. The missing term influence the predicted equivalent sound speed significantly and without this factor the plots in the work of Commander and Prosperetti cannot be reproduced correctly.

The work of Commander and Prosperetti includes a comparison between model results with many datasets. The considered data sets include cases for bubble ensembles of single radius, multiple radii and a distributions of bubble radii.
One of the main conclusions is that the theory works well for small void fractions and away from resonance. Criteria to quantify this are provided in the conclusion section. These criteria are based on the notions that the current theory will fail if “the average pressure field exciting a bubble is smaller than, or comparable with, the pressure wave scattered by a neighboring bubble” and the condition that “the multiple scattering field caused by the

insertion of a bubble be much smaller than the field exciting that bubble" should be satisfied. A third criteria provided depends on "condition of negligibility of two-particle correlation effects". In short, all these conditions relate to the fact that the theory presented by Commander and Prosperetti does not include bubble-bubble interaction and is expected to fail under conditions where bubble-bubble interaction is expected to become important. The criteria are frequency dependent and depend on void fraction directly or indirectly (through dependence on the number of bubbles). All criteria indicate the model will fail for higher void fractions and all criteria will become very stringent around bubble resonance. In other words, bubble-bubble interactions are expected to become important if bubbles are positioned in close proximity and/or if they are close to resonance.

The tone of the discussion in the conclusion suggest that the main reason for the break down close to resonance may not be due an inappropriate description of the behavior of individual bubbles close to or at resonance, but is linked to the fact that the model does not include the effects of interaction between multiple bubbles. This suggest that a model that correctly includes such interactions may be suitable for use at higher void fractions and/or closer to bubble resonance. On the other hand, the derivation requires many approximations needed for linearization. There is also an ad hock multiplication with a seemingly arbitrary term in final stage to arrive at the form of a harmonic oscillator after neglecting further terms (the authors indicate that these steps should lead to an acceptable approximation). The authors are aware of the limitations inherent to their approach and mention that "For the small-amplitude regime to which we have restricted our considerations, more sophisticated treatments than that afforded by the linearization of the model presented ... are available in the literature and it is conceivable the at a better agreement with the data can be obtained by use of some of those results." However, no criteria are provided to assess under which conditions the linearization steps and other approximations lead to acceptable errors. It is important to note that it is to be expected that the amplitude of the bubble vibrations is comparatively large at and close to resonance. Including bubble-bubble interaction may therefore be a necessary step towards extending the model to be appropriate to cases involving bubbles at or close to resonance, but it may only constitute a partial solution since non-linear effects and errors due to other approximations may quickly become significant in that regime.

Note that the provided criteria for the model results to not be dominated by errors due to omission of bubble-bubble interaction apply to the situation of bubbles of a single radius. It is mentioned that the measurement data for collections of bubbles with multiple radii suggest that the theory seems to work better (i.e. for higher void fractions) if there is a large spread in bubble radius. This can be related to the fact that the effect of bubble-bubble interaction is strongest for neighboring bubbles with similar resonance frequencies, and becomes less important as one of the bubbles involved in an interaction is farther away from resonance. If for a given void fraction the gas volume is spread out over a large range of bubble radii the number of bubbles that have a similar resonance frequency is smaller compared to a collection of bubbles of identical radius. Therefore, the effect bubble-bubble interaction remains limited even at higher overall void fractions. No guidance is given by Commander and Prosperetti on how the effect of a spread in bubble radii changes the criteria for void fractions that lead to acceptable results.

A.3.5 1994 Leighton, The acoustic bubble

For the case of non-linearity due to large vibration amplitudes there are different regimes identified. Three regimes that are described are excitation of higher harmonics, transient behavior (leading to growth and/or collapse of bubbles) and chaotic behavior. Criteria for the onset of non-linear behavior are not provided however, but identifiers (such as the presence of subharmonics and harmonics) are discussed.

The book also addresses vibration of bubbles in shapes other than breathing modes and the connection with the excitation of breathing modes is discussed. The main conclusion appears to be that oscillation in such shapes do not contribute significantly (also not through their coupling with the breathing mode) unless there is a mechanism delivering energy to such modes.
Relation between scattering cross section and transfer function between incident and scattered field for a damped forced oscillator is given in Section 4.1.2 of the book. This allows to interpret work done on scattering cross-section (for instance the overview of Ainslie and Leighton [25]) in the context of calculating equivalent fluid properties for bubble liquids.

A.3.6 1995 Ye and Li, Acoustic dispersion and attenuation relations in bubbly mixture

The work of Ye and Li [9] casts the problem of describing bubble-bubble interaction as a multiple wave scattering process which extends the work of Foldy [5]. They use the perturbative Feynman-diagram method to study the acoustic properties of bubbly mixtures, limiting their research to the case where waves are scattered by the same scatterer only twice, i.e., a second order correction to the theory of Foldy.
Besides giving an expression for the correction term, they provide a criterium for when this term due to second order scattering is needed for the case of single size bubbles. They also provide a guide on limiting behavior; For very low frequencies and frequencies well above the resonance frequency the correction term tends to zero. This indicates that for low frequencies the classical theory as described by C&P should suffice.
The numerical results show increase in damping and phase speed due to the correction term for most frequencies. These results are not in line with the trends in the corrections shown by Feuillade [11] [15] although the form of the correction term is similar[14].

A.3.7 1995 Feuillade et al., A low-frequency acoustic scattering model for small schools of fish

The work of Feuillade et al. [15] describes a model based on a self-consistent approach that describes full bubble-bubble interaction instead of using a scattering series. The authors state that “When applied to bubbles this predicts the important outcome that multiple scattering processes can have the effect of reducing the scattered acoustic pressure field, while broadening the bubble resonance and shifting the peak to a lower frequency.” They go on to say that “The model indicates that, for larger schools of commercially important fish in deep water, multiple scattering effects may severely reduce the target strength at frequencies close to the swim bladder resonance. The collective effects on the scattering of a single individual in a school show more fluctuations as the school size increases.” And point out that the model can be implemented to describe scattering from small bubble clouds, which Feuillade does in subsequent papers [11] [28].

A.3.8 1996 Feuillade, The attenuation and dispersion of sound in water containing multiply interacting air bubbles

In the work of Feuillade [11] the equations for the average sound speed of a bubble liquid mixture as presented by Commander and Prosperetti are derived in a slightly different way.

[14] With Equations (17)(18) in [8] Ye and Li arrive at a similar result to that obtained by Feuillade [10]. An identical expression is obtained if the Taylor expansion of Equation (36) in [10] is taken in terms of F around $F = 0$ and it is assumed that evaluation of the integral $\int_0^\infty re^{-ikr}\,dr$ equals $i/(2k)$.

The alternative derivation makes the connection with the equation of motion for a damped resonator and the scattering cross section explicit (in Commander and Prosperetti the equations are also cast in this form, but in an ad hoc manner). Feuillade illustrates that the solution by Commander and Prosperetti does not include effects due to bubble-bubble interactions. He proposes an approximation to include the 'symmetric mode' of bubble-bubble interaction where neighboring bubbles interact with each other and vibrate in unison and demonstrates these interactions can contribute significantly. The effect is a lowering of the damping and phase speed at and around bubble resonance and a shift of the resonance peak to lower frequencies.
Note that although most of the derivation of the presented work is either from first principle or based on established work an important aspect of how the theory is used in this publication is based on interpretation. In the expression for the equivalent speed of sound an integral from zero up to infinity is used over a term that is representative of the effect of propagation due to travelling between interacting bubbles. This integrant exhibits oscillatory behavior and its average value grows to infinity with increasing integration range. This makes direct evaluation of this integral impossible if the medium has no damping (i.e. if the sound speed of the host medium is used). On the other hand, If the equivalent sound speed is used based on a calculation without multiple bubble interaction (i.e. the theory in C&P) the effect of damping is so strong that the correction term becomes negligibly small. Feuillade argues that the proper value for the sound speed that needs to be used in the integral is dependent on the to the original scatterer. He proposes that the wave number of the water should be used up until a certain number of contacts with other bubbles. These first interactions change the equivalent sound speed so that the radiated field is damped out to levels that are no longer significant (i.e. the first interactions shield other bubbles). He does not comment on how this transition should occur, but proposes to evaluate the integral only up to a certain range (he uses the term radius of a sphere of influence) using the sound speed of the host medium. He then sets out to determine the appropriate range by fitting model data to measurement data for the cases considered in Commander and Prosperetti [7] and Fox [29].

For bubble ensembles with a single bubble radius and void fractions between 0.22% and 1% he gets radii for the sphere of influence that approximately contain a constant number of bubbles independent of bubble size and void fraction (ca. 8-9 bubbles). There is no measurement data presented for cases with larger void fractions. For cases with smaller void fractions the number of bubbles in the sphere of influence after fitting is found to be smaller (ca. 2-3 bubbles). Fueiladde does not provide a reason for this transition in behavior. Note that the fitting is always done using the predicted damping coefficient, since the data points for measured phase speed is limited. For the one case where more measured phase speed data points are available the prediction of the phase speed was overestimated using a sphere of influence containing only 2-3 bubbles, while a better match was obtained using a range leading to 8-9 bubbles in the sphere of influence.

Feuillade also considered two datasets with collection of bubbles with multiple radii. He fits the data using only one radius of influence which he admits is questionable since the radius depends on the number of bubbles per unit volume, which is dependent on bubble size for a given void fraction. He observes that the number of bubbles in the sphere of influence is larger than what he expected based on other cases with void fractions below 0.22%. A measurement dataset from Fox [29] is also considered involving an ensemble of bubbles with a distribution of bubble sizes. Again, Feuillade fits a single radius of the sphere of influence to the data for the damping coefficient. He finds a better match than the prediction by the model of Commander and Prosperetti using the same bubble size distribution and void fraction as input, but the match with the new model is less favorable than for previous cases. He then proceeds to fit the void fraction using the Commander and

Prosperetti model (i.e. he does not use the measured void fraction) and gets a better match. Feuillade tentatively concludes that these results be explained by the fact that measuring the void fraction accurately is difficult with such low void fraction values and the void fraction used in evaluation of his own model may be incorrect.

Based on these findings he concludes that the theory for multiple scattering is not needed for collections of bubble including a distribution of radii. This is in line with the conclusion of Commander and Prosperetti that for collections of bubbles including multiple radii the bubbles of similar resonance are spaced much further apart for a given void fraction compared to the case of single bubble radius with the same void fraction. However, it must be noted that both cases with a distribution of bubble radii that are considered by Feuillade have very low void fractions. Therefore, the possibility that the theory presented by Feuillade may be crucial for cases with a distribution of bubble radii at higher void fractions cannot be excluded.
Moreover, since Feuillade suggest that the results of the comparison at low void fraction values may unreliable since measuring the void fraction accurately is difficult at low void fraction values the overarching conclusion should be that any conclusions based on data for low void fraction values should be treated with caution.

A.3.9 1999 Henyey, Corrections to Foldy's effective medium theory for propagation in bubble clouds and other collections of very small scatterers

Henyey [10] takes the work of Ye and Li [9] and expands it to include additional higher order terms. He derives an analytic expression for the effective sound speed that includes all higher order terms of the scattering series.
In the derivation assumptions are made regarding when to use the wave number for the fluid and when to use the effective wavenumber when propagating between bubbles, making the model approximate. More specifically, as part of his derivation Henyey proposes to substitute the wave number in the fluid with that of the equivalent medium after scattering on a bubble has occurred, to account for the fact that after interaction with a bubble traveling distances through the medium involves the wave number in the equivalent medium. In contrast, in the work of Ye and Li and the work of Feuillade only the wave number in the fluid is used. However, the reasoning of Henyey to include the effective wave number for part of the propagation closely follows the arguments of Feuillade to only evaluate the integral which accounts for propagation between bubbles over a limited distance (see Section A.3.8). Both assumptions aim to accounting for the fact that propagation between scatterers cannot exclusively be described by the wave number of the fluid or the effective wave number. In fact, the expression obtained by Henyey for the effective wave number is identical to that provided by Feuillade if we set the integral

$\int_0^\infty re^{-ikr}\,dr$ in Feuillade to equal $i(K-k)/(4\pi N)$.

Henyey addresses the differences between his result and that of Feuillade and indicates that the order of the correction terms in Feuillade does not match the theory as proposed by Foldy. He demonstrates that a quadratic term of the form f^2 should not be present, but this is found in the theory of Feuillade upon taking the Taylor series in f. The theory proposed by Henyey and Ye and Li do not have a quadratic term, but include the next term f^3.
Note however that the integral in Feuillade is not evaluated up to infinity but up to a range that is determined by fitting. There is no expression given for this range, but it may dependent on f, making the quadratic term in the Taylor expansion of Feuillades

expression of a higher order, which would defuse the argument made by Henyey. Note that changing the range does not allow to match the expression of Feuillade to that of Henyey. Either the real or imaginary, or the absolute value or phase can be matched, but not the complementary value of one of these pairs, implying the two theories will resulting in different predictions independent of the choice of the bound of the integral in the solution of Feuillade.
Henyey also shows that for large values of the effective wavenumber compared to the wave number in the fluid the cubic term introduced by Ye and Li is largely cancelled by higher order terms (which are present in the expression by Henyey). This implies the result of Ye are invalid in case the actual effective sound speeds leads to large damping or large phase speeds (note that this does not imply that if small values are predicted by the model of Ye and Li it is guaranteed that their theory is correct).

Henyey also provides guidance on if and when the approach is valid for media that are (statistically) not uniform in space. He states “equation (11) is derived in a uniform medium. Clearly, one cannot use Ye and Ding’s evaluation of the integral when F and K are functions of position. Since the integral is dominated by r on the order of $1/(k+K)$, presumably one should use averages over such a sphere in the correction. If F and K vary little on the scale of $1/(k+K)$, then equation (11), evaluated locally, should be correct.“

Henyey does not provide any results from his theory. The expression that is given for the equivalent sound speed is implicit (i.e. it depends on the equivalent sound speed itself) and requires solving before obtaining an explicit expression for the equivalent sound speed. It can be solved iteratively, or it can be rewritten in the form of a cubic equation for K. Solving this cubic equation yields three roots. Since no solutions to an example are given in Henyey’s paper, both solutions where implemented[15] and used on the examples presented in Commander and Prosperetti [7]. The real and imaginary part of the equivalent sound speed predicted by the theory of Henyey and Commander and Prosperetti are given in Figure A-1 for an example in the form of parametrized curves (with frequency being the parameter that is varied). Note that for the third root resulting from the cubic equation in Henyey the negative value is plotted. This is done for readability (the plotting area is doubles otherwise), but this does not constitute a valid solution to the cubic equation! In fact, all values associated with this root lead to unphysical behavior (negative damping and negative phase speed).

[15] Note that for the form of the cubic solution that was used the branches in the different (quadratic) roots in intermediate solutions are determined by the software used for implementation (Matlab). The choice of these branches leads the three roots to ‘switch places’ depending on the frequency that is evaluated. It is possible to ‘untangling’ the results to arrive at three series of roots that depend ‘continuously’ on frequency.

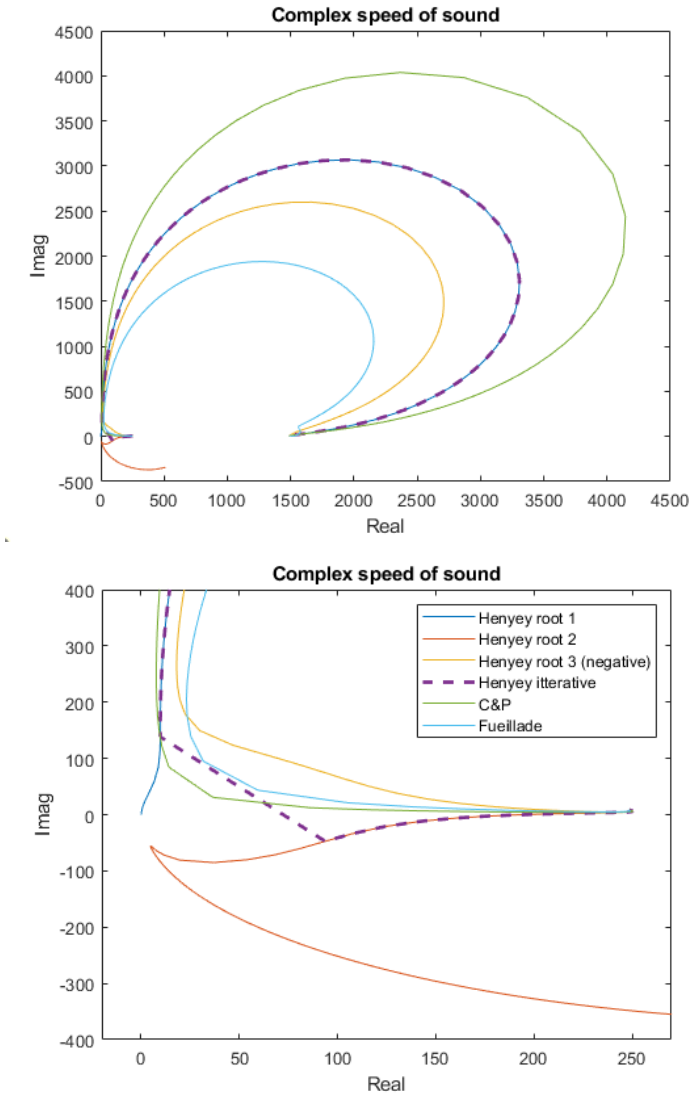

Figure A.2: Parametrized curves for the solution to the expression for the speed of sound in the complex plane for the model of Commander and Prosperetti (C&P), Henyey and Feuillade (with frequency being the parameter that is varied). The example corresponds to Figure 3 in Commander and Prosperetti with a collection of bubbles having a radius of $r = 1.77$ mm and a void fraction of $\beta = 0.22$ %. For the third root resulting from the cubic equation in Henyey the negative value is plotted. This is done only to limit the required plotting area, but this does not constitute a valid solution to the cubic equation. In the high frequency limit all curves approach speed of sound of the pure liquid, which is expected (see [3]). The lower plot is a zoomed in version highlighting the upper plot around the origin. In this plot it can be observed that not all solutions convergence to the same value for the speed of sound in the low frequency limit.

The associated real part of the sound speed and damping coefficient α of all solutions are plotted as a function of frequency in Figure A.2.

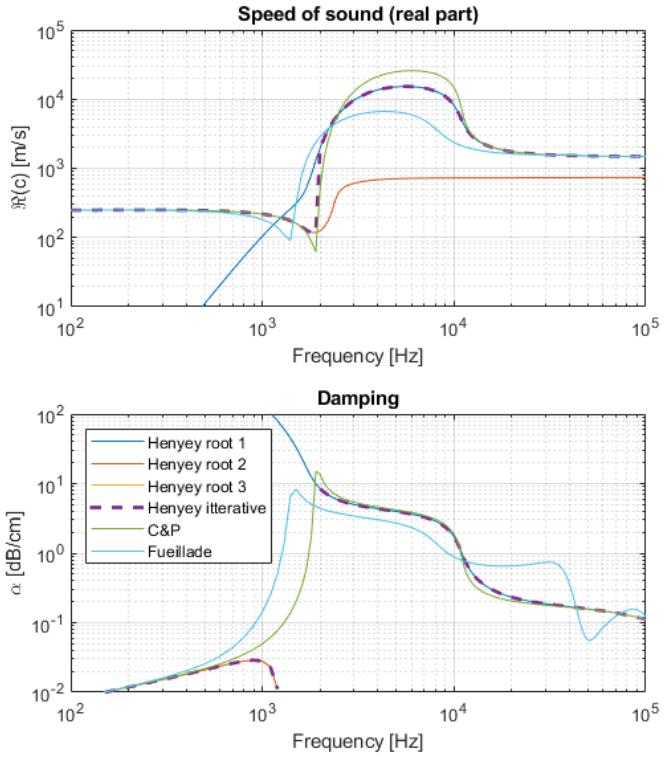

Figure A.3: The real part of the sound speed and damping coefficient α for the models of Commander and Prosperetti (C&P), Henyey and Feuillade as a function of frequency. The example corresponds to Figure 3 in Commander and Prosperetti with a collection of bubbles having a radius of $r = 1.77$ mm and a void fraction of $\beta = 0.22$ %. The underlying data for these plots is identical to that for the curves in Figure A.2. Note that the third root of the solution of Henyey lead to negative values for phase speed and damping and cannot therefore not be plotted on a log scale.

Each series of roots is different and only one leads to values that make physical sense (i.e. yielding a positive damping value and phase speed for all frequencies). This solution (root 1 in Figure A.1 and Figure A.2) does however not converge to the speed of sound predicted by Wood's equation and the theory of Commander and Prosperetti, which are known to correspond well with measurement in the low frequency limit. Instead, this solution converges to a sound speed and damping of zero for low frequencies. An additional solution was obtained by iteratively evaluating the expression in Henyey (starting with the solution provided by Commander and Prosperetti, since the starting value for the equivalent sound speed needs to include damping to get a non-trivial solution). This solution matches with the series of roots yielding physical values for most frequencies. Furthermore, below the frequency at which the solution from solving the cubic equation and solving it iteratively match the solution for Commander and Prosperetti, the solution from iteratively solving the equation iteratively 'jumps' to one of the other series of roots (one that converges to the sound speed predicted by Wood's equation and Commander and Prosperetti). However, with exception of the lowest frequencies ($f < 1300$ Hz) that solution consistently predicts negative damping values which is unphysical (since it implies sound levels are predicted to grow while traveling through the medium at these frequencies).
This leaves the theory in an awkward position: None of the individual solutions from solving the cubic equation predict both the converge at low and high frequency correctly (these converge behaviors have been demonstrated in measurements countless times) and produce physically relevant values. Only one solution produces consistently physical results, but that solutions does not converge to the expected value at low frequency. The iterative

solution does converge at high and low frequencies and matches solutions from solving the cubic equation, but 'jumps' at a certain frequency[16] to a different series of roots and has a region where its predicted values lead to unphysical behavior.
Note that the solutions of the cubic equation have been tested to indeed make the cubic expression equal to zero. It was tested that this also minimizes the residue of summing all terms of the original equation for K^2 after bringing all terms to one side. The same is true for the iterative solution since it always matches one of the roots. It can only be concluded that either the solution published by Henyey contains an unknown error or the solution strategy presented by Henyey, while based on an exact solution to the problem laid out by Foldy, does not automatically lead to a valid solution for the problem of finding equivalent fluid properties for a bubbly liquid (perhaps due to the assumptions made in the derivation). Note that the approach may still lead to valid solutions (or a useful approximation) under certain conditions, but a mention of the shortcomings listed above or guidance on when the proposed approach is expected to be successful is not given in the paper by Henyey. Based on the finding described above (and the comments of Feuillade on this approach in a later publication [28], see Section A.3.10) it was decided not to use the model proposed by Henyey for any calculations related to the properties of the bubble screens characterized by MARIN in the scope of the Bubble JIP.

A.3.10 2001 Feuillade, Acoustically coupled gas bubbles in fluids: Time-domain phenomena

In a later publication [28] Feuillade indicates that the theory of Foldy [5] (and all work based on it) may not lead to correct results in all cases. There is a fundamental difference between accounting for multiple interactions between objects with an infinite series of correction terms (i.e. the approach used by Foldy [5], Ye and Li [9] and Henyey [10]) and accounting for multiple interactions by considering a system of mutually interacting objects at once. A series of corrections may diverge if strong scatterers (such as resonating bubbles) are in close proximity of each other. As mentioned above, it is also not immediately clear that even if convergence of a series of correction terms is observed the solution will describe equivalent fluid properties correctly. Furthermore, it is not immediately clear which order of correction is needed to arrive at a suitable approximation. After examining a system of two bubbles Feuillade explains the difference between his approach and that using a multiple scattering series as follows:
"When the two bubbles are far apart the coupling is weak, and the rate of energy exchange due to cycling is less than the rate of energy loss which each bubble experiences as a result of its individual damping mechanisms. In this case, the time variation of the scattering amplitude of each bubble is predominantly determined by its damping parameter α rather than the cycling frequency... The interaction between the two bubbles can be treated as a perturbation of their individual motions, and characterized as a multiple scattering process whose magnitude may be determined via a power series expansion.
When the coupling is strong, however, so that the rate of energy exchange due to cycling is greater than the rate of individual energy loss due to damping ... the perturbation picture is no longer valid. The energy "stored" in the coupling is so great that it dominates the behavior of the two bubbles, which can then no longer be individually resolved insofar as the scattering process is concerned. In this case, a fully coupled self-consistent description

[16] Note that the 'jump' is a result of the relative 'distance' the starting value of the iteration has to the different solutions of the cubic equation. In the present study the C&P solution was used as a starting point. Above the frequency where one of the roots matches the C&P solution, this root is always the solution closest to the C&P solution and the iterative solution will converge to that root. For low frequencies that root converges to zero, while the C&P solution converges to the speed of sound predicted by Wood's equation. Another root also converges to the appropriate speed of sound in the gas for low frequencies, but as frequency goes up, this root exhibits negative damping. The iterative solution 'jumps' to this root for low frequencies, since this root and C&P converge to the same value.

is strongly indicated if the behavior of the ensemble is to be accurately determined. We can now see that the multiple scattering and self-consistent approaches to describing acoustic interactions between the two air bubbles should not be viewed as alternative ways of looking at the same phenomenon. Due to the strongly resonant character of bubbles, they actually represent distinct physical pictures. The multiple scattering approach imposes a paradigm which implicitly incorporates discretely separated scattering events as the primary means of energy exchange. The self-consistent methodology, conversely, while capable of characterizing the system as an interaction between multiple scatterers, can also describe it as an interaction between strongly coupled resonators wherein the energy exchange is primarily due to radiative cycling rather than scattering. Only when $|fe^{ikd}/d| \ll 1$ *are the two approaches formally equivalent."*

It is added that the conditions required for validity of the counting approach (which are provided for the case of two and three bubbles) will be more restrictive if additional bubbles are added. Feuillade expresses that he believes these that very tight restriction will also result for bubble ensembles consisting of multiple bubble radii (although he does not prove this).

A.3.11 2002 Kargl, Effective medium approach to linear acoustics in bubbly liquids

An alternative approach to solve the problem of multiple scattering is proposed by Kargl [8]. He identifies that the models of Commander and Prosperetti [7] (and by extend that of Ye and Li [9] and Henyey [10]) contain a system of equations that is not internally consistent. The expression for the response of the scatterer that is used in these models depends on the properties of the medium (such as the speed of sound) in which the bubbles reside. For instance, in the work of Commander and Prosperetti the sound speed and density that are used to evaluate the response of the scatterer are the values for pure water. Kargl argues that the response of the scatterer would be different if the properties of the effective medium are used, and that this is a more natural choice since the bubble interacts not with pure liquid but with a bubble mixture which is characterized by the equivalent medium properties. For instance, the ability of a scatterer to radiate sound should be considered using the effective impedance of the medium (bases on the equivalent speed of sound) and not the impedance of the undiluted medium. He deduces that for small void fractions the influence of taking the values for pure water instead of those for the equivalent fluid is small for most properties, with the exception of the speed of sound. His proposed method for solving the inconsistency in the model involves iteratively solving the expression for the sound speed proposed by Commander and Prosperetti (which makes the solution internally consistent if the iterative proses converges).
It is relevant to note that Feuillade [11] and Henyey [10] argue that the speed of sound that is used in their models to calculate the effect of traveling from one bubble to its nearest neighbor/neighbors is the unperturbed speed of sound, and only after re-scattering should an adjusted speed of sound be used. This specifically concerns the propagation between bubbles and does not involve the calculation of the scattering strength of the bubbles which is the focus of Kargl's proposed amendment to the Commander and Prosperetti model. Feuillade and Henyey do not explicitly address the issue of self-consistency, and the iterative approach proposed by Kargl could in theory also be applied to the models of Feuillade and Henyey. This was however not attempted in the scope of this study.
Note that the effects of Kargl's proposed iterative approach seems to be more or less opposite to the effects of including the effects of higher order scattering as is included in the models of Feuillade and Henyey.

The work of Kargl only includes a comparison between model and measurement data for one example. Measurement data is only available for the attenuation coefficient and the model of Kargl does not seem to offer an immediate improvement in fidelity of the results compared to the results of Commander and Prosperetti for the provided example.

A.3.12 2010 Lauterborn and Kurz, Physics of bubble oscillations

The work of Lauterborn and Kurz [30] contains an overview of the field of acoustic (and non-acoustic) interaction with bubbles in liquids. The publication contains a summary of three models of a bubble as an non-linear oscillatory system. All of these models include the effect of viscosity, surface tension and vapor pressure on the bubble oscillation. Two of these models include the effect of radiation by the bubble into the surrounding medium. The models do not explicitly include the effect of heat transport inside the bubble and over the bubble boundary (which is included in the linearized model of Commander and Prosperetti and the work based on it). Closed analytical solutions to the above bubble models are not known except for the empty bubble. The equations of motion for the bubble radius as a function
of time can be solved after initial conditions for the radius and for the velocity of the bubble wall have been specified. This has been done for a substantial part of the parameter space (with the main parameters of interest being the bubble radius
at rest, the sound field parameters pressure amplitude, and sound field frequency). However, due to the vast parameter space, the properties of spherical bubble oscillations are still not fully explored. Lauterborn also describes the different regimes (from linear behavior, through hysteresis, higher harmonics and subharmonics ending in chaos) that are observed when the amplitude of the driving signal exciting the bubble is increased. The publication does not deal with equivalent fluid properties of bubbly liquids and guidelines on when non-linear effect become relevant (for instance to estimating equivalent fluid properties) are not provided.

A.4 Summary

The field of acoustic models for the propagation of sound waves in bubbly liquids is not yet settled. The literature suggests that the propagation of sound waves in bubbly liquids can be modelled with good accuracy using linearized models for bubble clouds with bubbles of equal radius and for small amplitudes. However, for bubble clouds with a distribution of bubble radii experimental validation proves less successful and the considered distributions (relevant for bubbly liquids due to ocean waves) are not representative for the case at hand (bubble curtains).
In addition, there is still debate to what extend bubble-bubble interaction is relevant (for specific cases) and how it can be modelled best depending on the circumstances. In cases the interaction is relevant, bubble pairs/systems respond as a collective and instead considering the aggregate of individual responses does not lead to meaningful predictions (e.g. not including bubble-bubble interaction can lead to significant overestimation of damping and sound speed for certain cases). Modelling of bubble-bubble interaction for systems with a distribution of bubble radii and the validation thereof has not been attempted.
Apart from the literature on linearized system of equations describing bubble vibrations which is mainly cited here, there is an ample amount of literature available on models representing the non-linear regime suitable for larger amplitude vibration of bubbles (for in introduction/overview see for instance [30] or [31]). These publications are in general focused on the response of individual bubbles and tend to not include a derivation of equivalent fluid properties. A derivation for equivalent fluid properties include non-linear effects are presented in the literature for certain limiting cases (see Chapter 8 of [31] for an

overview). A derivation for expressions of equivalent fluid properties for the general case (arbitrary amplitude and frequency content) appears to be a non-trivial task and was not found in the literature. Moreover, criteria for when non-linear effects become significant to the equivalent fluid properties of bubble-fluid mixtures could also not be found in the literature.

Appendix B

Adiabatic vs Isothermal speed of sound

Note that van Wijngaarden [13] gives a different equation than the expression in equation (3.8) for the equivalent speed of which he states “This relation can be found in the textbook of Wood (1941)”

$$c_{\text{eff}} = \left\{\frac{(1-\beta)^2}{c_w^2} + \frac{\beta^2}{c_g^2} + \frac{\rho_w \beta(1-\beta)}{P}\right\}^{-1/2} \tag{B-1}$$

where P is the static pressure [Pa], which is assumed to be equal in water and gas. This is however an approximation of the original expression given by Wood which is stated in terms of fluid and gas stiffness and density. The last term between the outer brackets in equation (3.8), which does not contribute for $\beta = 0$ and $\beta = 1$, is used in approximate form in the equation above. Since $c_g^2 \rho_g^2$, the first term in the numerator of equation (3.8) is small compared to $c_w^2 \rho_w^2$, the second term, neglecting the second term leads to minor errors. The approximate expression of equation (3.8) is thus:

$$c_{\text{eff}} = \left\{\frac{(1-\beta)^2}{c_w^2} + \frac{\beta^2}{c_g^2} + \frac{\rho_w \beta(1-\beta)}{c_g^2 \rho_g}\right\}^{-1/2} \tag{B-2}$$

Comparing this equation with that provided by van Wijngaarden suggests that $p = c_g^2 \rho_g$, which is appropriate for the sound speed under isothermal conditions concurring with the assumption that van Wijngaarden makes. The relation between the adiabatic sound speed c, density ρ and pressure p for a perfect gas that is found in literature is[17]:

$$p = \frac{c^2 \rho}{\gamma} \tag{B-3}$$

with γ the ratio of specific heats.

[17] See e.g. https://en.wikibooks.org/wiki/Engineering_Acoustics/Speed_of_sound

Appendix C
Bubble damping

As long as an air bubble is small compared to the water in which it is immersed, its vibrations can be conveniently modelled in terms of a damped forced oscillator [4], for which the displacement ε of the bubble wall follows the equation of motion:

$$m\ddot{\varepsilon} + b_{\text{tot}}\dot{\varepsilon} + k\varepsilon = F \tag{C-1}$$

with mass m [kg], stiffness k [kgs^{-2}] and damping b_{tot} [kgs^{-1}].

In the Fourier domain ($\hat{\varepsilon}(f) = \int_{-\infty}^{\infty} \varepsilon(t)\mathrm{e}^{-\mathrm{i}2\pi f t}\mathrm{d}t$), the corresponding equation is:

$$(-m\omega^2 - \mathrm{i}\omega b_{\text{tot}} + k\,)\hat{\varepsilon} = \hat{F} \tag{C-2}$$

with $\omega = 2\pi f$. Defining the undamped natural frequency $\omega_0 = \sqrt{k/m}$ this yields:

$$\frac{\hat{\varepsilon}}{\hat{F}} = \frac{1}{m}(\omega_0^2 - \omega^2 - \mathrm{i}\omega b_{\text{tot}}/m)^{-1} \tag{C-3}$$

and with dimensionless damping factor $\delta_{\text{tot}} = \omega b_{\text{tot}}/m\omega_0^2$:

$$\frac{\hat{\varepsilon}}{\hat{F}} = \frac{1}{m\omega_0^2}\left(1 - \left(\frac{\omega}{\omega_0}\right)^2 - \mathrm{i}\delta_{\text{tot}}\right)^{-1} \tag{C-4}$$

For constant parameters m k and b_{tot} (and hence ω_0 and δ_{tot}) and for light damping ($\delta_{\text{tot}} < 1$), the dimensionless damping factor for a damped oscillator at resonance equals $\delta_{\text{tot}} = b_{\text{tot}}/m\omega_0$ and is related to other characteristic damping parameters:

- time constant of decay for the oscillation amplitude: $\beta = \frac{1}{2}\delta_{\text{tot}}\omega_0$ [s^{-1}]
- logarithmic decrement $\Lambda = \frac{2\pi\beta}{\omega_0} = \pi\delta_{\text{tot}}$
- quality factor $Q = \frac{\pi}{\Lambda} = \frac{1}{\delta_{\text{tot}}}$
- fraction of critical damping $\zeta = \frac{b_{\text{tot}}}{2\sqrt{km}} = \frac{\delta_{\text{tot}}}{2}$

Note that parameters m k and b_{tot} depend on frequency (ω) for a bubble oscillator.

The literature is inconsistent in parameter definitions.

Commander & Prosperetti

[7] define a 'damping constant' b, with contributions arising from viscous, thermal, and acoustic effects, respectively:

$$b^{\mathrm{C\&P}} = \frac{2\mu_w}{\rho_w a^2} + \frac{p_0}{2\rho_w a^2 \omega}\mathrm{Im}(\Phi) + \frac{\omega^2 a}{2c_w} \tag{C-5}$$

Note that the $\boldsymbol{\omega}$ in the denominator of the second term is incorrectly missing in eq.(33) in [7].

This $b^{\mathrm{C\&P}}$ [s^{-2}] relates to the b_{tot} [kgs^{-1}] as defined above according to

$$b^{\mathrm{C\&P}} = b_{\mathrm{tot}}/2m \tag{C-6}$$

So that

$$\delta_{\mathrm{tot}}^{\mathrm{C\&P}} = 2\omega b^{\mathrm{C\&P}}/\omega_0^2 \tag{C-7}$$

Kargl

[8] rewrites the expression from [7], into separate terms for the individual damping mechanisms, thereby replacing $2\omega b^{\mathrm{C\&P}}$ with $b_{\mathrm{tot}}^{\mathrm{Kargl}} = b_v^{\mathrm{Kargl}} + b_t^{\mathrm{Kargl}} + b_a^{\mathrm{Kargl}}$:

$$b_v^{\mathrm{Kargl}} = \frac{4\mu_w\omega}{\rho_w a^2},\ b_t^{\mathrm{Kargl}} = \frac{p_0}{\rho_w a^2}\mathrm{Im}(\Phi) \text{ and } b_a^{\mathrm{Kargl}} = \frac{\omega^3 a}{c_w} \tag{C-8}$$

Hence

$$\delta_{\mathrm{tot}}^{\mathrm{Kargl}} = b_{\mathrm{tot}}^{\mathrm{Kargl}}/\omega_0^2 \tag{C-9}$$

Appendix D

Derivation of the power transmission coefficient

Below a derivation of the power transmission coefficient as defined by Kinsler & Frey [16] is given. It concerns the power transmission coefficient for the case of a plane wave at normal insidence on a layer of uniform thickness. The media on both sides of the layer may be different. The setup is schematically depicted in Figure D.1.

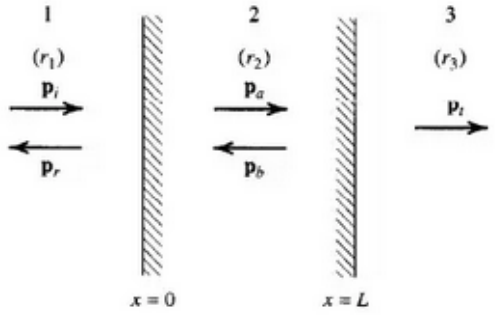

Figure D.1: Reflection and transmission of a plane wave normally incident on a layer of uniform thickness.

The specific impedance in the three media is defined as $r_i = \rho_i c_i$.

The waves traveling in positive and negative x-direction in each section are related by the boundary conditions imposed at the interfaces. The boundary conditions which ensure continuity of pressure and normal acoustic velocity across the interfaces can be written as the following system of equations

$$[M]p = p_i \tag{D-1}$$

where p contains the complex pressure of waves traveling away from the screen and inside the screen

$$p = \begin{bmatrix} p_r \\ p_{s+} \\ p_{s-} \\ p_t \end{bmatrix} \tag{D-2}$$

with p_r the complex pressure for the reflected wave, p_{s+} and p_{s-} for the waves in screen traveling in positive and negative direction, and p_t for the transmitted wave. The matrix M expresses the contributions of these waves to the equations describing continuity of the pressure and normal acoustic velocity at both interfaces:

$$M = \begin{bmatrix} 1 & 1 & 1 & 0 \\ r_1 & -r_2 & r_2 & 0 \\ 0 & e^{-ikL} & e^{ikL} & 1 \\ 0 & -r_2 e^{-ikL} & r_2 e^{ikL} & -r_3 \end{bmatrix} \tag{D-3}$$

The vector p_i contains the contributions of the incident wave to the equations describing continuity of pressure and normal acoustic velocity at the interface on which the incident wave impinges.

$$p_i = \begin{bmatrix} -1 \\ r_1 \\ 0 \\ 0 \end{bmatrix} \tag{D-4}$$

After solving for the vector of pressures p, the power transmission coefficient α_t can be calculated by

$$\alpha_t = |p_t|^2 = |p_t^2| \tag{D-5}$$

The system can be solved analytically by calculating the inverse of the matrix M. Alternatively, the system can be solved numerically at a given frequency. Both methods were implemented, and it was verified that they give near identical results for a large range of frequencies (1 Hz through 10 kHz), with the difference being caused by numeric rounding errors.

In the following, the definition of the inverse of a 4x4 matrix as given in: http://www.cg.info.hiroshima-cu.ac.jp/~miyazaki/knowledge/teche23.html was used.

The derivation begins by defining a 4x4 matrix A as

$$\mathbf{A} = \begin{pmatrix} a_{11} & a_{12} & a_{13} & a_{14} \\ a_{21} & a_{22} & a_{23} & a_{24} \\ a_{31} & a_{32} & a_{33} & a_{34} \\ a_{41} & a_{42} & a_{43} & a_{44} \end{pmatrix} \tag{D-6}$$

Assuming the matrix $\mathbf{A}$ has a nonzero determinant, the inverse is defined by

$$\mathbf{A}^{-1} = \frac{1}{\det \mathbf{A}} \begin{pmatrix} b_{11} & b_{12} & b_{13} & b_{14} \\ b_{21} & b_{22} & b_{23} & b_{24} \\ b_{31} & b_{32} & b_{33} & b_{34} \\ b_{41} & b_{42} & b_{43} & b_{44} \end{pmatrix} \tag{D-7}$$

With the determinant $\det(\mathbf{A})$ defined as

$$\begin{aligned} \det \mathbf{A} = {} & a_{11}a_{22}a_{33}a_{44} + a_{11}a_{23}a_{34}a_{42} + a_{11}a_{24}a_{32}a_{43} \\ & + a_{12}a_{21}a_{34}a_{43} + a_{12}a_{23}a_{31}a_{44} + a_{12}a_{24}a_{33}a_{41} \\ & + a_{13}a_{21}a_{32}a_{44} + a_{13}a_{22}a_{34}a_{41} + a_{13}a_{24}a_{31}a_{42} \\ & + a_{14}a_{21}a_{33}a_{42} + a_{14}a_{22}a_{31}a_{43} + a_{14}a_{23}a_{32}a_{41} \\ & - a_{11}a_{22}a_{34}a_{43} - a_{11}a_{23}a_{32}a_{44} - a_{11}a_{24}a_{33}a_{42} \\ & - a_{12}a_{21}a_{33}a_{44} - a_{12}a_{23}a_{34}a_{41} - a_{12}a_{24}a_{31}a_{43} \\ & - a_{13}a_{21}a_{34}a_{42} - a_{13}a_{22}a_{31}a_{44} - a_{13}a_{24}a_{32}a_{41} \\ & - a_{14}a_{21}a_{32}a_{43} - a_{14}a_{22}a_{33}a_{41} - a_{14}a_{23}a_{31}a_{42} \end{aligned} \tag{D-8}$$

And the factors b_{ij} defined by

$$
\begin{aligned}
b_{11} &= a_{22}a_{33}a_{44} + a_{23}a_{34}a_{42} + a_{24}a_{32}a_{43} - a_{22}a_{34}a_{43} - a_{23}a_{32}a_{44} - a_{24}a_{33}a_{42}\\
b_{12} &= a_{12}a_{34}a_{43} + a_{13}a_{32}a_{44} + a_{14}a_{33}a_{42} - a_{12}a_{33}a_{44} - a_{13}a_{34}a_{42} - a_{14}a_{32}a_{43}\\
b_{13} &= a_{12}a_{23}a_{44} + a_{13}a_{24}a_{42} + a_{14}a_{22}a_{43} - a_{12}a_{24}a_{43} - a_{13}a_{22}a_{44} - a_{14}a_{23}a_{42}\\
b_{14} &= a_{12}a_{24}a_{33} + a_{13}a_{22}a_{34} + a_{14}a_{23}a_{32} - a_{12}a_{23}a_{34} - a_{13}a_{24}a_{32} - a_{14}a_{22}a_{33}\\
b_{21} &= a_{21}a_{34}a_{43} + a_{23}a_{31}a_{44} + a_{24}a_{33}a_{41} - a_{21}a_{33}a_{44} - a_{23}a_{34}a_{41} - a_{24}a_{31}a_{43}\\
b_{22} &= a_{11}a_{33}a_{44} + a_{13}a_{34}a_{41} + a_{14}a_{31}a_{43} - a_{11}a_{34}a_{43} - a_{13}a_{31}a_{44} - a_{14}a_{33}a_{41}\\
b_{23} &= a_{11}a_{24}a_{43} + a_{13}a_{21}a_{44} + a_{14}a_{23}a_{41} - a_{11}a_{23}a_{44} - a_{13}a_{24}a_{41} - a_{14}a_{21}a_{43}\\
b_{24} &= a_{11}a_{23}a_{34} + a_{13}a_{24}a_{31} + a_{14}a_{21}a_{33} - a_{11}a_{24}a_{33} - a_{13}a_{21}a_{34} - a_{14}a_{23}a_{31}\\
b_{31} &= a_{21}a_{32}a_{44} + a_{22}a_{34}a_{41} + a_{24}a_{31}a_{42} - a_{21}a_{34}a_{42} - a_{22}a_{31}a_{44} - a_{24}a_{32}a_{41}\\
b_{32} &= a_{11}a_{34}a_{42} + a_{12}a_{31}a_{44} + a_{14}a_{32}a_{41} - a_{11}a_{32}a_{44} - a_{12}a_{34}a_{41} - a_{14}a_{31}a_{42}\\
b_{33} &= a_{11}a_{22}a_{44} + a_{12}a_{24}a_{41} + a_{14}a_{21}a_{42} - a_{11}a_{24}a_{42} - a_{12}a_{21}a_{44} - a_{14}a_{22}a_{41}\\
b_{34} &= a_{11}a_{24}a_{32} + a_{12}a_{21}a_{34} + a_{14}a_{22}a_{31} - a_{11}a_{22}a_{34} - a_{12}a_{24}a_{31} - a_{14}a_{21}a_{32}\\
b_{41} &= a_{21}a_{33}a_{42} + a_{22}a_{31}a_{43} + a_{23}a_{32}a_{41} - a_{21}a_{32}a_{43} - a_{22}a_{33}a_{41} - a_{23}a_{31}a_{42}\\
b_{42} &= a_{11}a_{32}a_{43} + a_{12}a_{33}a_{41} + a_{13}a_{31}a_{42} - a_{11}a_{33}a_{42} - a_{12}a_{31}a_{43} - a_{13}a_{32}a_{41}\\
b_{43} &= a_{11}a_{23}a_{42} + a_{12}a_{21}a_{43} + a_{13}a_{22}a_{41} - a_{11}a_{22}a_{43} - a_{12}a_{23}a_{41} - a_{13}a_{21}a_{42}\\
b_{44} &= a_{11}a_{22}a_{33} + a_{12}a_{23}a_{31} + a_{13}a_{21}a_{32} - a_{11}a_{23}a_{32} - a_{12}a_{21}a_{33} - a_{13}a_{22}a_{31}
\end{aligned}
\tag{D-9}
$$

Applying the expression for det(A) to matrix M yields

$$
\det M = \begin{array}{lll}
(\; r_2 r_3 e^{ikL} & -r_2^2 e^{-ikL} & +0 \\
+r_1 r_2 e^{ikL} & +0 & +0 \\
-r_1 r_3 e^{-ikL} & +0 & +0 \\
+0 & +0 & +0 \\
+r_2^2 e^{ikL} & r_2 r_3 e^{-ikL} & +0 \\
+r_3 e^{ikL} & +0 & +0 \\
+r_1 r_2 e^{-ikL} & +0 & +0 \\
+0 & +0 & +0)
\end{array}
\tag{D-10}
$$

Collecting al terms yields:

$$
\begin{aligned}
&\mathrm{Det}(M) = \\
&\; r_2 r_3 e^{ikL} - r_2^2 e^{-ikL} + r_1 r_2 e^{ikL} - r_1 r_3 e^{-ikL} + r_2^2 e^{ikL} + r_2 r_3 e^{-ikL} + r_1 r_3 e^{ikL} + r_1 r_2 e^{-ikL}
\end{aligned}
$$

Reordering and factoring yields:

$$\det(M) = r_2 r_3 (e^{ikL} + e^{-ikL}) + r_2^2 (e^{ikL} - e^{-ikL}) + r_1 r_2 (e^{-ikL} + e^{ikL}) + r_1 r_3 (e^{ikL} - e^{-ikL})$$

Applying the relation between the exponential function and sine and cosine functions yields:

$$\det(M) = 2(r_2 r_3 + r_1 r_2)\cos(kL) + i2(r_2^2 \sin(kL) + r_1 r_3 \sin(kL))$$

Since the main interest is in obtaining an expression for p_t only the coefficients b_{41} and b_{42} in the definition of the inverse are needed:

$$b_{41} = -r_1 r_2 e^{ikL} e^{-ikL} + 0 + 0 - r_1 r_2 e^{ikL} e^{-ikL} - 0 - 0 = -2 r_1 r_2$$

$$b_{42} = r_2 e^{-ikL} e^{ikL} + 0 + 0 + r_2 e^{-ikL} e^{ikL} - 0 - 0 = 2 r_2$$

Substituting the expressions for $\det(M)$ and b_{41} and b_{42} in the relevant part of the expression for the inverse, and applying it to the right hand side vector p_i yields the following expression for the complex pressure of the transmitted wave

$$p_t = [M]^{-1} p_i = \frac{-b_{41}+b_{42}r_1}{\det M} = \frac{4r_1r_2}{2(r_2r_3+r_1r_2)\cos(kL)+i2(r_2^2+r_1r_3)\sin(kL)}$$

which can be rewritten as:

$$p_t = \frac{2}{(\frac{r_3}{r_1}+1)\cos(kL)+i(\frac{r_2}{r_1}+\frac{r_3}{r_2})\sin(kL)} \tag{D-11}$$

Note that in case the media on both sides of the screen are identical, the specific acoustics impedances are equal ($r_1 = r_3$) and the equation can be simplified to:

$$p_t = \frac{2}{2\cos(kL)+i(\frac{r_2}{r_1}+\frac{r_1}{r_2})\sin(kL)} \tag{D-11}$$

For the power transmission coefficient α_t we is obtain using the relation

$$\alpha_t = |p_t|^2 = \left|\frac{2}{2\cos(kL)+i\left(\frac{r_2}{r_1}+\frac{r_1}{r_2}\right)\sin(kL)}\right|^2 \tag{D-12}$$

This is believed to be the correct expression; however, it cannot be brought closer to the expression in the fourth edition of the book of Kinsler & Frey without furhter assumptions. By manipulating the expression slightly it can be brought into the form

$$\alpha_t = \frac{4}{\left|2\cos(kL)+i\left(\frac{r_2}{r_1}+\frac{r_1}{r_2}\right)\sin(kL)\right|^2} \tag{D-13}$$

It was mentioned in Section 4.1 that as long as r_1, r_2 and k remain real valued the denominator in the right hand side takes the form of a complex number

$$z = x + iy \tag{D-13}$$

with $x = 2\cos(kL)$ and $y = \left(\frac{r_2}{r_1}+\frac{r_1}{r_2}\right)\sin(kL)$. In that case taking the square of the absolute value (also known as the squared norm) can be written as

$$|z|^2 = |x+iy|^2 = x^2 + y^2 \tag{D-14}$$

So, under this assumption and using this relation the expression for α_t can be rewritten as

$$\alpha_t = \frac{4}{4\cos^2(kL)+\left(\frac{r_2}{r_1}+\frac{r_1}{r_2}\right)^2\sin^2(kL)} \tag{D-15}$$

demonstrating that for this special case Equations (4.1) and (4.3) give identical results. However, in the more general case where the speed of sound in one of the media becomes complex, r_1 or r_2 and k becomes complex and the denominator in equation (4.3) is not of the form $z = x + iy$. In that case equation (4.1) and (4.3) will not lead to identical results and equation (4.3), which is based on the more general case, is the appropriate expression.

Observations from comparing results between the solution derived here (equation (4.3)) and that provided by the book (both second and fourth edition) by Kinsler & Frey (equation (4.1) and (4.2), respectively):

- The results using the equation in the book matches those for the equation derived here and the numerical solution in case there is no damping. So as long as real sound speeds are considered the equations produce identical results. This is true both for cases where the difference in specific impedance between water and screen are large and small.
- Things change as damping is added. More damping makes the solution in the book deviate more from the solution derived here and the numerical solution (the latter two remaining equal).
- If damping is present, decreasing the difference in specific impedance between water and screen increases the observed error for the solution in the book compared to the solution derived here and the numerical solution (the latter two remaining equal).
- The observed differences are negligible at low frequencies, grow with increasing frequency and ultimately the difference seems to settle to a constant offset in the high frequency limit.

Defence, Safety & Security

Oude Waalsdorperweg 63
2597 AK Den Haag
www.tno.nl

TNO innovation for life